BIOELECTRIC SOURCE CHARACTERIZATION OF ACUTE MYOCARDIAL ISCHEMIA

by

Kedar Kirtikumar Aras

A dissertation submitted to the faculty of
The University of Utah
in partial fulfillment of the requirements for the degree of

Doctor of Philosophy

Department of Bioengineering

The University of Utah

August 2015

The University of Utah Graduate School

STATEMENT OF DISSERTATION APPROVAL

The dissertation of **Kedar Kirtikumar Aras**

has been approved by the following supervisory committee members:

Robert S. MacLeod	, Chair	**06/02/2015**
		Date Approved
Alexey V. Zaitsev	, Member	**06/02/2015**
		Date Approved
Scott T. Youngquist	, Member	**06/02/2015**
		Date Approved
Edward W. Hsu	, Member	**06/02/2015**
		Date Approved
Edward V. R. DiBella	, Member	**06/08/2015**
		Date Approved

and by **Patrick A. Tresco**, Chair of

the Department of **Bioengineering**

and by David B. Kieda, Dean of The Graduate School.

ABSTRACT

Despite a century of research and practice, the clinical accuracy of the electrocardiogram (ECG) to detect and localize myocardial ischemia remains less than satisfactory. Myocardial ischemia occurs when the heart does not receive adequate oxygen-rich blood to keep up with its metabolic requirements, and severe ischemia can lead to myocardial infarction and life-threatening arrhythmias. Early and accurate detection is an essential component of managing this condition.

Ischemia is known to be a dynamic condition that reflects a changing imbalance between blood supply and metabolic demand so that it is natural that examination under physical stress conditions or exercise testing (ET) is in widespread clinical use. However, ET is characterized by poor sensitivity (68%) and specificity (77%), limiting its diagnostic usefulness and providing the motivation to address some gaps in our understanding of myocardial ischemia and its ECG signature.

This dissertation is composed of three studies. The aim of the first study was to evaluate the conventionally held mechanisms for nontransmural ischemia using intramural electrodes to measure three-dimensional potential distributions in the ventricles of animals exposed to acute ischemia. We demonstrated that contrary to accepted dogma, the electrocardiographic response of acute myocardial ischemia originated throughout the ventricular wall, i.e., in the subendocardium, midmyocardium, or the subepicardium, under various conditions.

Our goal in the second study was to evaluate whether acute myocardial ischemia follows a similar pattern of spatial and temporal evolution as seen in myocardial infarction. Our findings show that the spatial and temporal evolution of acute ischemia is characterized by multiple distinct regions that expand in all three directions, with maximal expansion in the circumferential direction, especially in the early stages of ischemic development. Furthermore, with increased stress, these regions continue to expand and eventually merge into one another, and in the extreme become transmural. The progression of myocardial infarction, by contrast, was very quickly transmural in extent and formed a cohesive block of affected tissues.

The aim of the third study was to evaluate the sensitivity of epicardial electrical markers of acute ischemia relative to direct evidence of ischemia derived from intramural electrograms. The key finding from this study is that the epicardial T-wave is a more sensitive index of acute ischemia than epicardial ST segment changes, especially in the early stages of acute ischemia development.

I dedicate this dissertation to my parents, Kirtikumar and Padma. I hope that this achievement will complete the dream that you had for me all those many years ago when you chose to give me the best education you could.

CONTENTS

ABSTRACT ..... **iii**

ACKNOWLEDGMENTS ..... **ix**

CHAPTERS

1. INTRODUCTION **1**

1.1 Background and Significance 2
1.1.1 Myocardial Ischemia Profile 2
1.1.2 Coronary Perfusion and Myocardial Ischemia 3
1.1.3 Pathophysiology of Myocardial Ischemia 4
1.1.4 ECG Markers for Myocardial Ischemia 4
1.1.5 ECG-Based Detection of Ischemia 6
1.1.6 Clinical Modalities for Detecting Ischemia 7
1.2 Study Aims 8
1.2.1 Aim 1 - Spatial Organization of Ischemia 8
1.2.2 Aim 2 - Spatio-Temporal Evolution of Ischemia 9
1.2.3 Aim 3 - Sensitivity of Electrical Markers to Ischemia 9
1.3 Organization of the Dissertation 9

2. BACKGROUND **11**

2.1 Cardiac Anatomy 11
2.1.1 Pericardium and Heart Wall 11
2.1.2 Cardiac Cell Types 12
2.1.3 Cardiac Chambers 14
2.1.4 Cardiac Skeleton and Cardiac Valves 16
2.1.5 Coronary Arteries and Veins 18
2.1.6 Electrical Conduction System 20
2.1.7 Comparative Cardiac Anatomy 20
2.2 Cardiac Electrophysiology 21
2.2.1 Cardiomyocyte 21
2.2.2 Cardiac Cell Membrane 24
2.2.3 Resting Potential 26
2.2.4 Action Potential 29
2.2.5 Excitation-Contraction Coupling 33
2.2.6 Gap Junctions 35
2.2.7 Myocardial Anisotropy 36
2.2.8 Cardiac Propagation 37
2.2.9 Cardiac Activation Sequence 38
2.2.10 Electrocardiogram (ECG) 40
2.3 Cardiovascular Physiology 45

2.3.1 Cardiac Cycle . . . 45
2.3.2 Hemodynamics . . . 48
2.3.3 Coronary Circulation . . . 49
2.3.4 Integrated Control of Cardiovascular Physiology . . . 51
2.4 Coronary Heart Disease (CHD) and Ischemia . . . 53
2.4.1 Definition and Classification . . . 55
2.4.2 Metabolic Consequences . . . 57
2.4.3 Structural Consequences . . . 58
2.4.4 Ionic Consequences . . . 58
2.4.5 Neurohumoral Consequences . . . 61
2.4.6 Electrical Consequences . . . 62
2.4.7 Functional Consequences . . . 64
2.4.8 Diagnosis . . . 65
2.4.9 Treatment . . . 71
2.4.10 Prevention . . . 72
2.5 Literature Review . . . 73
2.5.1 Pre-1950s . . . 74
2.5.2 1950s - 1990s . . . 74
2.5.3 2000s - Present . . . 78

3. DESIGN OF EXPERIMENTS . . . 79

3.1 Animal Models . . . 79
3.2 Experimental Setups . . . 80
3.2.1 In Situ Setup . . . 81
3.2.2 Isolated Heart Perfused by Support Animal . . . 81
3.3 Study Protocols . . . 82
3.4 Data Acquisition . . . 83
3.4.1 Time Signal Acquisition . . . 83
3.4.2 Image Acquisition . . . 85
3.4.3 Registration Data Acquisition . . . 86
3.5 Data Processing . . . 86
3.5.1 Time Signal Processing . . . 87
3.5.2 Image Processing (Segmentation) . . . 88
3.5.3 Geometry Processing . . . 88
3.6 Data Visualization . . . 89

4. SPATIAL ORGANIZATION OF MYOCARDIAL ISCHEMIA . . 91

4.1 Abstract . . . 91
4.2 Introduction . . . 92
4.3 Methods . . . 94
4.3.1 Experimental Preparation . . . 94
4.3.2 Experimental Protocols and Data Acquisition . . . 95
4.3.3 Postexperiment Imaging and Signal Processing . . . 96
4.3.4 Statistical Analysis . . . 97
4.4 Results . . . 98
4.5 Discussion . . . 102
4.6 Conclusion . . . 105

5. SPATIO-TEMPORAL EVOLUTION OF ACUTE MYOCARDIAL ISCHEMIA **107**
5.1 Abstract 107
5.2 Introduction 108
5.3 Methods 109
5.3.1 Experimental Preparation 109
5.3.2 Experimental Protocols and Data Acquisition 111
5.3.3 Postexperiment Imaging and Signal Processing 111
5.3.4 Statistical Analysis 112
5.4 Results 113
5.5 Discussion 116
5.6 Conclusion 118

6. EPICARDIAL SENSITIVITY TO MYOCARDIAL ISCHEMIA **119**
6.1 Abstract 119
6.2 Introduction 120
6.3 Methods 121
6.3.1 Experimental Preparation 121
6.3.2 Experimental Protocols and Data Acquisition 122
6.3.3 Postexperiment Imaging and Signal Processing 123
6.3.4 Statistical Analysis 123
6.4 Results 124
6.5 Discussion 127
6.6 Conclusions 129

7. CONCLUSIONS AND FUTURE WORK **130**
7.1 Conclusions 130
7.2 Future Work 133
7.2.1 Spatial Organization of Ischemia 134
7.2.2 Spatio-Temporal Evolution of Ischemia 136
7.2.3 Sensitivity of Electrical Markers to Ischemia 137
7.2.4 Design of Experiments 137

REFERENCES **140**

ACKNOWLEDGMENTS

I'd like to express my gratitude to my colleagues, friends, and family. Their unwavering support has been instrumental in completing my dissertation. First and foremost, I would like to thank my advisor, Dr. Rob Macleod, for giving me the opportunity to pursue this doctoral research. He has been my teacher, mentor, father figure, and role model. Thank you for providing an incredibly supportive learning environment and helping me become a better scientist. I could not have imagined having a better advisor for my doctoral study. I would like to thank Dr. Alexei Zaitsev, Dr. Edward Hsu, Dr. Edward DiBella, and Dr. Scott Youngquist for their guidance, patience, and suggestions for this research. In addition, I'd like to thank Dr. Andrews Michaels, Dr. Elizabeth Shiu, and Dr. Bonnie Punske for also serving on my PhD committee.

I am also grateful to the other students and postdocs in our research lab including Darrell Swenson, Josh Blauer, Jess Tate, Brett Burton, Wilson Good, and Moritz Dannhauer for their time, support, and advise. This work would not have been possible without contributions from everyone at the Cardiovascular Research and Training Institute (CVRTI). I am grateful to Jayne Davis, Nancy Allen, Alicja Booth, Phil Ershler, and Bruce Steadman for their invaluable help in conducting the ischemia experiments. I'd also like to thank members of Dr. Ed Hsu's small animal imaging group including Osama Abdullah and Samer Merchant for their expertise in generating CT, MRI, and DT-MRI scans. I'd also like to thank the research and development (Ayla Khan, Dan White) and also the media development staff (Nathan Galli, Chems Touti) at the Scientific Computing and Imaging (SCI) Institute for resources, including support software used in this research.

Finally, I thank my family for their unyielding support and encouragement. I would like to express my eternal gratitude to my parents, Kirtikumar Narayan Aras and Padma Aras, my brother, Kaushal Aras, and my sister, Radhika Aras Kharpate, for their numerous sacrifices, and their love, patience, and support. I would also like to thank my partner, Holly Majszak, for her patient support and constant encouragement.

CHAPTER 1

INTRODUCTION

Coronary artery disease (CAD) is one of the leading causes of mortality in the United States, affecting over 13 million people, with half suffering from myocardial (cardiac) ischemia [1]. Cardiac ischemia is a pathological condition that occurs when the heart does not receive enough oxygen-rich blood to keep up with its metabolic requirements. Severe ischemia leads to a heart attack, cell damage, and life-threatening arrhythmias so that early and accurate detection is an essential component of managing this condition.

The electrocardiogram (ECG) records the electrical activity of the heart and is used as a central tool to establish the diagnosis of myocardial ischemia. ECG evidence of myocardial ischemia includes shifts in the ST segment, the portion of the ECG between the end of the QRS complex and the beginning of the T-wave, all of which are described below in more detail. The use of ECG for ischemia diagnosis is most critical in two clinical settings and the consequences of errors in interpretation most costly. The first is the emergency room (ER), in which an ECG is often recorded in patients with symptoms of chest pain. Unfortunately, a relatively high percentage of the cases of myocardial ischemia occur without chest pain symptoms [1], a syndrome known as silent ischemia. Moreover, the ECG may also be normal or nonspecific in a patient with myocardial ischemia, leading to diagnostic errors of 30-50% [1]. The second setting is exercise stress testing (ET), which is a noninvasive tool to evaluate cardiovascular response to exercise under controlled conditions. If the heart does not receive enough oxygenated blood during the test, it may produce abnormalities in the ECG suggestive of myocardial ischemia and underlying CAD. However, ET has poor sensitivity (68%) and specificity (77%) [1].

This poor performance of the ECG for detecting ischemia provides powerful motivation to address some gaps in our understanding of myocardial ischemia and its electrocardiographic signature. Additional motivation comes from the fact that the ECG remains the most widely available diagnostic tool that is painless, noninvasive, safe, and easy to perform. Accurate and robust characterization of the heart's electrocardiographic response

to acute episodes of cardiac ischemia would provide the basis for improving the accuracy of myocardial ischemia detection and result in more effective treatments. The research in this dissertation focused on advancing this goal through a series of acute ischemia studies using high-resolution mapping of cardiac potentials.

We first investigated the spatial origins of acute myocardial ischemia through qualitative and quantitative analysis of different types and degrees of cardiac ischemia that we could induce in animal models. We began with an evaluation of the current dogma regarding the spatial organization and distribution of especially nontransmural ischemia and suggested an alternative formulation that better supports the available data. Next, we characterized the spatio-temporal progression of acute cardiac ischemia, again with the goal of establishing a robust description of the sequence of ischemia development over the acute time frame. The third and most clinically relevant component of the research was to extend these results to the cardiac surface with the goal of establishing realistic estimates of the degrees to which ischemic changes are detectable from the heart surface. The results from the third project provided valuable insights about information available on the cardiac surface relative to the location of nontransmural ischemia. The cumulative results from our studies have provided new understanding of the underlying bioelectric sources, their spatial organization and temporal progression, and the extent to which the cardiac surface ECG is sensitive to them.

1.1 Background and Significance

1.1.1 Myocardial Ischemia Profile

Each year in the Western world, there are about 5.8 million new cases of coronary artery disease (CAD), and about 40 million individuals with prevalent CAD are alive today [2]. In the United States, CAD is the single leading cause of death in adults, accounting for one in five deaths [2]. It is estimated that over 13 million Americans have CAD, about one half of whom experience episodes of myocardial ischemia [2]. The estimated annual health care burden in the US associated with CAD is about $142.5 billion USD [2]. Myocardial ischemia can be defined as an imbalance between the supply of oxygenated blood and the oxygen requirements of the heart [3]. Myocardial ischemia resulting predominantly from increased myocardial oxygen demand in the presence of critical narrowing of a coronary artery is termed *demand ischemia*. By contrast, myocardial ischemia caused predominantly by reduction of coronary blood flow is termed *supply ischemia*. Demand ischemia occurs in most episodes of *stable angina* (chest pain), whereas supply ischemia is associated with

most episodes of *unstable angina*. Myocardial ischemia can also arise from a combination of both an increase in oxygen demand and a reduction in supply, i.e., supply **and** demand ischemia. According to its location, cardiac ischemia is also classified as *transmural ischemia* if it affects the full thickness of the ventricular wall or *nontransmural ischemia* if the injury does not span the entire thickness of the ventricular wall.

1.1.2 Coronary Perfusion and Myocardial Ischemia

Since ischemia reflects an imbalance between blood supply and metabolic demand, it is important to understand the many parameters and regulatory mechanisms that control this central homeostatic system. On the side of metabolic demand, the main parameters dictating cardiac oxygen consumption are heart rate (chronotropy), cardiac contractility (inotropy), and left ventricular (LV) wall stress. At maximal levels, heart rate can increase threefold, contractility three- to fivefold [1]. The main mechanism to bring more oxygen to the myocardium upon increased demand is to increase coronary blood flow, which is regulated to continuously and dynamically match variation in metabolism. In fact, at maximal metabolic load (e.g., maximal exercise), coronary blood flow can reach values up to three to five times those at rest [1]. This difference between values at rest and maximal levels of coronary flow represents the *coronary flow reserve*. What is known as "coronary autoregulation" is the most powerful mechanism by which coronary flow reserve is recruited to maintain the desired perfusion level. Autoregulation is a local mechanism, i.e., it requires no control from the brain or nervous system, that has the ability to maintain a suitable blood flow despite changes in metabolic demand and local perfusion pressure. When the blood pressure falls, arterial resistance is reduced as the small arteries and arterioles dilate. The reduction in resistance causes blood flow to remain stable despite the presence of reduced perfusion pressure.

Myocardial ischemia represents a breakdown in this homeostasis and has a variety of consequences depending on the severity of the reduction in coronary blood flow, the length of the ischemic insult, the area of the myocardium served by the occluded artery, and the presence of collateral vessels from other adjacent beds within the heart. Under the most severe instances of complete occlusion of blood flow, myocardial ischemia can progress to myocardial infarction (heart attack) characterized by tissue death and, if left untreated, necrosis and scar.

1.1.3 Pathophysiology of Myocardial Ischemia

While the origins of ischemia are hemodynamic, there are rapid and profound electrophysiological consequences, changes that often represent the most lethal clinical impacts of this condition. Carmeliet [4], in his exhaustive review of the electrophysiological changes during myocardial ischemia, described a series of metabolic, ultrastructural, mechanical, and electrical changes within myocardial cells and tissues that occurs during acutely compromised coronary blood flow. The myocardium becomes cyanotic because of the consumption of freely diffusible oxygen, causing decreased tissue oxygen tension. With increasing tissue hypoxia, intracellular respiration shifts from aerobic to anaerobic form. Adenosine triphosphate (ATP) stores are rapidly depleted, and characteristic metabolic changes occur in the ischemic tissue, including accumulation of tissue lactate, H^+ ions, phosphate, and potassium. Ultrastructural changes consist of reduction in the size and number of glycogen granules, intracellular edema, swelling and distortion of mitochondria, and eventually margination of nuclear chromatin and relaxation of myofibrils. Diminished ATP stores and alteration of Ca^{++} lead to impairment of cardiac contractile function.

The most important consequences of ischemia from the perspective of the ECG and this research are those related to altered action potential shape and amplitude. The electrical changes in ischemic cells include a marked elevation in resting membrane potential due to increased extracellular K^+ concentration, reduced action potential (AP) amplitude and a reduced rate of AP upstroke due to decreased inward Na^+ current, and shortened AP duration due to reduced inward Ca^{++} current. These changes do not occur uniformly in space, and the resulting variations in action potential amplitude and morphology in different parts of the heart lead to what are known as "injury currents," which ultimately cause important changes in the ECG that we describe in the next section.

1.1.4 ECG Markers for Myocardial Ischemia

ECG records the electrical activity of the heart from the body surface and can detect noninvasively the occurrence of myocardial ischemia. The waves in the ECG reflect the sequence of electrical excitation and recovery as it moves through the atria and the ventricles. Fig. 1.1(a) shows schematically the relationship between the activation sequence and the resulting phases/waves of the ECG. The P-wave represents the progression of atrial depolarization as it moves from the sino-atrial (SA) node across the right and then left atria. The QRS complex reflects the corresponding rapid depolarization of the right and left ventricles initiated when activation passes from the atria through the specialized conduction system of the atrio-ventricular (AV) node and the Bundle of His into the Purkinje

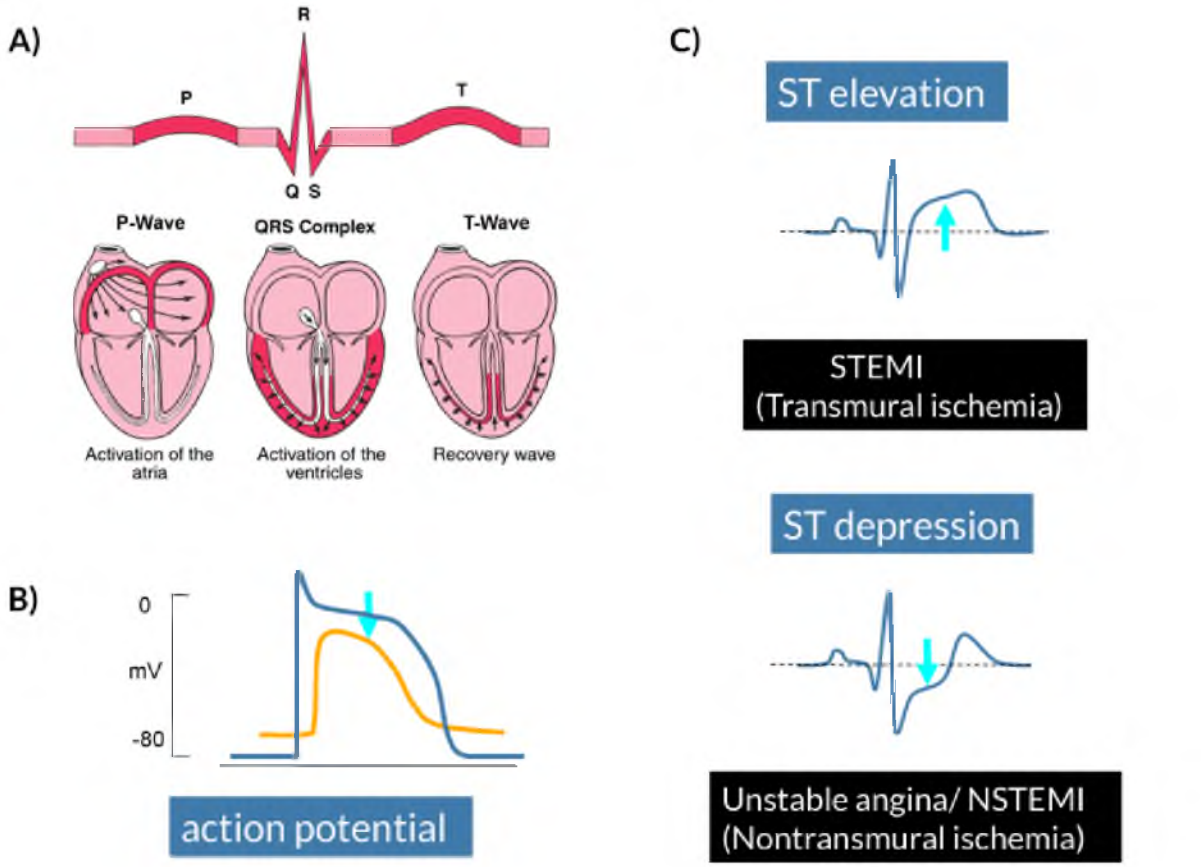

Fig. 1.1. Clinical model of ischemia: (a) Electrocardiogram (ECG), (b) ventricular action potentials (AP) under normal (blue) and ischemic (orange) conditions, (c) classical electrocardiography theory. ST segment elevation is diagnosed as ST segment elevation myocardial infarction (STEMI) or transmural ischemia, whereas ST segment depression is diagnosed as non-ST segment elevation myocardial infarction (NSTEMI) or unstable angina or nontransmural ischemia.

fiber network. The T-wave represents the repolarization of the ventricles, i.e., the gradual return of ventricular action potentials to resting values. Of special importance in the setting of ischemia is the "ST segment," which connects the QRS complex and the T-wave and represents the period when the ventricles are depolarized. Under normal conditions, the ST segment is isoelectric, i.e., the action potentials all reach approximately the same value and so there are no potential differences across the myocardium and hence no current.

During cardiac ischemia, regional changes in the AP morphology of ischemic cells bring about alterations in the ECG. Best documented and used for clinical diagnosis are changes in the ST segment (described in more detail below). However, there are also changes in the QRS complex that include changes in amplitude, inversion of complex polarity, loss of some

constituent waves, and in the case of conduction slowing, widening of the QRS complex. Abnormal repolarization during ischemia may also change the amplitude and polarity of the T-wave.

The most important ECG diagnostic marker for ischemia detection remains the upward or downward shifts in the ST segment, which occur within 15–30 seconds after the onset of ischemia [5]. ST segment shifts are caused by localized electrical changes that occur in the action potentials of ischemic cells, especially shortening of duration, diminished amplitude, and elevation of resting membrane potential. Fig. 1.1(b) shows these changes schematically, with the blue line indicating a normal action potential and the orange line a typical ischemic action potential. Regional differences in membrane action potentials generate injury currents and produce deflections from the isoelectric potentials of a healthy heart. Fig. 1.1(c) shows the resulting changes in ST segments, the orientation of which depends on a set of geometric factors, both of the ischemic region and the location of the sensing electrode relative to the ischemic zone. For example, a positive deflection (upward shift) occurs if the injury current is flowing toward the recording electrode and a negative deflection (downward shift) if the injury current is oriented away from the electrode. For electrodes located over the heart, ST segment elevation (upward shift) is often thought to represent transmural ischemia, usually leading, if untreated within 1–2 hours, to an infarction (heart attack), whereas ST segment depression is considered a sign of nontransmural, typically transient ischemia.

This diagnostic model for ischemia detection is based in part on the dogma that myocardial ischemia arises first in the subendocardium, thus generating intracellular injury current flowing towards the endocardium and away from precordial ECG electrodes. Over time or under increased stress, the ischemic region expands towards the epicardium, eventually becoming transmural, and the injury current begins to flow towards the recording electrode and thus produce ST segment elevation.

1.1.5 ECG-Based Detection of Ischemia

The use of ECG for ischemia diagnosis is critical in two clinical settings: the emergency room (ER) and exercise testing (ET). In the ER, a 12-lead ECG with the patient at rest is often recorded in patients with symptoms suggestive of ischemia, e.g., chest pain (angina), shortness of breath, or dizziness; however, the ECG is normal in up to 50% of the patients who actually have chronic stable angina [1]. A further source of confounding error is the finding that in approximately 70% of cases of true cardiac ischemia, there are no clear symptoms of chest pain, a syndrome known as *silent ischemia* [1]. Exercise testing (ET)

is a very broadly used method to evaluate the functional reserve present in a patient with suspected CAD. It is based on the simple idea that by increasing metabolic demand through physical or pharmacological stress, it is possible to exceed the coronary flow reserve and elicit electrocardiographic symptoms of ischemia. While simple and safe to carry out in the carefully controlled conditions of the hospital, ET has poor accuracy (sensitivity of approximately 70% and specificity of only 80%) [6], which has motivated the development of other, typically slower and/or more costly approaches to ischemia diagnosis.

1.1.6 Clinical Modalities for Detecting Ischemia

In large part because of the limited accuracy of ECG-based diagnosis, there are other clinical modalities available, both noninvasive and invasive, to establish the diagnosis of ischemia with varying degrees of accuracy. Echocardiography (Echo) is a noninvasive approach based on ultrasound to evaluate cardiac structure and function with images that have limited resolution and high noise levels but can capture two and even three dimensions as functions of time. In this way, Echo can establish diagnosis of ischemia based on regional systolic or diastolic wall motion abnormalities. Echo has a mean sensitivity of 70% and mean specificity of 80%, which is similar to the ECG. Myocardial perfusion imaging (MPI) using any one of several imaging modalities is another noninvasive approach available for ischemia diagnosis. Single-photon emission computed tomography (SPECT) MPI is performed using a scintillation camera and an intravenously injected nuclear tracer (e.g., isotope thallium-201) that over time, distributes itself through the heart in proportion to the regional myocardial perfusion, thus providing a map of blood flow to the heart. MPI has higher sensitivity (90%) and lower specificity (70%) compared to ECG and also requires tens of minutes to acquire and so cannot capture rapid changes in ischemia. Biochemical assays that detect cardiac markers such as creatine kinase (CK) and cardiac troponins T (cTnT) and I (cTnI) released into the blood by damaged cardiomyocytes are also used for diagnosis of ischemia. These markers have high sensitivity to detect cardiac injury, but they are also very slow (typically tens of minutes) and not specific for the etiology of cardiac injury, i.e., they may be the result of any number of illnesses, including diabetes, hypertrophy, etc. Perfusion can also be traced using coronary angiography, which is a marginally invasive procedure that entails passing a catheter through an artery into the heart and uses a special dye and x-rays to detect blood flows through the heart and into the myocardium. The dye highlights any restrictions or blockages in the coronary blood flow and remains the gold standard against which the accuracy of all other CAD diagnostic tools is measured. A

related, novel approach that eliminates the burden of ionizing radiation is angiography and perfusion imaging based on MRI [7, 8]. Conceptually similar to X-ray-based approaches, MRI perfusion imaging also has poor temporal resolution and high cost and functions poorly as a monitoring approach.

1.2 Study Aims

Early and accurate detection of myocardial ischemia remains a key component of managing this condition. ECG remains the most widely available diagnostic tool that is painless, noninvasive, safe, and easy to perform. Moreover, the equipment is readily available, inexpensive, and portable. However, the clinical performance of ECG in detecting and localizing the extent of cardiac ischemia remains unsatisfactory, providing the motivation to address some gaps in our understanding of myocardial ischemia and its ECG signature. The goal of this research was to characterize the electrocardiographic response of the heart during acute myocardial ischemia through a series of acute ischemia studies using high-resolution mapping of cardiac potentials. The ischemia studies included canine and swine animal models. The study protocol was designed to simulate stress testing and entailed inducing demand or supply ischemia by controlling the heart rate and coronary perfusion. During the ischemia study, electrograms were recorded from the cardiac surface as well as the intramural regions. These recorded electrical potentials were used to generate high-resolution potential maps and analyzed to determine the spatial origins and distribution of ischemia, determine the spatio-temporal progression of nontransmural ischemia, and finally evaluate the sensitivity of cardiac surface electrograms to variations in location and extent of nontransmural ischemia.

To address these research goals, we have carried out studies focused around the following three specific aims.

1.2.1 Aim 1 - Spatial Organization of Ischemia

Current literature suggests that myocardial ischemia originates from the subendocardium. However, studies done in the past have relied on measurements primarily on the epicardial and endocardial surfaces. Moreover, those relatively few reported cases of intramural measurements have been limited by sparse spatial resolution. The goal of this study was to characterize the electrocardiographic response of the heart during acute myocardial ischemia through a series of acute ischemia studies using high-resolution mapping of cardiac potentials. We investigated the spatial origins of different types and degrees of acute myocardial ischemia. Despite widespread use, the link, especially quantitatively, between

the direction and extent of ST segment shifts and the putative mechanisms of ischemia is equivocal and thus the cause of persistent clinical error. Based on our findings, we suggest an alternative formulation that better supports the available data and provides a better understanding of bioelectric sources during cardiac ischemia.

1.2.2 Aim 2 - Spatio-Temporal Evolution of Ischemia

Reimer et al. [9] in their study on canine models induced irreversible ischemic injury characterized by necrosis and suggested that ischemia progresses as a transmural wavefront from the subendocardium to subepicardium. We profiled the spatio-temporal progression of acute ischemia in order to characterize the way ischemia develops over the acute time frame and determine whether it follows a similar pattern of spatial and temporal evolution as is seen in myocardial infarction. The high-resolution mapping of cardiac potentials enabled us to provide a much more refined description of the progress of nontransmural acute to transmural ischemia.

1.2.3 Aim 3 - Sensitivity of Electrical Markers to Ischemia

Classical electrocardiographic theory suggests that ST segment elevation on the body surface ECG reveals transmural ischemia, whereas ST segment depression is the result of subendocardial ischemia [10]. However, numerous clinical and experimental studies suggest that this theory is, at best, incomplete. Some studies have suggested that ST segment depression is "reciprocal" to the presence of ST segment elevation [11]. Li et al. used a sheep model in their acute ischemia studies and showed that reducing flow in two different major coronary arteries produced similar epicardial ST segment potential distribution, even though intramural recordings showed that occlusion of different arteries resulted in distinctly different ischemic zones [12]. We evaluated the sensitivity of cardiac surface electrograms to localize acute myocardial ischemia. The goal of this study was to evaluate different electrical markers for their potential to detect the earliest phases of acute myocardial ischemia. Our findings indicate that a combination of markers may provide a more reliable index of acute ischemia.

1.3 Organization of the Dissertation

The dissertation is divided into seven chapters. Chapter 1 provides an overview of the dissertation. Chapter 2 includes background on cardiac anatomy, physiology, electrophysiology, pathophysiology of myocardial ischemia, and patient evaluation tools to diagnose CAD and a review of relevant literature to appreciate the subsequent chapters. Chapter 3 provides

an overview of the study design including the data acquisition and processing pipeline. Chapter 4 is a journal paper that has been submitted to the *Journal of Electrocardiology* and presents the results from spatial organization of myocardial ischemia. Chapter 5 is a journal paper that has been submitted to the *Journal of Electrocardiology* and deals with the spatio-temporal progression of ischemia. Chapter 6 is a paper published in the *Journal of Electrocardiology* 2014 and presents the results of a sensitivity study of cardiac surface electrograms. Chapter 7 concludes the dissertation and outlines future directions for this research.

CHAPTER 2

BACKGROUND

This chapter provides the necessary background to appreciate the research behind the electrocardiographic characterization of acute myocardial ischemia. Accordingly, we cover elements of cardiac anatomy and physiology, include an overview of cardiac electrophysiology, describe the pathophysiology of myocardial ischemia, highlight the clinical diagnostic tools and techniques used to evaluate and treat patients with myocardial ischemia, and finally include a summary of the literature relevant to this research.

2.1 Cardiac Anatomy

The heart is a hollow, cone-shaped muscular organ that serves as the blood circulatory pump for the body. It is located in the thoracic cavity medial to the lungs and behind the sternum. The heart has four chambers: the right atrium, left atrium, right ventricle, and left ventricle. The atria act as receiving chambers for blood and pass blood through one-way valves to the ventricles. They are the pumping chambers that carry blood through arteries to the rest of the body. To prevent blood from flowing backwards or regurgitating back into the heart, a system of four one-way valves is present in the heart: atrioventricular valves (tricuspid, mitral) and semilunar valves (pulmonary, aortic). We briefly cover the structural and functional anatomy of the heart below.

2.1.1 Pericardium and Heart Wall

The heart sits within a fluid-filled sac-like membrane known as the pericardium, as shown in Fig. 2.1. The pericardium is a type of two-layer membrane that produces fluid to lubricate the heart and prevent friction between the beating heart and the surrounding organs. The two layers of the pericardium are the outer fibrotic layer and the inner, serous layer, which, in turn, consists of parietal and inner visceral layers [1]. The fibrous parietal pericardium envelopes the heart and attaches to the great vessels and to the delicate parietal layer of the serous layer. The inner visceral layer of the serous pericardium forms the outer

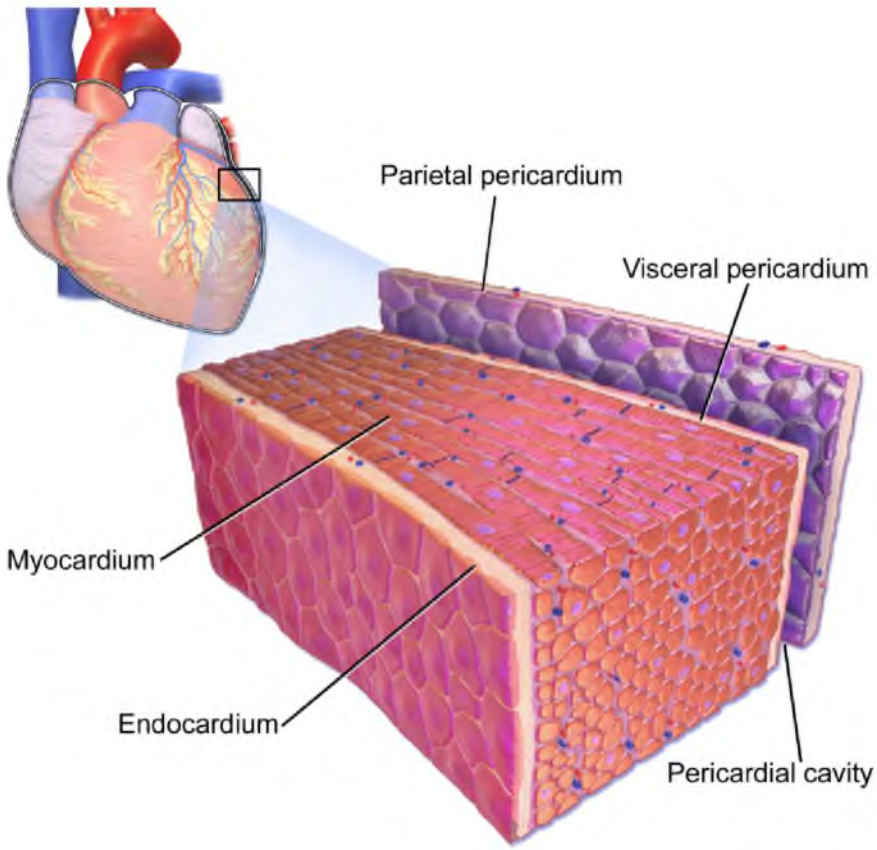

Fig. 2.1. Structure of heart wall. Reprinted with permission from Wikimedia and Bruce Blausen. Retrieved from `http://commons.wikimedia.org`. Used under creative commons attribution-noncommercial-sharealike 3.0 generic license (`http://creativecommons.org/`).

lining of the heart and great vessels. Besides lubrication, the pericardium also serves to hold the heart in position and maintain a hollow space for the heart to expand into when it is full. The heart wall contains three loosely defined concentric regions: the epicardium, midmyocardium, and endocardium. The epicardium is the outermost layer of the heart and is just another name for the visceral pericardium [1]. The myocardium is the muscular middle layer of the heart and makes up the majority of the thickness and the mass of the heart wall. The endocardium forms the inner lining of the heart.

2.1.2 Cardiac Cell Types

The heart is composed of different types of cells including epicardial cells, working cardiomyocytes, smooth muscle cells, cardiac fibroblasts, endothelial cells, pacemaker cells, Purkinje fibers, and the other elements of the conduction system [13], as shown in Fig. 2.2.

All these cell types play a role in the structural, biochemical, and electrical functioning

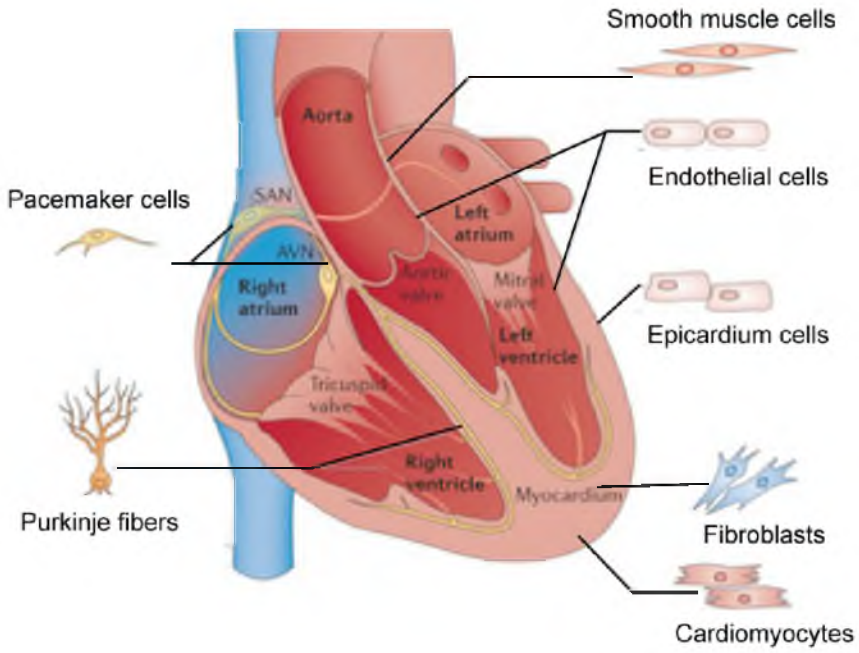

Fig. 2.2. Cardiac cell types. Reprinted with permission from Nature Publishing Group. M. Xin, E. Olson, and R. Bassel-Duby, "Mending broken hearts: Cardiac development as a basis for adult heart regeneration and repair," *Nature Reviews Molecular Cell Biology*, vol. 14, pp. 529-541, 2013.

of the heart. The epicardium is derived from a cluster of mesothelial cells, called the proepicardium [1]. The proepicardium gives rise not only to the epicardium but also to epicardium-derived cells: smooth muscle cells, cardiac fibroblasts, and possibly endothelial cells [13]. The myocardium is composed of cardiomyocytes, which are the cells that generate contractile force in the heart required for pumping blood. The atrial and ventricular myocytes are rod shaped and contain a large amount of contractile proteins, organized in clearly periodic myofibrils, a large number of mitochondria, and glycogen deposits [14]. Smooth muscle cells contribute to the formation of coronary arteries, as well as the inflow and outflow vasculature [13]. Cardiac fibroblasts play an important role in maintaing normal cardiac function (e.g., synthesis and deposition of extracellular matrix, cell-cell communication with cardiomyocytes), as well as in cardiac remodeling during pathological conditions such as myocardial infarction [15]. Endothelial cells line the endocardial region, the interior lining of the blood vessels, and cardiac valves [13]. Pacemaker cells (SA and AV nodal cells) and Purkinje fibers are specialized cardiac cells that form the electrical conduction system in the heart. The SA and AV nodal cells are small and generally spindle

shaped with little contractile material (myofibrils) but a high density of mitochondria. Moreover, in lieu of a less-developed T-tubule system, they have many caveolae that contain a high density of receptor and channel proteins [16]. The Purkinje cells are similar in shape to contractile myocytes but are larger, have less contractile material, and contain a high concentration of glycogen deposits [14]. The pacemaker cells generate and conduct electrical impulses but due to the lack of contractile machinery do not contract like the atrial and ventricular cardiomyocytes.

2.1.3 Cardiac Chambers

The cardiac chambers are shown in Fig. 2.3. The right atrium (RA) is the first cardiac structure to receive blood returning from the body. It has a prominent internal muscle ridge, the crista terminals, which is nonconductive and separates the right atrial free wall into a smooth-walled posterior region that receives the venae cavae and coronary sinus [1]. There is also a muscular anterior region lined by parallel pectinate muscles and from which

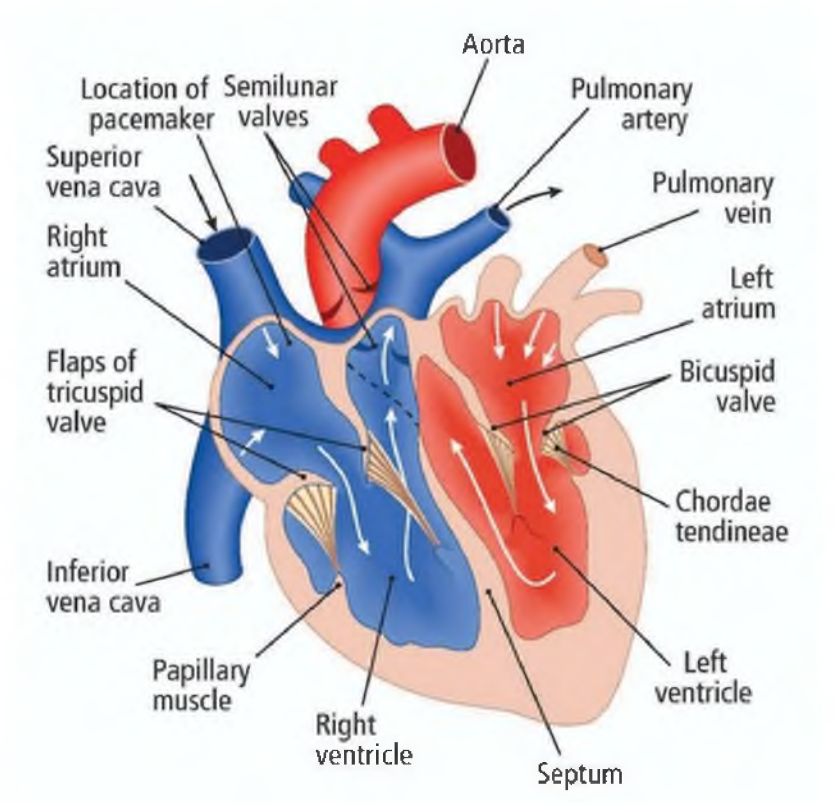

Fig. 2.3. Cardiac chambers. Reprinted with permission from leavingcertbiology.net (John Loughlin). Retrieved from `http://leavingcertbiology.net`, 2015.

the right atrial appendage emanates. The right atrial appendage abuts the right aortic sinus and overlies the right coronary artery [1].

The atrial septum (AS) divides the right and left atrial chambers. It is composed of interatrial and atrioventricular regions. The interatrial portion is highlighted by the fossa ovalis [1]. During the fetal development of the heart, the fossa ovalis is known as the foramen ovale and serves as an opening between the right and left atria, allowing blood to pass from the right to left atrium and into the left ventricle, effectively bypassing the lungs [1]. After birth, the opening closes as the blood flow shifts through the right ventricle into the lungs and enters the left atrium by way of pulmonary veins. The atrioventricular (AV) portion of the atrial septum is made up of major muscular and minor membranous components and separates the right atrium from the left ventricle. It corresponds roughly to the "triangle of Koch," which contains the AV node and the proximal portion of the AV (His) bundle [1].

The left atrium (LA) usually receives four pulmonary veins that connect to the posterior wall of the chamber. The atrial appendage arises anterolaterally and lies atop the proximal portion of the left circumflex coronary artery [1]. The left atrial appendage is smaller, more tortuous, and less pyramidal than its right atrial counter part and is often multilobed [1]. In contrast to the right atrial free wall, the left has no crista terminals and no pectinate muscles outside its appendage. The coronary sinus travels along the posterior wall of the left atrium.

The right ventricle (RV) receives blood from the right atrium. It is composed of an inlet and trabecular and outflow segments [1]. The inlet component extends from the tricuspid annulus to the insertions of the papillary muscles. An apical trabecular zone extends inferiorly beyond the attachments of the papillary muscles toward the ventricular apex [1]. The outflow portion, also known as the conus or the infundibulum, is a smooth-walled muscular subpulmonary channel. A prominent arch-shaped muscular ridge known as the *crista supraventricularis* separates the tricuspid and pulmonary valves and is made up of four distinct components: parietal band, infundibular septum, septal band, and the moderator band [1]. These components encircle the main region of the right ventricle.

The left ventricle (LV) is the largest and the strongest chamber of the heart and like the right ventricle is made of an inlet portion composed of the mitral valve apparatus, a subaortic outflow portion, and a finely trabeculated apical zone [1]. The upper aspect of the ventricle, the area where the mitral and aortic valves are located, is referred to as the base of the chamber. At the far end of the chamber is the ventricular apex. The LV free wall is thickest towards the base and thinnest towards the apex. The LV free wall is nearly

three times thicker than the right ventricular free wall [1]. The LV apex shows much less trabeculation than its counterpart on the right. LV false tendons are discrete, thin, cordlike fibromuscular structures that connect two walls, the two papillary muscles, or a papillary muscle to a wall, usually the ventricular septum [1].

The ventricular septum (VS) is a complex intracardiac partition separating the left and right ventricles. It is slanted backwards and to the right, and it also curves to the right following the course of an inverted S (moving from apex to aortic valve) [1]. The VS can also be divided into muscular and membranous portions. The upper portion, which separates the aortic vestibule from the lower part of the right atrium and the upper part of the right ventricle, is much thinner and fibrous and is termed the membranous VS [1]. The greater part of the VS is thick and muscular and constitutes the muscular VS. The basal half of the VS is smooth-walled, whereas the apical half is characterized by numerous small and irregularly arranged trabeculation [1].

2.1.4 Cardiac Skeleton and Cardiac Valves

The cardiac valves are anchored to their annuli or valve rings. These fibrous rings, at the base of the heart, join to form the fibrous skeleton of the heart. The centrally located aortic valve forms the cornerstone of the cardiac skeleton, and its fibrous extensions abut each of the other three valves. The four rings are mutually supported and held together by the right and left fibrous tissues and by the conus tendon [1]. From the right side of the aortic ring, the membranous portion of the interventricular septum extends downward to meet the muscular portion of the septum. The central fibrous body joins the aortic, mitral, and tricuspid valve annuli [1]. The aortic and pulmonary valve rings are joined together by a stout band of fibrous tissue, the tendon of the conus [1]. Other than the atrioventricular Bundle of His, the fibrous cardiac skeleton serves to electrically isolate the atria from the ventricles.

The tricuspid valve allows the blood to flow from the right atrium into the right ventricle. It is so called because it is made of three cusps (leaflets) that separate to allow the blood to pass through and connect to block regurgitation of blood. The tricuspid valve is composed of five components, i.e., annulus, leaflets, commissures, chordae tendinae, and papillary muscles [1]. The anterior tricuspid leaflet is the largest and most mobile. The posterior leaflet is usually the smallest. The septal leaflet is the least mobile because of its many direct chordal attachments to the ventricular septum [1]. The commissures are cleftlike splits in the leaflet tissue that represent the sites of separation of the leaflets, as shown in Fig. 2.4. The tricuspid valve is attached on the ventricular side to tough strings called

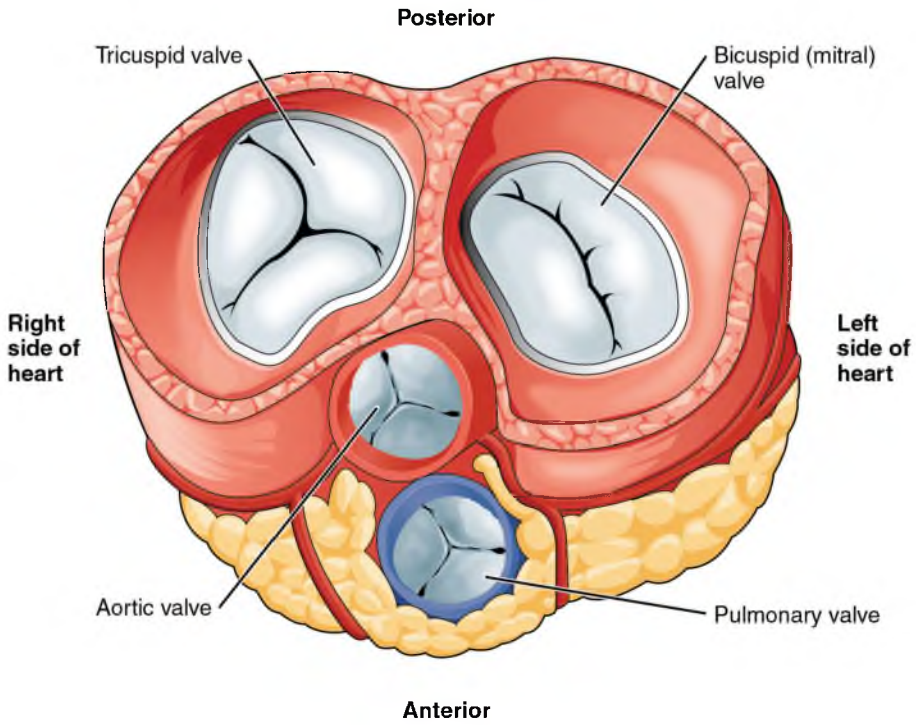

Fig. 2.4. The four cardiac chamber valves including tricuspid valve, bicuspid valve, aortic valve, and pulmonary valve. Reprinted with permission from Wikimedia and OpenStax College. Retrieved from `http://commons.wikimedia.org`. Used under creative commons attribution-noncommercial-sharealike 3.0 generic license (`http://creativecommons.org/`).

the chordae tendinae. The chordae tendinae anchor and support the leaflets and keep them from folding backwards (prolapse) and allowing blood to regurgitate past them. The chordae tendinae are attached to papillary muscles, which are fingerlike projections arising from the ventricular wall. Papillary muscle contraction pulls the leaflets toward one another and thereby promotes valve closure [1].

The mitral valve allows blood to flow from the left atrium into the left ventricle. It is composed of the same five components as the tricuspid valve. Unlike the other cardiac valves, the mitral valve has only two leaflets. The anterior leaflet is large and semicircular. The posterior mitral leaflet is rectangular and usually divided into three scallops [1].

The aortic valve prevents blood from regurgitating back into the left ventricle. It is composed of three components: annulus, cusps or leaflets, and commissures. In contrast to the mitral and tricuspid valves, the aortic valve has no tensor apparatus (i.e., chordae tendinae or papillary muscles) [1]. The commissures form tall, peaked spaces between the attachment of adjacent cusps. The three half-moon shaped (semilunar) aortic cusps — left, right, and posterior — form pocketlike tissue flaps that are avascular [1]. The pulmonary

valve prevents the back flow of blood from the pulmonary trunk into the right ventricle.

2.1.5 Coronary Arteries and Veins

The patterns of coronary distribution are highly variable and as such the correlations between coronary vessel architecture and the regions of the heart they supply are not precise [1]. The right and left coronary arteries arise from the right and left aortic sinuses, respectively. The right coronary artery (RCA) arises nearly perpendicular from the aorta and is embedded in the adipose tissue throughout its course within the right atrioventricular groove, as shown in Fig. 2.5.

The first branch of the RCA is typically the conus artery, which supplies the right ventricular outflow tract and forms an important collateral anastomosis, just below the pulmonary valve, with an analogous branch from the left anterior descending coronary artery (LAD) [1]. Among the numerous marginal branches of the RCA that supply the remainder of the RV wall, the largest branch travels along the acute margin from base to apex. The posterior descending and distal posterolateral branches of what is known as a "dominant" RCA supply the basal and middle inferior wall, basal inferior septum, right bundle branch, AV node, AV bundle, posterior portion of the left bundle branch, and

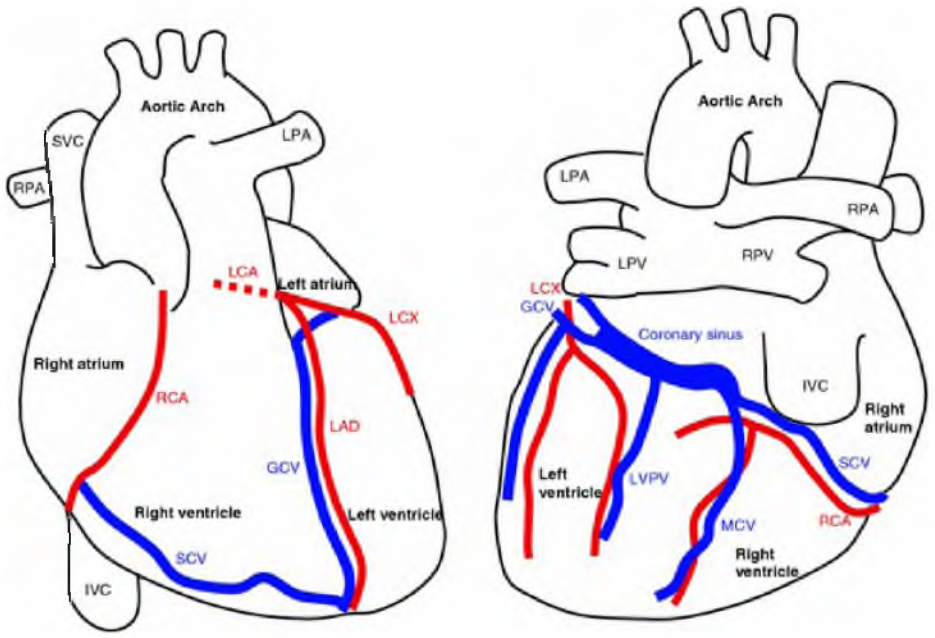

Fig. 2.5. Coronary arteries and veins. Reprinted with permission from Springer. J. Lee and N. Smith, "The multi-scale modeling of coronary blood flow," *Annals of Biomedical Engineering*, vol. 40(11), pp. 2399-2413, 2012.

posteromedial mitral papillary muscle [1].

The left main coronary artery (LCA) travels a very short distance along the epicardium between the pulmonary trunk and left atrium before dividing into the anterior descending and circumflex arteries. The LAD courses within the epicardial fat of the anterior interventricular groove and travels a variable distance along the inferior interventricular groove toward the cardiac base [1]. Its septal perforating branches supply the anterior septum and apical septum. The epicardial diagonal branches of the LAD supply the anterior LV free wall, part of the anterolateral mitral papillary muscle, and the medial one-third of the anterior RV free wall [1]. The left circumflex coronary artery (LCX) courses within the adipose tissue of the left atrioventricular groove and commonly terminates just beyond its large obtuse marginal branch. It supplies the lateral LV free wall and a portion of the anterolateral mitral papillary muscle [1].

The coronary veins typically run parallel to the entire course of the coronary arteries. The coronary venous circulation is composed of the coronary sinus, cardiac veins, and thespian venous systems. The great cardiac vein travels in the anterior interventricular groove beside the LAD and in the left anterior interventricular groove beside the LCX [1]. The great cardiac vein and other cardiac veins, such as the left posterior and middle cardiac veins, drain into the coronary sinus, which courses along the posteroinferior aspect of the left atrioventricular groove and empties into the right atrium [1].

Collateral channels provide blood flow between the major coronary arteries and their branches. If stenosis of an epicardial coronary artery produces a pressure gradient across such a vessel, the collateral channel can dilate with time and provide a bypass avenue for blood flow beyond the obstruction. Such functional collaterals can develop between the terminal extensions of two coronary arteries, between the side branches of two arteries, between branches of the same artery, or within the same branch [1]. These collaterals are common in the ventricular septum, ventricular apex, anterior RV free wall, anterolateral LV free wall, and along the atrial surfaces [1].

The microcirculation is composed of arterioles (10–150 μm in diameter), capillaries (0.5–0.8 μm), and venules (10–40 μm). The independent vasoactivity of different-sized arterioles affects the flow of blood to the tissue locally [1]. The flow of blood through the arterioles is usually rapid, continuous, and unidirectional, whereas capillary flow can be highly variable. Oxygen and nutrients diffuse through the capillaries into surrounding tissues, whereas venules are involved in the transvascular exchange of fluid and macromolecules [1]. The veins collect blood that is eventually returned to the heart.

2.1.6 Electrical Conduction System

The cardiac conduction system consists of the sinus node, internodal tracts, AV node, AV (His) bundle, and the right and left bundle branches, as shown in Fig. 2.6. The sinus node is located subepicardially in the terminal groove, close to the junction between the superior vena cava and right atrium, whereas the AV node is a subendocardial structure that is located within the triangle of Koch [1]. The AV (His) bundle arises from the distal portion of the AV node and travels along the ventricular septum. The right bundle branch emanates from the distal portion of the AV bundle and forms a cordlike structure that travels towards the anterior tricuspid papillary muscle. The left bundle branch represents a broad fenestrated sheet of subendocardial conduction fibers that spread along the septal surface of the left ventricle [1].

2.1.7 Comparative Cardiac Anatomy

As most mechanistic research studies depend on animal models of healthy and diseased organs, it is critical to appreciate variations in structure and function between humans and the typical animal species. All mammals (including dogs, pigs, and sheep) have principally

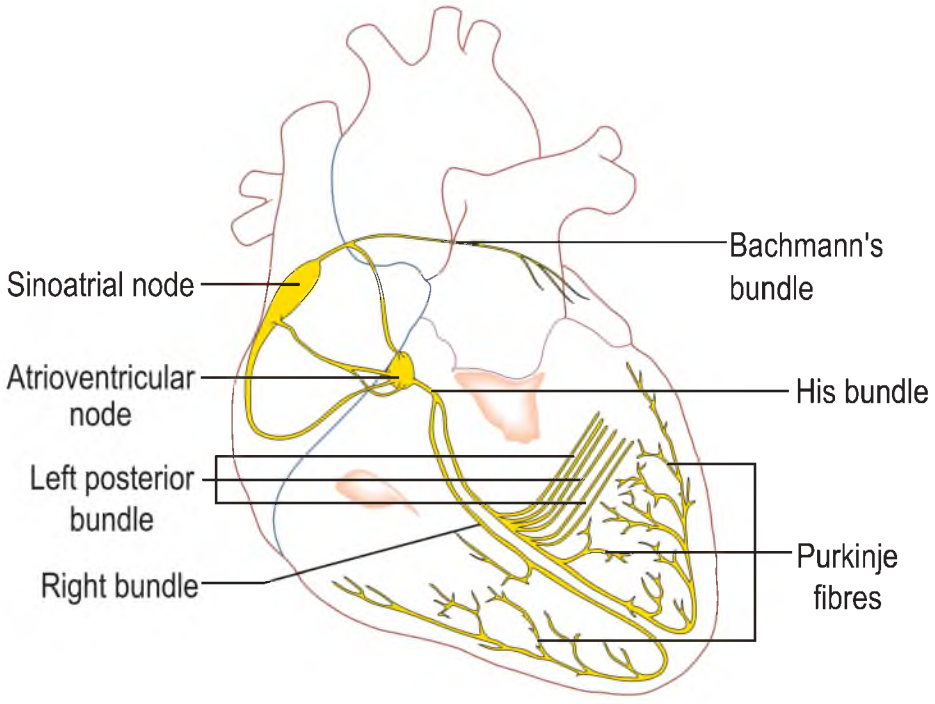

Fig. 2.6. Cardiac conduction. Reprinted with permission from Wikimedia and Madhero. Retrieved from `http://commons.wikimedia.org`. Used under creative commons attribution-noncommercial-sharealike 3.0 generic license (`http://creativecommons.org/`).

the same atrial and ventricular architecture. However, they do not have the same degree of trabeculation, which is coarser compared to adult human hearts [17]. Differences in aortic valve anatomy have also been reported in the literature relative to the shape of the leaflets [17]. Additional differences exist with respect to coronary structure and perfusion. Dogs and sheep typically have a left coronary type of supply, such that the majority of the myocardium is supplied via branches arising from the LCA. In contrasts, pigs and humans typically have a coronary supply balanced between the LCA and the RCA, and in some cases even a supply dominated by the RCA [18]. In addition, human and pig hearts have only a sparse coronary collateral network located subendocardially. In contrast, an extensive collateral network located near the epicardial surface can be seen in dogs [19]. However, with CAD and over time, collateral vessels become prevalent in humans [20]. All mammalian hearts have a similar conduction system except for differences in the transmural penetration of the Purkinje network between pigs and other species (e.g., dog and human). All Purkinje system fibers originate in subendocardium, but in pigs they penetrate more deeply than in other species and thus alter the time of activation in different depths of the ventricles [21].

2.2 Cardiac Electrophysiology

The heart can be construed as mechanical pump driven by an internal electrical system that generates the power and determines the timing necessary for the heart to eject blood effectively. Myocytes represent the functional unit of this system, and collectively myocytes form tissues that behave as an electrical syncytium [14]. In this section, we explore the basic mechanisms behind the electrical activity of the cardiomyocytes including action potentials, excitation-contraction coupling, cardiac excitation, repolarization, and automaticity.

2.2.1 Cardiomyocyte

The working myocytes of the atria and ventricles are roughly rectangular in shape, 50–200 μm long and 10–40 μm wide; they generate force only along the long axis [22]. Individual cells often bifurcate, with the result that a single cell may connect with more than one neighboring cell. Myocytes contain a specialized cisternal system, the sarcoplasmic reticulum (SR), in which Ca^{++} is actively accumulated by ATP-driven transport. Most of the internal volume is devoted to a cytoskeletal lattice of contractile proteins that gives rise to a striated appearance. The contractile proteins are organized into sarcomeres, which are contractile functional units, bordered on each end by a protein matrix known as the "Z line," as shown in Fig. 2.7.

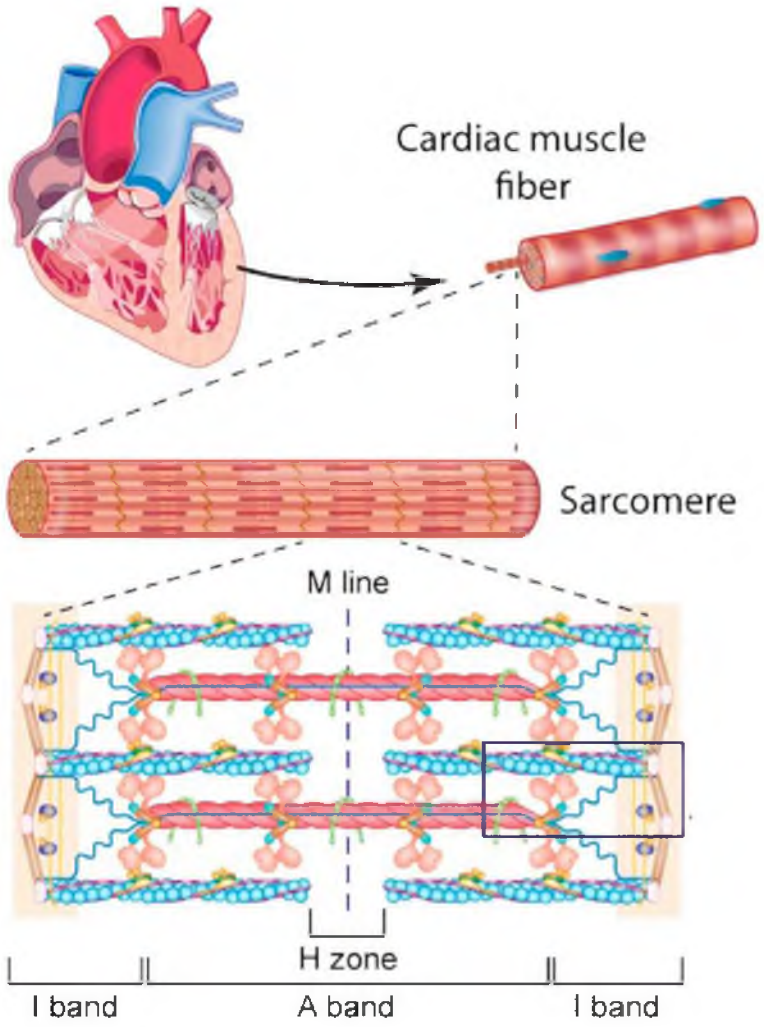

Fig. 2.7. Cardiomyocte. Reprinted with permission from American Society for Biochemistry and Molecular Biology. Y. Peng, Z. Gregorich, S. Valeja, H. Zhang, W. Cai, Y. Chen, et al., "Top-down proteomics reveals concerted reductions in myofilament and Z-disc protein phosphorylation after acute myocardial infarction," *Molecular Cell Proteomics*, vol. 13(10), pp. 2752-2764, 2014.

The Z lines are primarily composed of the protein a-actinin. Within each sarcomere, there is an interdigitating lattice of thick and thin protein filaments. The thin filaments extend from the Z line for about 1 μm toward the center of the sarcomere and are polymeric assemblies of globular subunits of protein actin [22]. The thick filaments are bipolar assemblies of the protein myosin.

Myosin molecules have long α helical tails that form the backbone of thick filaments, and each has two globular head domains, which possess the ability to form cross-bridges with

the actin filaments. Upon binding with actin, the cross-bridges act as molecular motors responsible for contraction [22]. The region of the sarcomere in which the myosin filaments reside is known as the "A band." The area between the A bands of adjacent sarcomeres is known as the "I band." This area is bisected by the Z lines and is traversed by actin thin filaments that extend from the Z line toward the center of both sarcomeres [22]. The thin actin filaments also carry regulatory proteins tropomyosin and troponin. Tropomyosin is a double-stranded, α helical, coiled-coil protein that spans seven actin monomers [22]. Troponin is a globular protein complex with three subunits: 1) TnC, a calcium binding subunit, 2) TnI, a subunit that inhibits muscle contraction, and 3) TnT, a subunit that connects the troponin complex to tropomyosin and actin [22]. Tropomyosin molecules are aligned end to end around the helical coil of the thin filament with the troponin complex attached to each tropomyosin molecule.

In relaxed muscle, tropomyosin binds to actin and impedes the binding of myosin heads to actin binding sites. However, on muscle activation and subsequent increase in myoplasmic calcium concentrations, free calcium binds to troponin, inducing a conformational change that is transmitted to tropomyosin. It shifts the position on the actin thin filament to reveal the site on actin required for strong myosin binding. Myosin can then bind to the thin filament in a manner conducive to force production.

Force production occurs as follows. First, during muscle relaxation, myosin can bind to ATP and hydrolyze it, but cannot use the energy released during hydrolysis to create force because of the inhibition of its binding to the thin filament by tropomyosin and troponin [22]. Next, after calcium binding to troponin has released the inhibition of the tropomyosin-troponin complex on the thin filament, an energized myosin crossbridge can attach to the thin filament. This association with actin catalyzes the release of the products of hydrolysis (ADP and inorganic phosphate) and a concomitant conformational change of myosin head occurs while it is bound to actin [22]. This conformational change pulls the actin thin filament past the thick filament. Once this is completed, myosin can rebind ATP, which reduces the affinity of myosin for actin and allows for crossbridge detachment. The subsequent hydrolysis of ATP in turn reenergizes the myosin crossbridge and prepares it for the next force generating cycle. As long as the calcium concentration is high enough to keep tropomyosin-troponin complexes from blocking the myosin binding sites on actin, the cycle continues [22].

There is a direct connection between the overlap of thick and thin filaments and the resultant force developed by cardiac muscle cells. Sarcomere length is defined as the distance

between Z lines. In general, maximal isometric force can be elicited when this distance is approximately 2.2 μm [22]. Force generation is decreased when the sarcomere length is reduced as the contractile proteins are too crowded to work optimally. Likewise, force is reduced if the sarcomere length is increased because of the decrease in the overlap of thick and thin filaments, reducing the potential for possible crossbridge formation. This association between myocyte length and amount of force that can be generated is called the length-tension relationship and plays an important role across scales to explain the response of the heart to changes in ventricular filling [22].

Sarcomeres are linked end to end into assemblies known as myofibrils, which run the length of the long axis of the cardiac cell and are also placed side to side to fill most of the internal volume of the cell. The nucleus is found on the periphery of the cell along with the sarcoplasmic reticulum (SR), which is a vesicular structure that acts as an internal calcium store [22].

Cardiac cells are connected and communicate with one another by junctions of two types. First, intercalated discs form strong mechanical bonds between myocytes that allow force to be transmitted across the myocardium. These structures are formed by the protein-protein associations at the membrane surface of the neighboring cells [22]. Second, gap junctions form an electrical connection between the cardiac cells. They provide direct electrical and chemical communication between the cytoplasmic spaces of the adjoining cells. The electrical communication facilitates the coordinated contractions of the cardiac muscle [22].

2.2.2 Cardiac Cell Membrane

While contraction occurs mostly inside a cardiac myocyte, the electrical function of that cell is largely determined by the membrane that surrounds it, hence the overwhelming focus in electrophysiology on membrane structure and function. The plasma membrane defines the exterior of the cell and controls the movement of molecules between the cytosol and the extracellular medium. It also facilitates cell-to-cell signaling and cell adhesion [22]. The basic structural component of the cell membranes is a phospholipid bilayer, formed by molecules in opposing orientation that contain a hydrophilic head and a hydrophobic tail, as shown in Fig. 2.8.

The hydrocarbon chains of the phospholipids in each layer form a hydrophobic core within a lipid bilayer that has two important properties: 1) The hydrophobic core is an impermeable barrier that prevents diffusion of water soluble solutes across the membrane. Moreover, this simple barrier is modulated by the presence of membrane proteins that mediate transport of specific molecules across this otherwise impermeable bilayer [22]. 2)

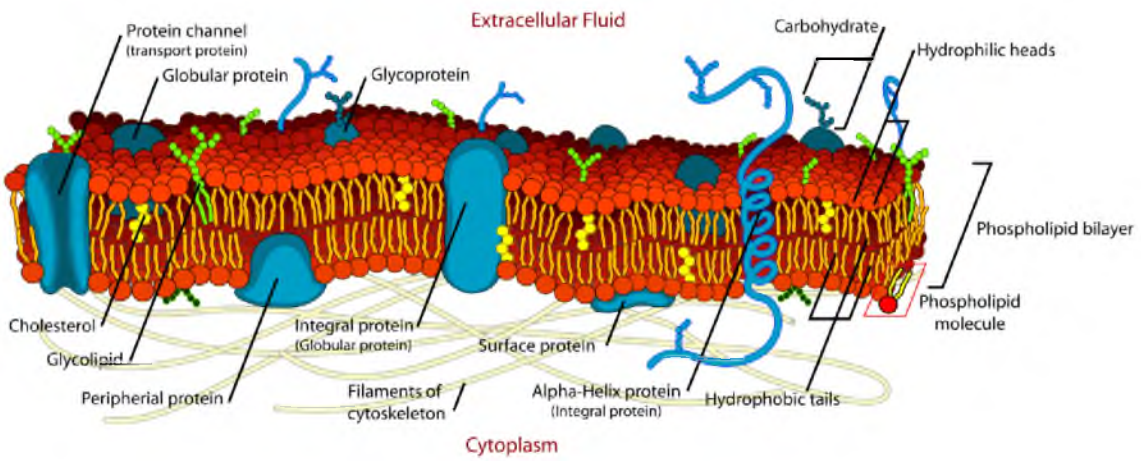

Fig. 2.8. Plasma membrane structure and function. Reprinted with permission from Wikimedia and Mariana Ruiz (LadyofHats). Retrieved from `http://commons.wikimedia.org`. Used under creative commons attribution-noncommercial-sharealike 3.0 generic license (`http://creativecommons.org/`).

The bilayer is stable. The bilayer structure is maintained by hydrophobic van der Waals interactions between lipid chains. Even though the exterior aqueous environment can vary widely in ionic strength and pH, the bilayer has the strength to retain its characteristic architecture [22]. A typical biomembrane is assembled from phosphoglycerides (at high concentrations in cardiac cells), sphingolipids, and steroids (Cholesterol). All three classes of lipids are amphiphatic molecules with a polar head and hydrophobic tail [22]. Natural biomembranes have fluidlike consistency, which is decreased by sphingolipids and cholesterol and increased by phosphoglycerides [22].

The sarcolemma forms multiple invaginations perpendicular to the long cell axis, named "T-tubules," which serve as extensions of the cell surface and host a large density of transport proteins. The T-tubules are well developed in ventricular myocytes but poorly so in atrial myocytes [14]. The cell membrane usually contains both integral (transmembrane) and peripheral membrane proteins, which do not enter the hydrophobic core of the bilayer. Most integral proteins contain membrane-spanning hydrophobic α helices and hydrophilic domains that extend from the cytosolic and exoplasmic faces of the membrane [22]. The binding of a water soluble enzyme (e.g., phospholipase, kinase or phosphatase) to a membrane surface brings the enzyme close to its substrate and in some cases activates the substrate. Such interfacial binding is due to the attraction between positive charges on basic residues in the protein and negative charges on phospholipid head groups in the

bilayer [22].

The selective permeability of the plasma membrane allows the cell to maintain a constant internal environment. The cell membrane is permeable to gases, small hydrophobic molecules, and small uncharged polar molecules via passive diffusion. It is slightly permeable to water due to specialized aquaporins embedded in the membrane and urea, and essentially impermeable to ions and to large polar molecules [23]. Thus, the cell membrane, due to its ability to keep ions separated across its phospholipid bilayer, functions as an electrical capacitor. The specific capacitance is approximately constant across all cell membranes at $1\mu\text{F}/cm^2$ [14, 22].

The transport of most molecules into and out of cells requires the assistance of specialized transport proteins (transmembrane proteins) including ATP powered pumps, channel proteins, and transporters. ATP powered pumps are ATPases that use energy to move ions or small molecules across the membrane against a chemical gradient, electrical gradient, or both [22]. This process is referred to as active transport. Channel proteins form a hydrophilic passageway and transport water or specific types of ions and hydrophilic small molecules down their concentration or electrical gradient [24]. Such protein-assisted transport is referred to as facilitated diffusion. Some ion channels are nongated (open much of the time), but most are open only in response to specific chemical or electrical signals (gated). Transporters (carriers) move a wide variety of ions and molecules across cell membranes. Three types of transporters have been identified: uniporters, antiporters, and symporters [22]. Uniporters transport a single type of molecule down its concentration gradient via facilitated diffusion (e.g., glucose, amino acids). In contrast, antiporters and symporters couple the movement of one type of ion or molecule against its concentration gradient with the movement of one or more different ions down its concentration gradient [22]. These proteins, often called cotransporters, transport two solutes simultaneously using energy stored in the electrochemical gradient. This latter process is sometimes called the secondary active process [22].

2.2.3 Resting Potential

The movement of ions across membranes is influenced by two energetic factors: chemical gradient and electrical gradient. Consider a two-compartment system, with both compartments containing KCl, but in compartment 1 at a higher concentration. If the membrane allowed K^+ and Cl^- ions to cross, they would diffuse from compartment 1 to compartment 2. If, however, the membrane were permeable only to K^+, it would tend to diffuse from compartment 1 to 2, but Cl^- ions would be left behind. As soon as this happens, there

will be a net transfer of positive charge from compartment 1 to 2 (carried by K^+ ions), and consequently compartment 2 will become electrically positive with respect to compartment 1. The resulting electrical gradient will push K^+ ions from compartment 2 to compartment 1. Very quickly an equilibrium will be established where the electric gradient will be just large enough to move K^+ ions to the left at the same rate as they tend to diffuse to the right due to the concentration gradient. The potential at which the electrical gradient and the concentration gradient balance each other is called the equilibrium potential or the Nernst potential for that specific ion. In this instance, the membrane potential is equal to potassium equilibrium potential, because only K^+ ions can cross the membrane and thus influence the electrical gradient. The Nernst potential for a specific ion is given by

$$E = \frac{RT}{zF} ln \left(\frac{[C]_o}{[C]_i} \right), \tag{2.1}$$

where R is the universal gas constant, T is the absolute temperature, z is the valance, i.e., the charge of the ion, F is the Faraday constant, $[C]_o$ is the concentration of ions outside the cell, and $[C]_i$ is the concentration of ions inside the cell.

The resting membrane potential of a cell is the voltage difference between the interior and exterior of the cell under resting conditions. It is calculated as a weighted average of the equilibrium potentials of the individual ions. The size of each weight is the relative permeability (P_i) of each ion and the result is given by the Goldman-Hodgkin-Katz equation.

$$E_m = \frac{RT}{F} ln \left(\frac{\Sigma_i^N P_{M_i^+} [M_i^+]_{out} + \Sigma_i^N P_{A_i^-} [A_i^-]_{in}}{\Sigma_i^N P_{M_i^+} [M_i^+]_{in} + \Sigma_i^N P_{A_i^-} [A_i^-]_{out}} \right). \tag{2.2}$$

Neutral ions do not contribute to the membrane potential. In a cardiomyocyte, four ions—potassium (K), sodium (Na), calcium (Ca), and chloride (Cl)—contribute to the membrane potential, as shown in Fig. 2.9. Thus, the resting potential is given by

$$E_m = \frac{P_{K^+}}{P_{total}} E_{K^+} + \frac{P_{Na^+}}{P_{total}} E_{Na^+} + \frac{P_{Ca^{++}}}{P_{total}} E_{Ca^{++}} + \frac{P_{Cl^-}}{P_{total}} E_{Cl^-}. \tag{2.3}$$

A central concept in cellular electrophysiology is that of "driving force," a measure of the potential energy for a particular ion. Driving force describes the impetus for an ion to move across the cell. The driving force for an ion increases or decreases depending upon how

A) Major Ions in a Cardiac Cell

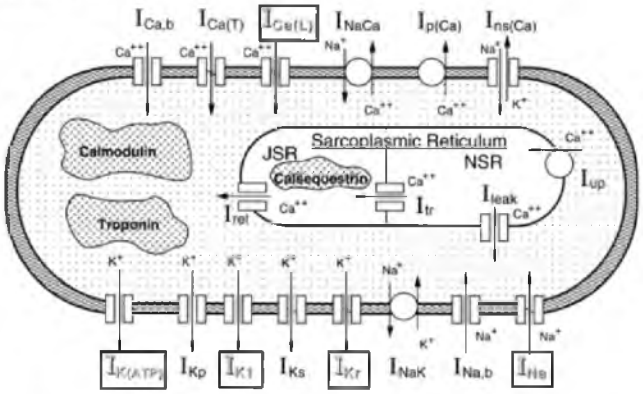

B) Ion Concentrations & Equilibrium Potentials

Ion	Intracellular concentration (mEq/L)	Extracellular concentration (mEq/L)	Equilibrium potential (mV)
Na^+	15	140	70
K^+	135	4	−94
Ca^{2+}	2×10^{-4}	4	132
Mg^{2+}	40	2	
Cl^-	4	120	−90
HCO_3^-	10	24	
HPO_4^{2-}	20	4	
SO_4^{2-}	4	1	
Proteins$^-$, Amino acids$^-$, Urea, etc.	152	1	

Fig. 2.9. Cardiac cell ions: (a) Cardiac cell model, (b) ionic concentrations of the major ions and the corresponding equilibrium potentials. Reprinted with permission from Circulation Research. R. Shaw and Y. Rudy, "Electrophysiologic effects of acute myocardial ischemia," *Circulation Research*, vol. 35, pp. 256-272, 1997.

close its equilibrium potential is to the membrane potential and is given by the equation

$$V_D = V_m - V_{eq}, \tag{2.4}$$

where V_m is the membrane potential and V_{eq} is the equilibrium potential.

At rest, the membrane potential of a cardiomyocyte is close to E_{K^+} (-94 mV), as potassium has the highest permeability compared to other ions. The equilibrium potential for Na^+, is +70 mV, for Ca^{++}, it is +132 mV and for Cl^- it is -90 mV [25]. The resulting cardiac membrane potential is approximately -85 mV. Thus, the driving force for K^+ (9 mV) is smaller than that for Cl^- (5 mV), which in turn is much smaller than the driving force

for Na^+ (-160 mV), which is smaller than that for Ca^{++} (-222 mV). The sign indicates the direction of the driving force. Outward (-) and inward (+). The resulting current due to a specific ion is given by Ohm's law

$$I_{ion} = \frac{V_m - V_{eq}}{R_m}, \tag{2.5}$$

where R_m is the membrane resistance. One consequence of this behavior is that if the membrane is not permeable to the ion, there will be no ionic current generated regardless of the driving force.

2.2.4 Action Potential

Action potentials (AP) are the result of transient changes in the cellular permeability to sodium, calcium, and potassium—charged ions capable of facilitated diffusion through ion channels. A brief increase in Na^+ permeability depolarizes the cell and drives the membrane potential toward the Na^+ equilibrium potential, which activates the voltage-gated calcium and potassium channels. The subsequent opening of calcium channels allows calcium to enter the myocyte and sustain the depolarized state. The opening of potassium channels allows potassium efflux from the cell and thus drives the membrane potential back toward the potassium equilibrium potential. The timing of these changes depends on isoforms of channel proteins present in each cell. For example, the most numerous ventricular myocytes, have durations of approximately 250 milliseconds, whereas sinoatrial and atrial muscle action potentials last approximately 150 milliseconds and Purkinje cells about 300 milliseconds.

Another morphological feature of action potentials that differs across cell types and has direct impact on macroscopic tissue behavior is the rate of rise, also known as "Phase 0" of the action potential. Atrial and ventricular muscle and Purkinje cells have an extremely rapid Phase 0, as shown in Fig. 2.10. As a result, they also conduct excitation more rapidly than other myocyte types.

Before discussing additional specific mechanisms and features, we outline the nomenclature and descriptions of the phases of the action potential:

- **Phase 0:** Phase 0 is supported by activation of two inward (depolarizing) currents, I_{Na} and I_{CaL}. Membrane depolarization rapidly activates these channels and with a delay of several milliseconds for I_{Na} and tens of milliseconds for I_{CaL} inactivates them [14].

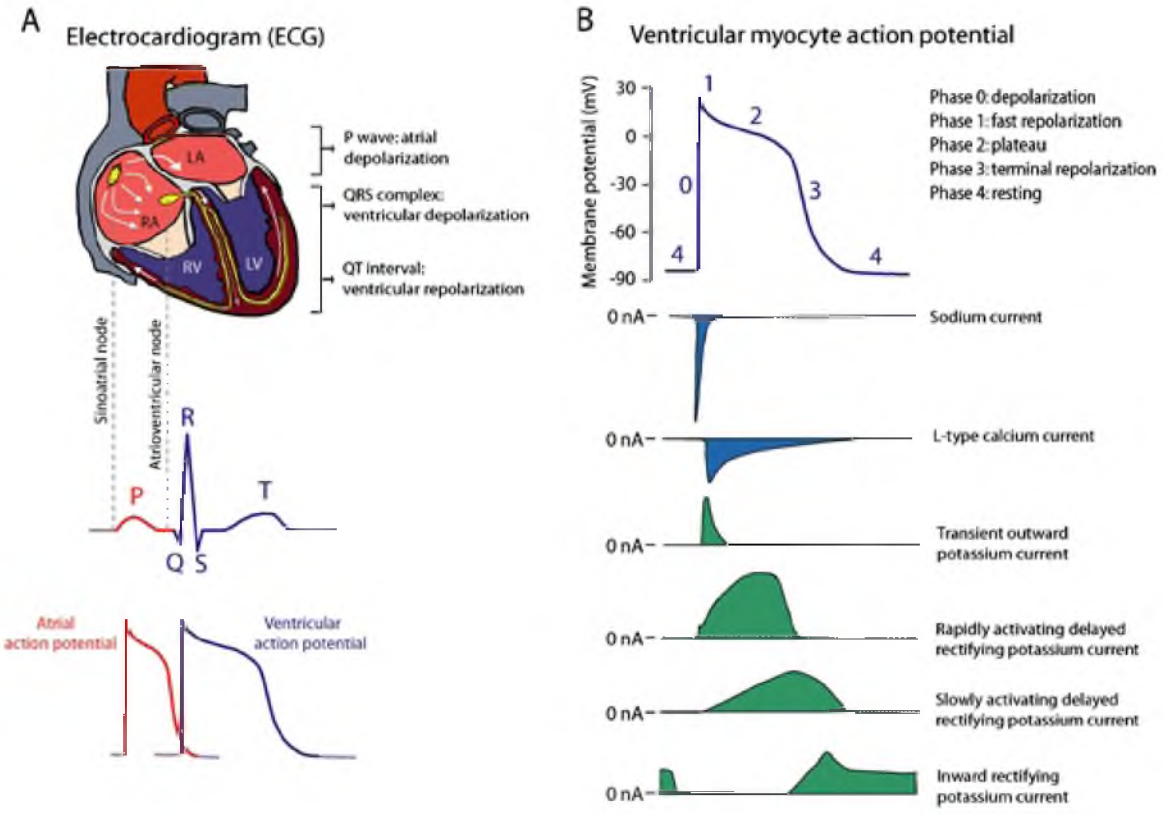

Fig. 2.10. Cardiac action potentials: Different action potentials seen within the myocardium. Reprinted with permission from Springer. A. Amin, A. Asghari-Roodsari, and H. Tan, "Cardiac sodium channelopathies," *European Journal of Physiology*, vol. 460(2), pp. 223-37, 2010.

- **Phase 1:** As the sodium channels begin to close, an initial, brief repolarization occurs that is labeled Phase 1. This transient event is primarily supported by I_{to}, a K^+ current that is activated and quickly inactivated by depolarization.

- **Phase 2:** The opening of L-type calcium channels and voltage-gated potassium channels results in a calcium influx that balances potassium efflux, which results in the positive plateau (Phase 2) of the action potential profile. This phase is perhaps the most varied across different myocytes types, lasting from just a few to several hundred milliseconds. This variation arises because the net current flow in this phase is the result of a dynamic balance of inward and outward currents. The inward currents are mainly carried by and I_{CaL} [26]. The outward currents include the rapid (I_{Kr}) and slow (I_{Ks}) components of delayed rectifier K^+ currents [27]. As long as the currents in both directions are balanced, there is an approximately constant transmembrane

potential, but this balance is tenuous and varies across cell types and also across the regions of the heart and even in time through physiological changes, like ischemia.

- **Phase 3:** Phase 3 is the fast repolarization phase. As the calcium channels close and inward currents diminish, the potassium currents begin to dominate, and full repolarization of the cells occurs. I_{K1} takes over during the final part of Phase 3 and returns the membrane potential back to its resting (diastolic) value [28].

- **Phase 4:** Phase 4 represents the membrane resting potential during diastole. After repolarization, the Na^+/K^+ ATPase extrudes the accumulated intracellular Na^+ ions and pumps the extracellular K^+ into the cell. The Na^+/Ca^{++} exchanger and the Ca^{++} ATPase also contribute to the ionic balance across the cell membrane.

The expression of channel proteins is not uniform throughout even regions containing otherwise identical cell types. As a result, there are associated regional variations in action potential morphology. For example, I_{to} is expressed more in the subepicardial region compared to subendocardial region, and as a result, Phase 1 is more prominent in the subepicardial cardiomyocytes [29]. A lower expression of I_{Ks} in the midmyocardial layers [30] may also contribute to electrical heterogeneity across the ventricular wall.

The cells of the working myocardium have stable resting potentials, i.e., the cell has to be stimulated to induce an action potential. In contrast, cells of the specialized conduction systems, such as sinoatrial and atrioventricular nodal cells, have unstable resting potentials (-60 to -40 mV), which allows them to serve as pacemakers. The mechanism of this behavior is that they lack I_{K1} expression [31]. Moreover, at these relatively positive resting potential values, I_{Na} cannot fully recover and so becomes inactive, so that depolarization is mainly driven by I_{CaL} [14]. The resulting sequence of events is as follows: I_f is activated by I_{KACh}-induced [32] membrane hyerpolarization [33], which causes the membrane potential to begin depolarizing, thereby initiating Phase 4. At -60 mV, the I_f inward current (funny currents) carried by Na^+ begins to flow [34]. The resulting gradual rise in resting potential crosses the threshold (-50 mV) for opening T-type calcium channels and the resulting inward I_{CaT}. A further depolarization to about -40 mV causes the inward I_{CaL} to activate and an action potential to fire. The resulting Phase 0 depolarization is primarily induced by I_{CaT}. The other inward currents including I_f and I_{CaT}, decline as their respective channels close. The influx of calcium is slow, resulting in a slower rate of depolarization compared to other contractile myocytes and Purkinje cells. No initial repolarization or plateau occurs,

so Phases 1 and 2 are said to be absent. Repolarization (Phase 3) is accomplished through the opening of voltage-gated potassium channels (I_{K1}).

During Phases 0, 1, 2 and part of Phase 3, the cell is refractory to the activation by depolarizing signals. This stability is described by the wavelength (λ) as

$$WL = ERP \times CV, \tag{2.6}$$

where CV is the conduction velocity. This is termed the "effective refractory period" (ERP) and is attributed to the slow recovery of the inactivated Na^+ channels [34]. The ERP acts as a protective mechanism and ensures cardiac electrical stability and protection against premature reexcitation.

Table 2.1 shows a summary of the key currents in the cardiac action potential and their contributions to each phase, including those responsible for maintaining homeostatic ion concentrations. Membrane depolarization rapidly activates the I_{Na} and I_{CaL} channels. As the calcium and sodium channels close, the potassium currents begin to dominate, and full repolarization of the cells occurs. The Na^+/Ca^{++} exchanger and the Ca^{++} ATPase also contribute to the ionic balance across the cell membrane.

Table 2.1. Cardiac ion currents for a ventricular action potential.

Ion	**Current**	**Transportation**	**Phase/role**
Na^+	I_{Na}	Facilitated diffusion via ion channels	Phase 0
Ca^{++}	$I_{Ca(L)}$	Facilitated diffusion via ion channels	Phase 0–2
K^+	I_{to1}	Facilitated diffusion via ion channels	Phase 1, notch
K^+	I_{Ks}	Facilitated diffusion via ion channels	Phase 2–3
K^+	I_{Kr}	Facilitated diffusion via ion channels	Phase 3
K^+	I_{K1}	Facilitated diffusion via ion channels	Phase 3–4
Na^+, Ca^{++}	I_{NaCa}	Na-Ca exchanger (cotransporter). 3:1 ratio favoring Na	ion homeostasis
Na^+, K^+	I_{NaK}	Na-K ATP pump 3:2 ratio in favor of Na	ion homeostasis
Ca^{++}	I_{pCa}	Ca ATP pump	ion homeostasis

2.2.5 Excitation-Contraction Coupling

Excitation contraction (EC) coupling describes the process from electrical excitation of the myocyte to its eventual contraction [35], as shown in Fig. 2.11. During the cardiac AP, Ca^{++} enters the cell through activated L-type calcium channels (LTCC), also called dihydropyridine receptors (DHPRs). These channels are located in the T-tubules at the sarcolemmal-SR junctions, where the SR calcium release channels, also called ryanodine receptors (RyRs), are also found [36]. RyRs are arranged in large organized arrays at the junctions between SR and sarcolemma beneath DHPR (on the surface of and in T-tubules) and form a large functional Ca release complex at the junction called the couplon [37].

SR calcium release is triggered by the Ca^{++}-induced Ca release (CICR) mechanism mediated by I_{CaL} [35]. Activation of one local DHPR channel can trigger the calcium release for all the RyRs at the couplon. Typically, there are 10–25 DHPR for every 100 RyR, which provides the safety margin for the couplon to function properly [35]. Even so, only a small fraction of DHPRs and RyRs in a cell or couplon needs to fire to generate measured Ca^{++} fluxes. The calcium release from the sarcoplasmic reticulum(SR) increases

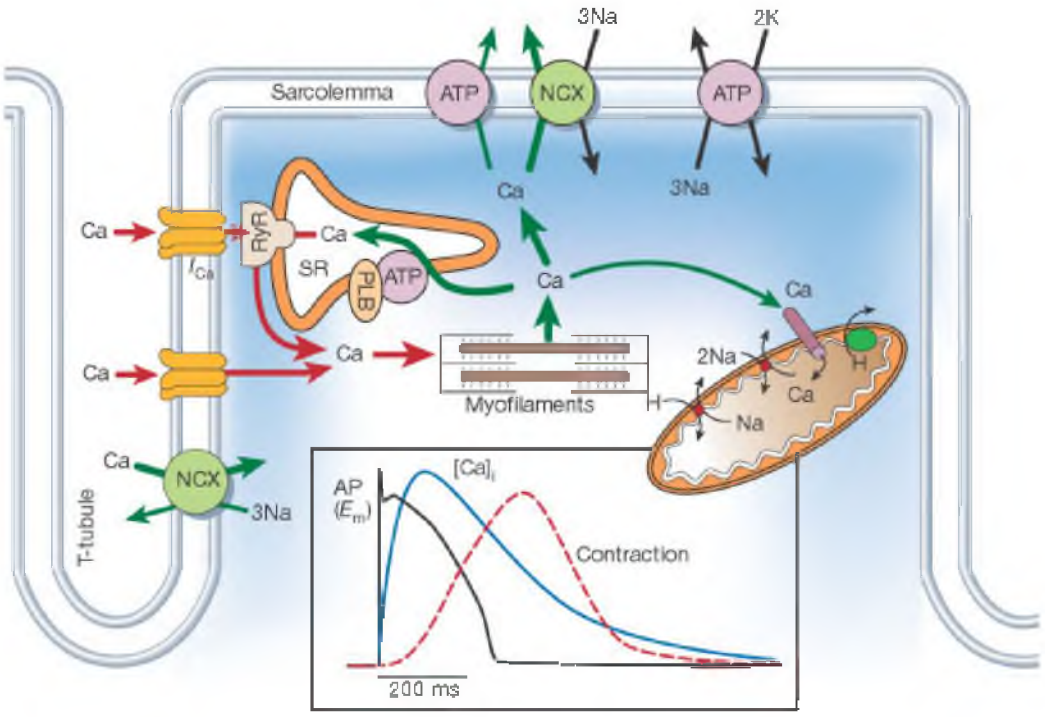

Fig. 2.11. Mechanism of EC coupling in a contractile myocyte. Reprinted with permission from Nature Publishing Group. D. Bers, "Cardiac excitation-contraction coupling," *Nature*, vol. 415, pp. 198-205, 2002.

the intracellular calcium concentration from about 10^{-4} to 10^{-2} mM [34].

A high load of SR Ca^{++} directly increases the amount of Ca^{++} released for a given I_{CaL} because of the potentiating effect of high $[Ca]_{SR}$ on the open probability of RyRs [38]. SR Ca^{++} content can be increased by increasing Ca^{++} influx, decreasing Ca^{++} efflux, or enhancing Ca^{++} uptake into the SR [35]. The combination of calcium influx and release increases the cytosolic calcium concentration, allowing Ca^{++} to bind to myofilament protein troponin C, which activates the contractile machinery.

The strength of contraction, which is graded, can be regulated by altering the amplitude or duration of Ca^{++} transient and also by altering the sensitivity of myofilaments to calcium [35]. Myofilament Ca^{++} sensitivity is enhanced dynamically by stretching the myofilaments (due to preload), resulting in stronger contraction. On the other hand, myofilament sensitivity is reduced by acidosis, elevated phosphate, and magnesium concentrations (all of which occur during ischemia), and β adrenergic activation, enhanced by caffeine and certain inotropic drugs [35].

The SR calcium release contributes to calcium-dependent inactivation of I_{CaL} [39]. Moreover, Ca^{++}-dependent inactivation at the cytosolic side also limits the amount of Ca^{++} entry during the AP. When there is high concentration of cytosolic Ca^{++}, further influx of Ca is suppressed. Thus, SR Ca^{++} release and I_{CaL} provide a local negative feedback on Ca^{++} influx [35].

Terminating calcium release is needed for diastolic refilling of the heart and is achieved by inactivation of RyR [35]. During relaxation, cytosolic calcium declines, allowing Ca^{++} to unbind from troponin. Calcium is then transported out of the cytosol primarily through the SR Ca^{++} ATPase. Phospholamban is an inhibitor of the SR Ca^{++} ATPase and its phosphorylation by cAMP-dependent or calmodulin-dependent protein kinases (PKA or CaMKII) removes this inhibition, allowing more rapid SR uptake of Ca^{++} and subsequent decline of $[Ca]_i$ [35]. There are also other pathways for calcium transport out of the cytosol: Na^+/Ca^{++} exchanger, sarcolemmal calcium ATPase, and mitochondrial Ca^{++} uniport. In human, canine, and rabbit ventricle myocytes, SR Ca ATPase removes 70% of activator Ca^{++} and the Na^+/Ca^{++} exchanger removes 28% and 1% each for the sarcolemmal Ca^{++} ATPase and the mitochondrial Ca^{++} uniporter [35]. For homeostasis, the amount of calcium influx must be equal to the calicum efflux for each beat.

2.2.6 Gap Junctions

The propagation of action potentials from cell to cell occurs through specialized, non-selective large-conductance ion channels packed in arrays called gap junctions [40], as shown in Fig. 2.12. Each cardiac gap junction channel is composed of 12 connexin molecules, with 6 embedded in the cell membranes on each side of the junction. The heart expresses three connexin isoforms, Cx40, Cx43, and Cx45, which are available to form heteromeric channels [41]. Six connexins form a hemichannel called the connexon, which faces another connexon in the neighboring myocyte. In combination, they function as a complete channel enabling electrical continuity between neighboring myocytes. The gap junctions are located within the intercalated disks connecting myocytes along the ends of the cell long axis, but are also present albeit in lower density along the sides of the cells, to provide some side-to-side connections. These intercalated disks also provide the physical framework for mechanical force of contraction generated by each myocyte to be transmitted [14].

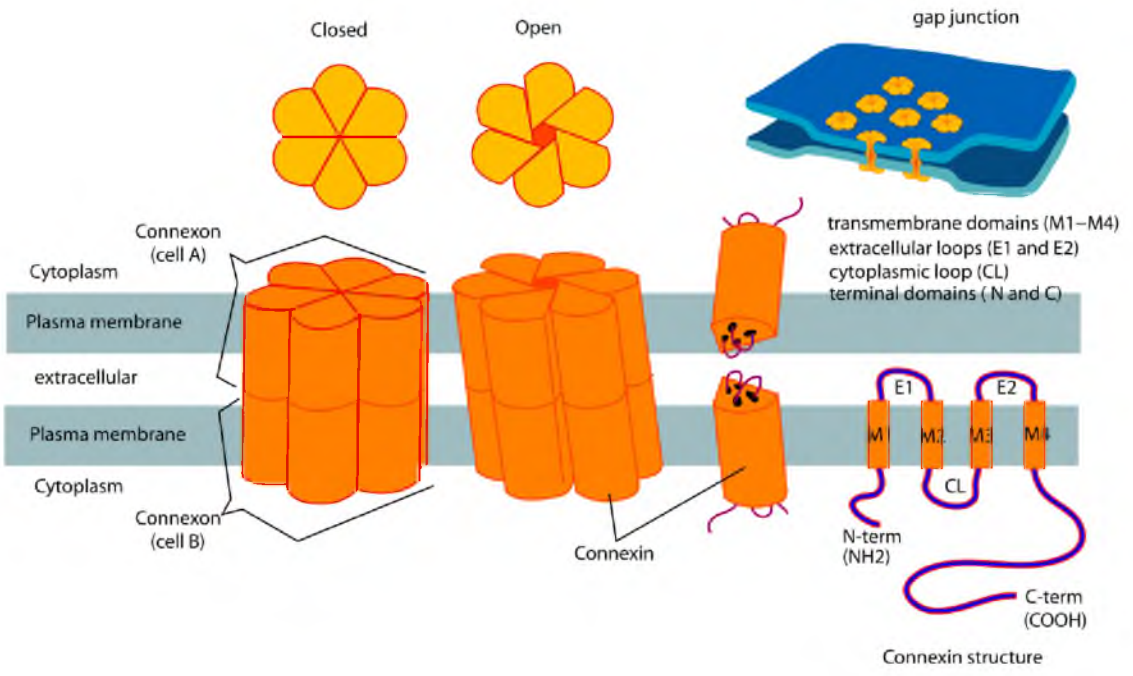

Fig. 2.12. Gap junctions: Structure of a gap junction. Reprinted with permission from Wikimedia and Mariana Ruiz (LadyofHats). Retrieved from `http://commons.wikimedia.org`. Used under creative commons attribution-noncommercial-sharealike 3.0 generic license (`http://creativecommons.org/`).

2.2.7 Myocardial Anisotropy

Myocardial anisotropy refers to directionally dependent variation in properties such as conduction velocity [42] and repolarization [43]. The structural determinants of anisotropy include cell geometry, cell size, and distribution of gap junction and ion channels. Moreover, since gap junctions behave as voltage- and chemically-gated ion channels, there is dynamic regulation of gap junction conductance, which contributes to transient anisotropy modulation [44].

The myocardial fiber orientation within myocardial tissue is anisotropic, as shown in Fig. 2.13. In ventricles, the fiber inclination angle ranges from 90–180 degrees of rotation. Moreover, the rate of rotation is slightly more rapid near ventricular walls. This three-dimensional spatial organization of myocardial fibers influences electrical propagation [44] and mechanical contraction [45]. Alterations in fiber architecture can occur during pathological conditions such as cardiac infarction [46], which may predispose the heart to arrhythmias.

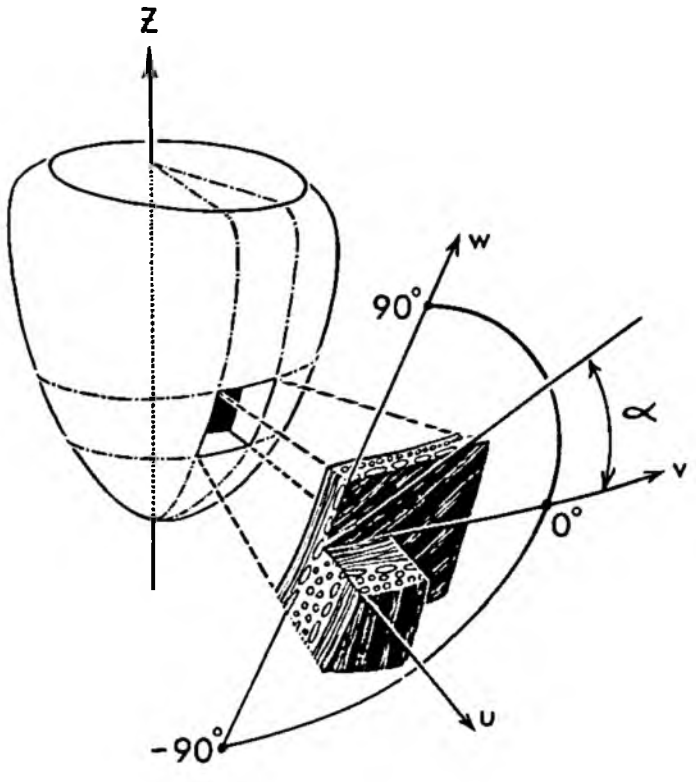

Fig. 2.13. Myocardial anisotropy. Reprinted with permission from Wolters Kluwer Health, Inc. D. Streeter, H. Spotnitz, D. Patel, J. Ross, and E. Sonnenblick, "Fiber orientation in canine LV during diastole and systole," *Circulation Research*, vol. 24, pp. 339-347, 1969.

2.2.8 Cardiac Propagation

When a cardiomyocyte is depolarized to a positive membrane voltage, it creates a difference in membrane potential with respect to the neighboring myocytes, which are still at the negative resting potential. This potential difference causes the intracellular depolarizing currents to flow across the gap junctions into the unexcited cells. Thus, the positive charge moves from the depolarized cell to the resting cells. At the same time, in the extracellular space, the local current flows in the opposite direction, as the extracellular site is made negative by the flow of Na^+ ions into the depolarized cell, thus forming a complete propagation circuit, as shown in Fig. 2.14.

As the positive charge continues to accumulate in the resting cell, its membrane potential starts rising and when the excitation threshold is reached, triggers an action potential. The newly excited cell now serves as a source for exciting the next neighboring cell. This wave of propagation from cell to cell is called the "activation wavefront," which eventually spreads through the heart. The spread of activation wavefront continues as long as the depolarizing charge supplied by the excited cell is enough to activate the neighboring resting cells.

Cardiac propagation is influenced by many factors, including the action potentials of

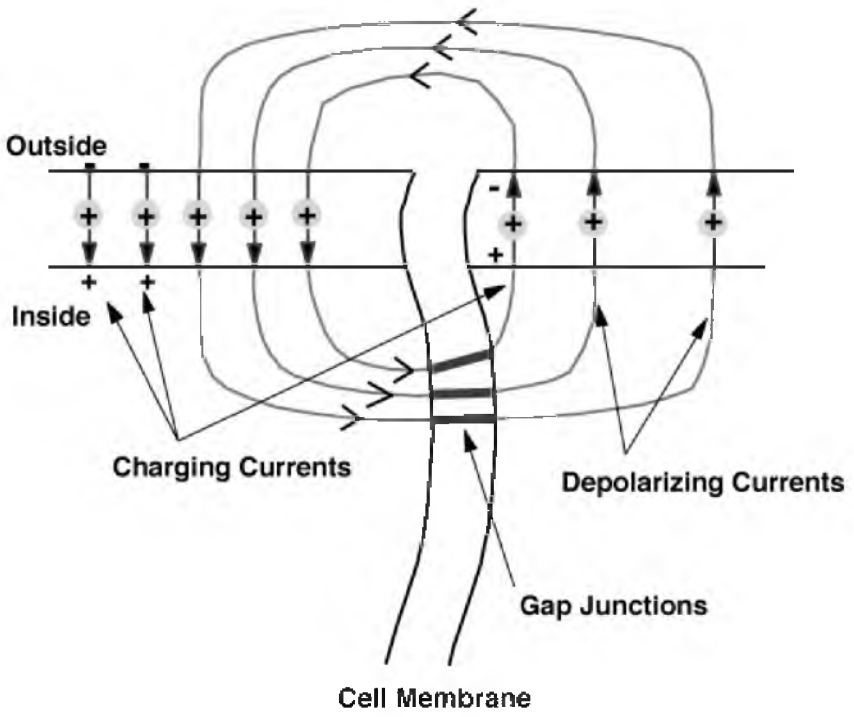

Fig. 2.14. Propagation circuit: Spread of excitation from one cardiac cell to another.

the individual cells, the tissue structure and connectivity, and can be captured by the value of the conduction velocity. One way to capture electrical connectivity in the myocardium is the "space constant" (λ), which describes how far along the tissue current can travel before it dissipates into the extracellular space. The space constant is defined by the equation

$$\lambda \approx \sqrt{\frac{R_m}{R_i}}, \tag{2.7}$$

where R_m is the specific membrane resistance per cross-sectional area and R_i is the specific axial resistance per cross-sectional area.

Conduction velocity is faster along the longitudinal direction than in the transverse direction of the myocardium as the current crosses more cell borders and thus gap junctions to cover the same distance [47]. This difference in conduction velocities is referred to as "electrical anisotropy." Conduction velocity is also influenced by the amount of electrical source (higher I_{Na} density in contractile myocytes and relatively lower I_{CaL} density in pacemaker cells) [14]. Conduction velocity is approximated using the equation

$$v = \sqrt{\frac{KD\frac{dV}{dt}}{R_i C_m}}, \tag{2.8}$$

where K is a constant, D is the diameter of the fiber, $\frac{dV}{dt}$ is the rate of rise of action potential, R_i is the intracellular resistivity, and C_m is the membrane capacitance.

A related parameter known as the "propagation safety factor" is determined by the electrical source and electrical load ratio. Under normal conditions, the current size in a single cell is large enough to depolarize a number of connected cells [14]. Source/load mismatch, perhaps due to depressed charge (I_{Na} or I_{CaL}) or expanded load (e.g., patchy fibrosis), can trigger arrhythmias resulting from unidirectional block (reentry) (described in more detail below).

2.2.9 Cardiac Activation Sequence

The cardiac electrical impulse originates in the SA node and propagates through the entire heart, as shown in Fig. 2.15. Through connections from the SA node fibers, the action potentials travel outwardly into adjacent atrial muscle fibers and spread rapidly over the entire atria with conduction velocities of 0.3 m/s [22]. The SA node is also believed to be connected to the AV node via internodal pathways. The conduction of impulse across

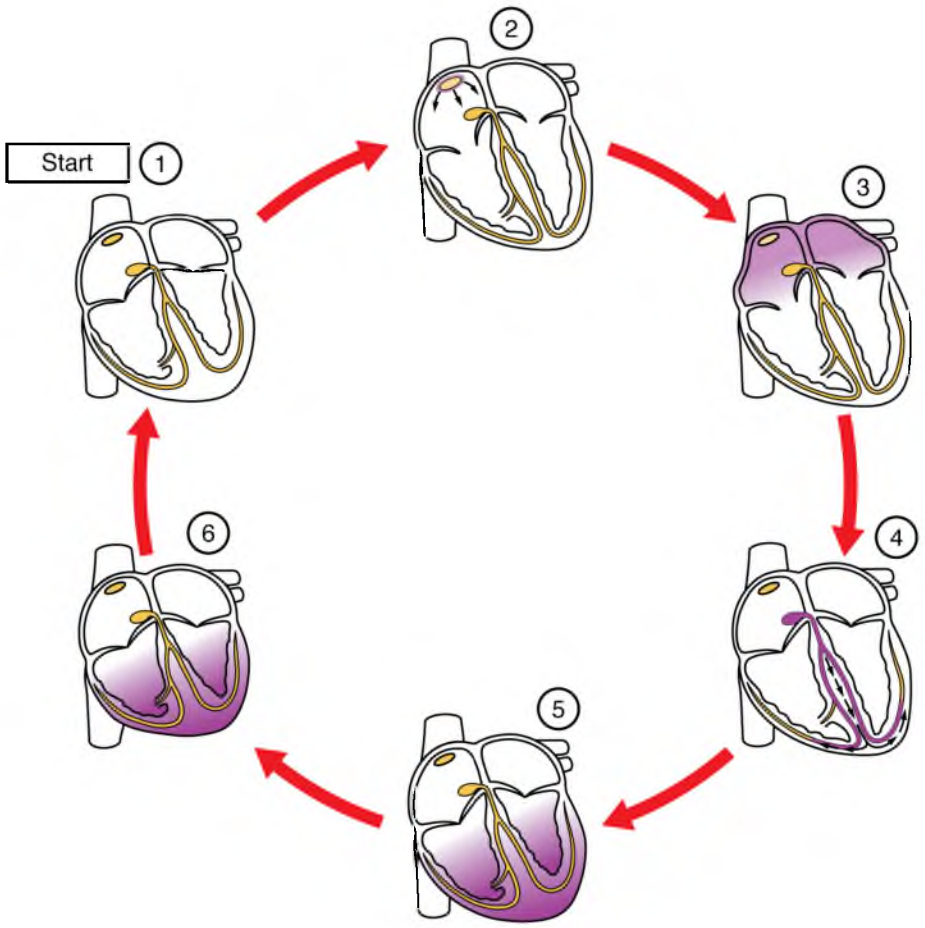

Fig. 2.15. Spread of excitation through the heart. The cardiac electrical impulse originates in the SA node and propagates through the entire myocardium. Reprinted with permission from Wikimedia and OpenStax College. Retrieved from `http://commons.wikimedia.org`. Used under creative commons attribution-noncommercial-sharealike 3.0 generic license (`http://creativecommons.org/`).

these specialized fibers is more rapid, at about 1 m/s [22]. The electrical impulse from the SA node reaches the AV node in about 30 milliseconds [22]. In the AV node, the electrical impulse is delayed by another 90 milliseconds before an impulse enters the distal portion of the AV bundle and into the ventricles [22]. The slow conduction in the AV node is attributed to the low density of gap junctions, resulting in higher intracellular resistance to conduction. This delay allows the atria to contract following excitation and pump a small amount of blood into the ventricles. Normally, the only pathway for electrical impulses to travel from the atria into the ventricles is through the AV node due to the electrical insulation provided by the cardiac skeleton. Moreover, under normal physiological conditions, the electrical impulse cannot travel back from the ventricles to the atria.

The cardiac impulse exits the AV node and travels through the Bundle of His, the right and left bundle branches, and the Purkinje system for another 30 milliseconds before reaching the ventricles [22]. The Purkinje fibers have higher density of gap junctions and as result, the conduction velocity reaches 1.5–4 m/s [22]. As the Purkinje fibers penetrate into a large portion of the endocardial myocardium and become continuous with cardiac muscle, they provide for almost instantaneous propagation of cardiac impulse throughout the remainder of the ventricles.

The conduction velocity of propagation within the ventricles is between 0.3 to 0.5 m/s [22]. The cardiac impulse spreads generally from the apex to the base, anterior to posterior, and from endocardium to the epicardium [48]. The transmission of cardiac impulse from the endocardium to the epicardium takes another 30 milliseconds [22] so that the total time of propagation from the SA node to the last of the ventricular muscle fibers is approximately 190 milliseconds. The penetration and spread of Purkinje fibers into the ventricular myocardium varies across species, affecting the ventricular activation sequence. For example, in pigs, the endocardium and the epicardium get activated more simultaneously than in other species [49].

2.2.10 Electrocardiogram (ECG)

The ECG represents the electrical activity of the heart recorded using body-surface electrodes as potential differences over time. To understand the complex relationship between the ECG and the electrical activity of heart, we first look at the potential field generated by a single cell, then a single fiber, a tissue composed of many fibers, and finally the integrated heart and torso volume conductor model.

For a single cell model as shown in Fig. 2.16, the potential, $\phi(\vec{r}')$ at some external observation point, $\vec{r}'$ is given by the equation

$$\phi(\vec{r}') = \frac{1}{4\pi\sigma_e}\sigma_i(V_d - V_r)\Omega(\vec{r}'), \tag{2.9}$$

where V_d and V_r denote the transmembrane potentials over the depolarized and resting regions of the cell and σ_i and σ_e denote the homogeneous isotropic electrical conductivity inside and outside the cell. The term $\Omega(\vec{r}')$ represents the solid angle subtended by the cross-section A at the external observation point $\vec{r}'$. Moreover, the expression $\sigma_i(V_d - V_r)$ represents the equivalent current density double layer and thus a distributed current dipole source [50]. If the cell is completely depolarized or completely repolarized, the

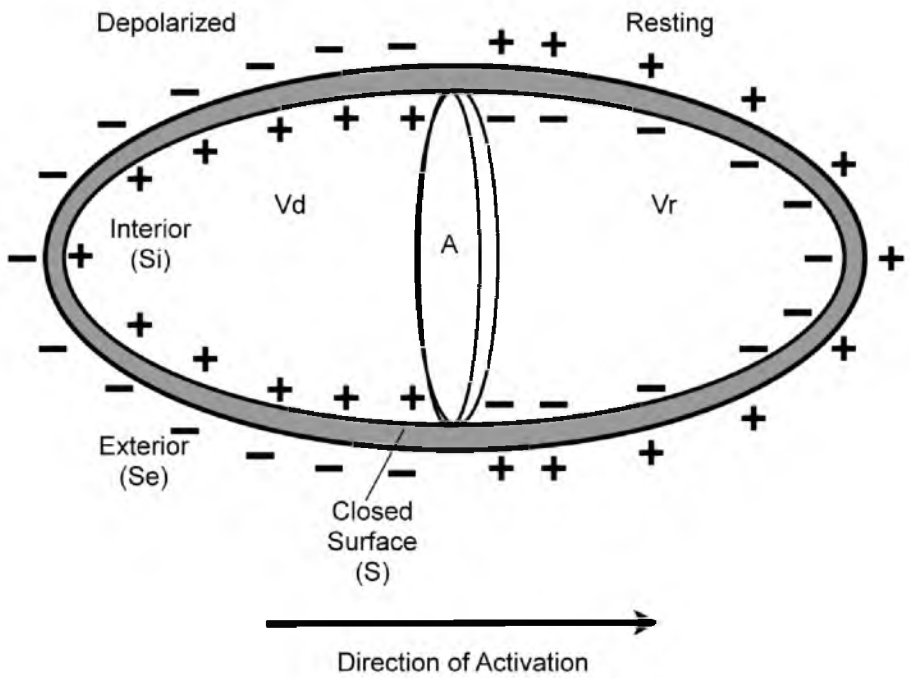

Fig. 2.16. Cardiac cell model: Cell model to evaluate a theoretical external potential field.

transmembrane voltage V_m over the entire closed surface, S, is a constant, and thus the potential field in the exterior region is zero. It is only when the part of the cell is depolarized and the other part is at rest that we see an external potential field.

Expanding this same concept to the single fiber model, the depolarizing wave produces a current entering the extracellular space just ahead of the depolarizing wavefront. There is also a current sink just behind it. The intracellular current I_i travels down the gradient from the location of the (extracellular) sink to the (extracellular) source.

Outside the fiber, a passive return current travels from the source to the sink, taking more than one path, and thus generating an external potential field throughout the external volume by passive current flow. For the observation points at some distance from the fiber, the potential field is indistinguishable from the one created by lumping the inward currents together into a single monopole $-I_o$ (sink) and all the outward currents into a single current monopole I_o (source) separated by a distance d. Moreover, at distances from the monopole pair that are much greater than d, the external potential field can be approximated as one generated by a dipole ($\vec{D} = I_o\vec{d}$) [14], as shown in Fig. 2.17. The external potential field can now be expressed as

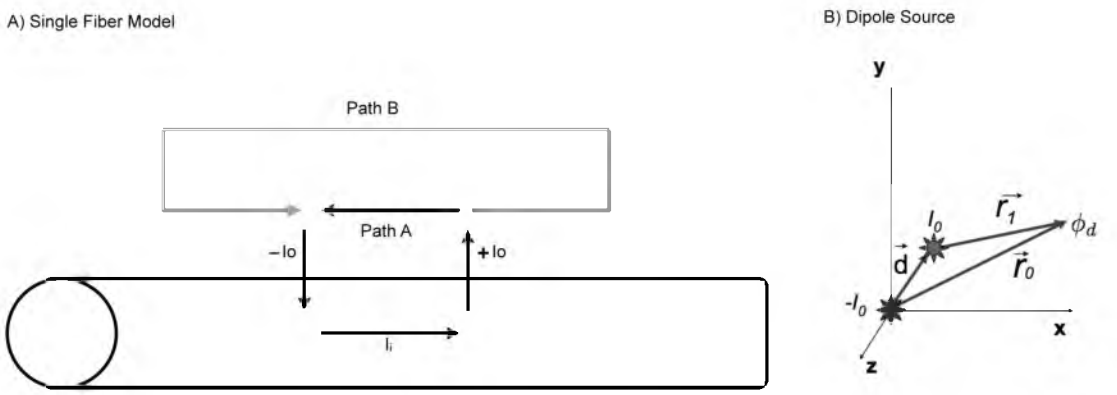

Fig. 2.17. Cardiac fiber model: (a) Single fiber model, (b) dipole source.

$$\phi_d(\vec{r}^{\,'}) = \frac{1}{4\pi\sigma_e}\frac{Dcos\varphi}{R^2}, \tag{2.10}$$

where D is the magnitude of the dipole, φ is the angle between the dipole direction (from sink to source) and the line from dipole location to the field point, and R is the distance from the dipole location to the field point.

Expanding the concept further to many fibers or a tissue model, the first simplification is to sum the potentials generated by each fiber by viewing the collection of elementary dipoles distributed over the surface $S(t)$ of the wavefront at time t.

Another simplification step is to assume that the direction of dipole density is aligned with the direction of the propagation wavefront and has a uniform strength, thus forming a uniform double layer (UDL) [14]. The external field can then be expressed as

$$\phi_e(\vec{r}^{\,'};t) = \frac{M_S}{4\pi\sigma_e}\Omega(\vec{r}^{\,'};t), \tag{2.11}$$

where M_S is the dipole density and $\Omega(\vec{r}^{\,'};t)$ is the solid angle subtended by the entire wavefront S(t) from the observer point.

The expression of external fields assumes a uniform medium of homogeneous conductivity around the active cell, fiber, and tissue [51]. In actuality, the cardiac sources are in a volume conductor with different conductivities attributed to lungs, blood, skeletal muscle, fat, etc. Moreover, instead of an infinite medium, the volume conductor has a sharp torso-air boundary, as shown in Fig. 2.18. The distance between the cardiac current source location

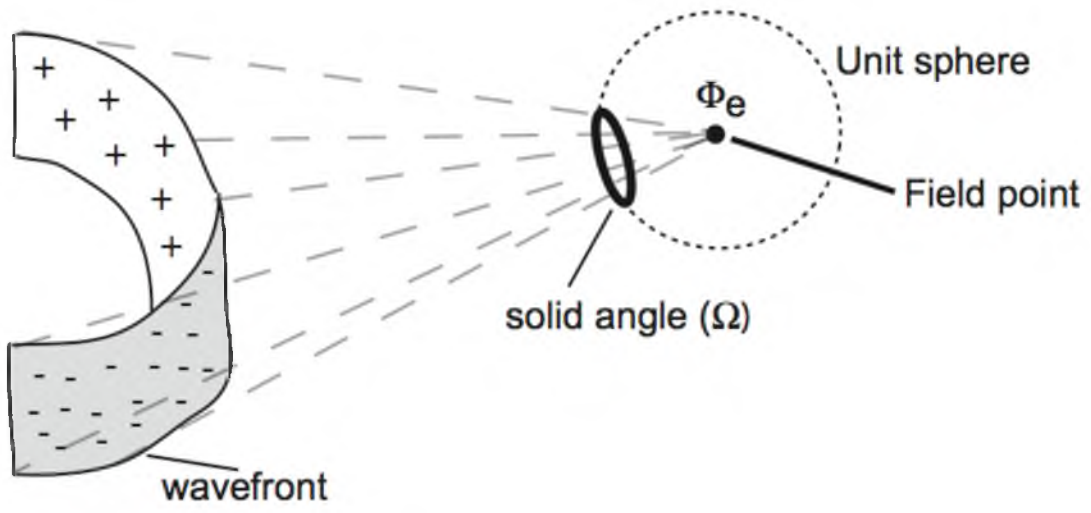

Fig. 2.18. Cardiac tissue model: External potential field generated by distributed sources.

and observation point (electrode location) plays a critical role in determining the magnitude of potentials recorded on the body surface. Since the potential field from a dipole source declines as $1/R^2$, the ability of the body surface ECG to measure potential fields from smaller current sources is diminished greatly [52, 14]. Moreover, the ECG measures the potential difference between two recording sites (electrodes), with one being used as a reference. However, this assumption is inaccurate for a bounded volume conductor [53].

The normal ECG waveform is shown in Fig. 2.19, and the key features include the P-wave, QRS complex, ST segment, T-wave, and the U-wave. The P-wave represents atrial depolarization. The QRS complex reflects the ventricular repolarization, and the T-wave indicates ventricular repolarization. The U-wave is believed to represent isovolumetric relaxation [14].

The P-wave has a relatively a small amplitude (60–120 μV), which can be attributed to smaller current sources (as the atria are smaller in size with thin walls). The P-wave is followed by an interval of approximately 70 milliseconds referred to as the "PQ segment" and corresponds to atrial repolarization [54] as well as the excitation wave progressing through the AV node and the His-Purkinje system [55]. Because of the small magnitudes of current generated during this interval, it registers minor, if any, deflection on the ECG.

QRS complex deflections are the result of ventricular depolarization, and since the RV and LV are excited almost simultaneously, the ECG reflects the superposition of the effects

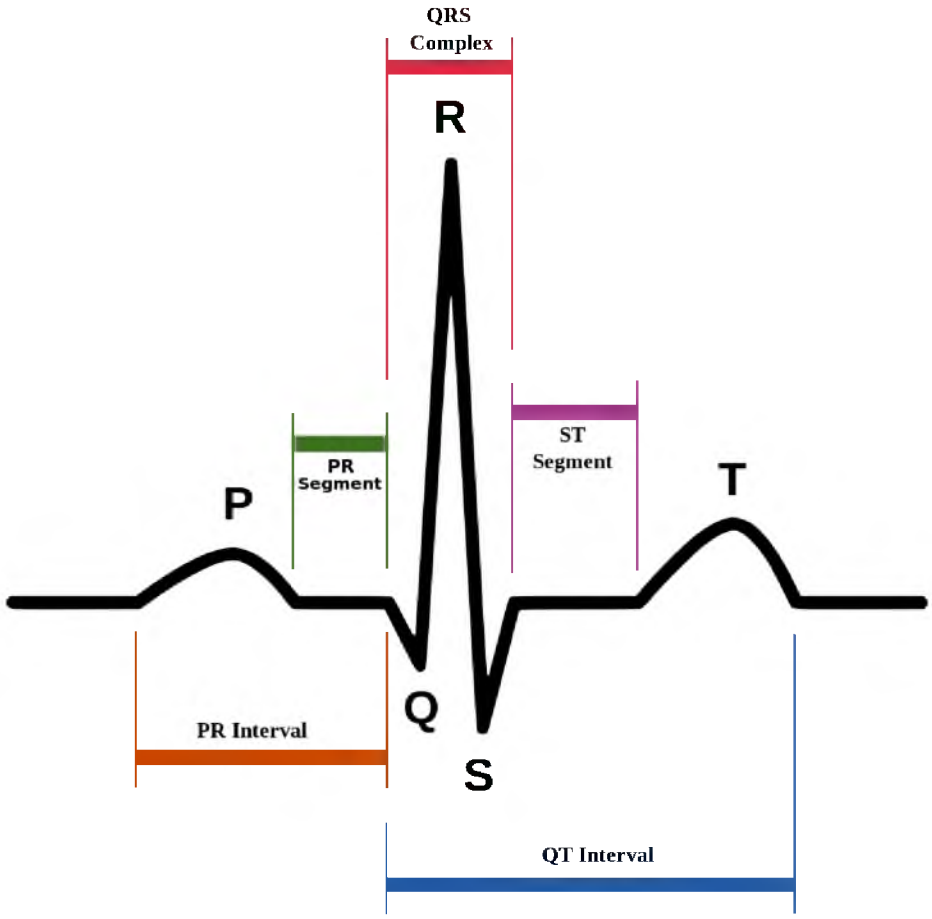

Fig. 2.19. Electrocardiogram (ECG) features including the ST segment, and the T-wave. Reprinted with permission from Wikimedia and Anthony Atkielski (Agateller). Retrieved from `http://commons.wikimedia.org`. Used under creative commons attribution-noncommercial-sharealike 3.0 generic license (`http://creativecommons.org/`).

of both wavefronts, which often results in electrical cancellation [56]. Moreover, since the RV wall is thinner, its excitation wavefront terminates earlier than the LV wavefront. Consequently, the early portion of the QRS complex receives contributions from both ventricles, whereas the latter portion of the QRS complex waveform is driven primarily by LV excitation.

Following the QRS complex deflection, the ECG reflects a relatively quiet period represented by the ST segment. The J-point is marked as the time point when the tracing changes slope sharply at the end of the S-wave [14] and is believed to represent the end of ventricular depolarization and the beginning of ventricular repolarization. As such, there is a period of overlapping potentials between regions at the end of depolarization and those at the beginning of repolarization. Moreover, this potential difference is relatively small,

resulting in the ECG returning to a voltage near baseline [14]. The primary reason for the isoelectric potentials during the ST segment in the normal ECG is that all action potentials have such similar plateau potentials that there is no current flow in the heart and hence no body-surface voltage.

The T-wave is produced by the repolarization of ventricular myocytes and is attributed to transmural dispersion of repolarization from the epicardium (shorter APD) to endocardium (longer APD) [14]. Moreover, the repolarization appears to occur earlier at the base than at the apex [57]. The U-wave is a low amplitude, usually monophasic ECG feature following and often partly merged with the T-wave [14]. The origins of U-wave remain controversial, although a negative U-wave, if present, is believed to signify the presence of cardiac diseases: ischemia, hypertension, and aortic regurgitation [58].

2.3 Cardiovascular Physiology

The cardiovascular system is designed to deliver oxygen and nutrients to the cells of the body and remove carbon dioxide and metabolic wastes from the cells. It is made up of two major circulatory systems working in tandem: pulmonary circulation and systemic circulation. The low resistance pulmonary circulation constitutes the right side of the heart pumping the deoxygenated blood to the lungs through the pulmonary artery and pulmonary capillaries and then returning the oxygen-rich blood to the left atrium through the pulmonary veins. The high-resistance systemic circulation is composed of the left side of the heart pumping oxygenated blood to the rest of the body through the aorta, arteries, arterioles, and systemic capillaries and subsequently returning deoxygenated blood to the right atrium through the venules and veins. We briefly cover the key concepts of cardiovascular physiology in this section.

2.3.1 Cardiac Cycle

The cardiac cycle describes the pressure, volume, and flow in the atria and ventricles as a function of time, as shown in Fig. 2.20. A single cycle of cardiac activity is composed of two phases: diastole and systole. Diastole constitutes the time period when the ventricles are relaxed, whereas systole represents the time during which the ventricles contract. The cardiac cycle diagram highlights the changes in aortic pressure, left ventricular pressure, left atrial pressure, and left ventricular volume and their relation to the heart sounds and the morphology of the electrocardiogram. The cardiac cycle is typically divided into five phases: atrial contraction, iso-volumetric contraction, ventricular ejection, iso-volumetric relaxation, and ventricular filling. The phases are detailed in the following:

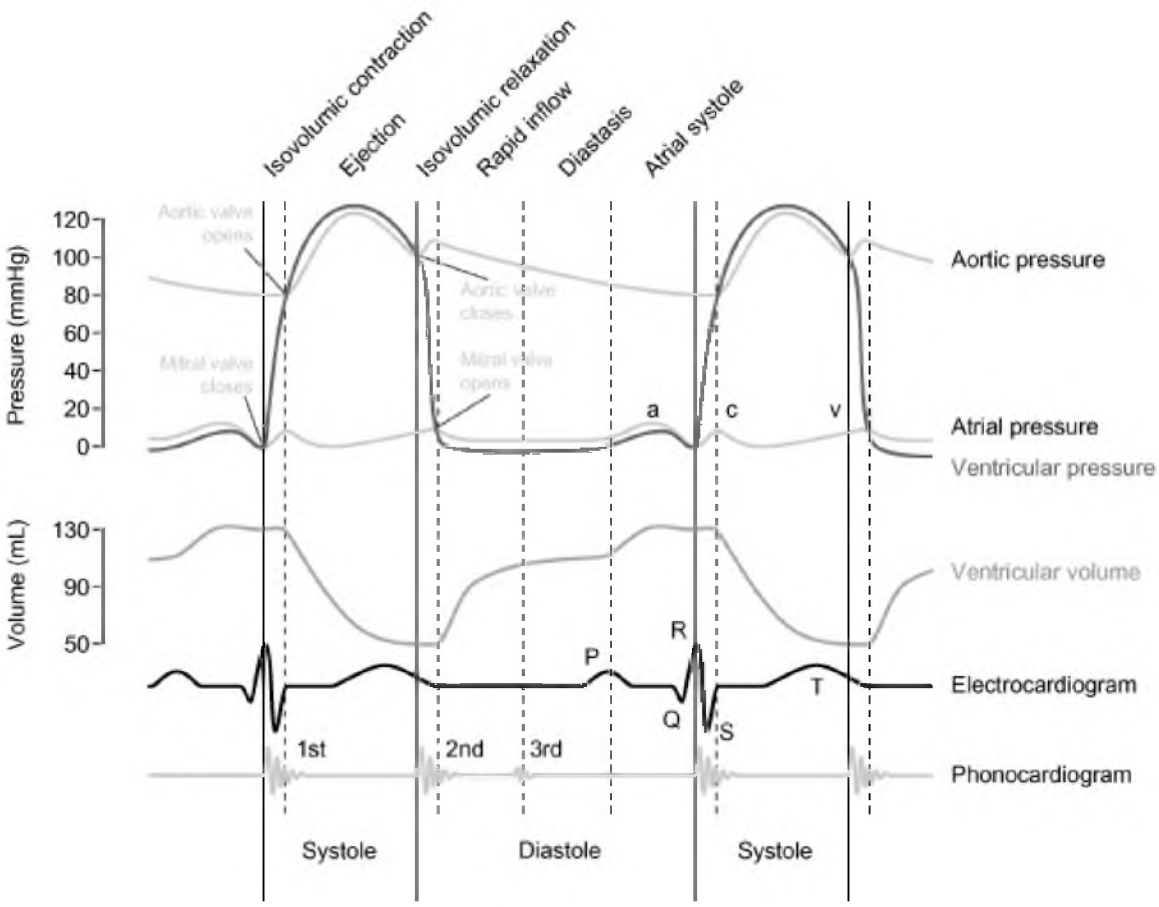

Fig. 2.20. Cardiac cycle: Wiggers diagram highlighting various events of a cardiac cycle. Reprinted with permission from John Wiley and Sons. B. Smith, "Classifying processes: An essay in applied ontology," *Ratio*, vol. 25(4), pp. 463-488, 2012.

- **Atrial Contraction Phase:** The atrial contraction phase is initiated by the P-wave on the ECG, reflecting the atrial activation, which causes the atria to contract. The pressure in the atrial chambers increases, forcing rapid flow of blood into the ventricles across the open atrio-ventricular valves. Following atrial contraction, the atrial pressure begins to fall, which causes the AV valves to float upwards before closure [34]. The ventricular volume is maximal at this stage and is called the end-diastolic volume (EDV), representing the ventricular preload. At resting heart rates, the atrial contraction accounts for 10% of the left ventricular filling as most of the ventricular filling happens before atrial contraction through the passive flow of blood through the open valves. However, at high heart rates, it can rise to as much as 40% of ventricular filling [34].

- **Iso-volumetric Contraction Phase:** The iso-volumetric contraction phase coincides with the QRS complex on the ECG representing ventricular activation, which triggers EC coupling, ventricular contraction, and a rapid increase in intraventricular pressure corresponding to maximal dP/dt. The AV valves close as the intraventricular pressure exceeds the atrial pressure, resulting in the first heart sound (S_1). During this time period, there is an increase in pressure without a change in volume as the ventricles contract, hence the iso-volumetric contraction. However, individual myocytes and fibers may contract isotonically (shortening), isometrically (no change), or eccentrically (lengthening), resulting in the heart becoming more spheroid with circumference increases and atrial base-to-apex shortening [34].

- **Ventricular Ejection Phase:** The ventricular ejection phase represents the ejection of blood from the ventricles. The intraventricular pressure exceeds the aortic and pulmonary pressures, causing the semilunar valves to open, and blood is rapidly ejected into the aorta from the left ventricle and into the pulmonary artery from the right ventricle. Approximately 200 milliseconds after the QRS complex, the ventricles begin to depolarize, which coincides with the T-wave on the ECG [34]. Ventricular pressure begins to fall, whereas atrial pressure begins to rise due to continued venous return from the lungs and systemic circulation.

- **Iso-volumetric Ventricular Relaxation Phase:** The iso-volumetric ventricular relaxation coincides with the closure of the semilunar valves, which causes the second heart sound (S_2). Valve closure is associated with a small back flow of blood into the ventricles characterized by the dicrotic notch [34]. Although the ventricular pressures decrease during this phase, the volumes remain constant as all the valves are closed. The volume of blood that remains in the ventricle is called the end-systolic volume (ESV). Moreover, the difference between EDV and ESV represents the stroke volume (SV). The atrial pressure continues to rise.

- **Ventricular Filling Phase:** The ventricular filling phase represents the opening of AV valves as the atrial pressure exceeds the intraventricular pressure. Despite the inflow of blood, the intraventricular pressure continues to fall briefly as ventricles are still undergoing relaxation. Once the ventricles are completely recovered, their pressure begins to rise slowly. As the ventricles continue to fill with blood and expand, the intraventricular pressure rises. During this time period, the aortic and pulmonary

arterial pressure continues to fall. In normal hearts, 90% of the ventricular filling occurs by the end of this phase [34].

2.3.2 Hemodynamics

Hemodynamics constitutes the physical factors that govern cardiac output and blood flow: blood flow velocity, pressure, and resistance. Cardiac output (CO) is the amount of blood pumped by the ventricles in 1 minute and is given by the equation: Cardiac Output (Q) = SV × Heart Rate (HR). Blood flow refers to the bulk flow of fluid during circulation. Blood flow velocity refers to the speed with which the blood moves during circulation and is directly related to blood flow and inversely related to the cross-sectional area, as shown in Fig. 2.21.

The systolic blood pressure decreases as the blood flows from the aorta (120 mmHg) through the arteries (100 mmHg), arterioles (80 mmHg), capillaries (35 mmHg), and venules (5 mmHg), and falls to near atmospheric pressure in the veins (1 mmHg) [1]. Moreover, the oscillations of blood pressure are abolished in the arteriolar portion of the systemic

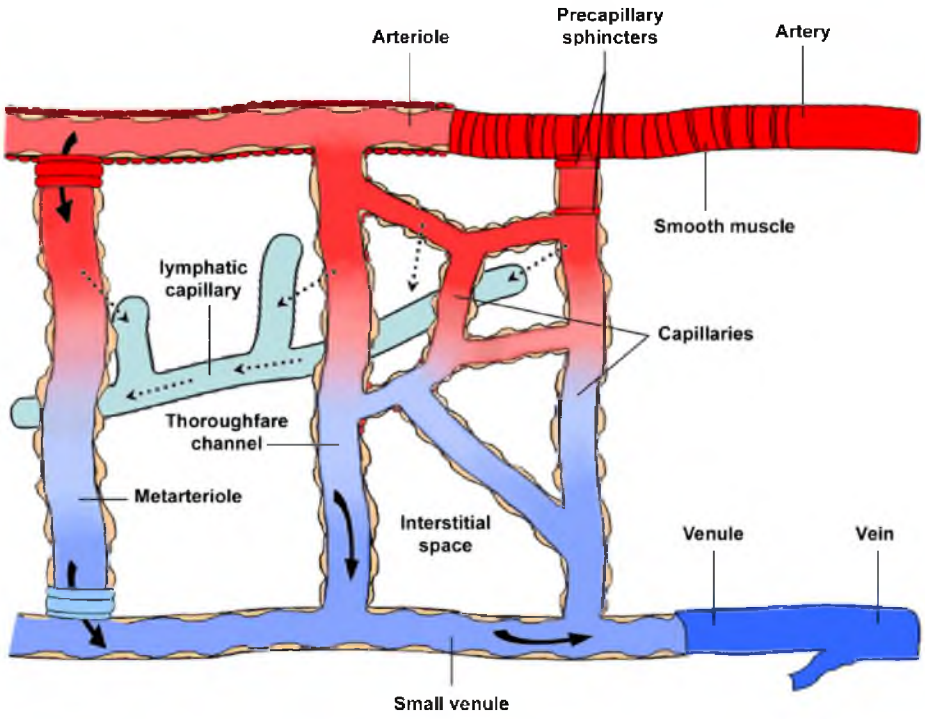

Fig. 2.21. Circulatory system. Reprinted with permission from Vascular Cell. M. Scioli, A. Bielli, G. Arcuri, A. Ferlosio, and A. Orlandi, "Ageing and microvasculature," *Vascular Cell*, vol. 16, pp. 6-19, 2014. © 2014 BioMed Central Ltd.

circulation. The arterial pulse is altered by such factors as heart rate (increased diastolic pressure), stroke volume (increased systolic pressure), and arterial compliance (decreased systolic pressure) [1]

Resistance (R) to blood flow is affected by vessel radius (r) and fluid viscosity (n) such that R is given by Poiseuille's law $R = 8nL/\pi r^4$. Thus, when the vessel radius is halved, resistance increases by a factor of 16. Viscosity is affected by temperature, red blood cell mass, and protein concentration [1].

2.3.3 Coronary Circulation

Coronary circulation is of special interest in the setting of this research as it is closely tied to ischemia. The energy requirements of the heart include basal metabolism (20%), electrical activation (5%), and mechanical contraction (75%). The major determinants of local metabolic rate and oxygen delivery are shown in Fig. 2.22.

Myocardial oxygen demand is directly related to heart rate, wall tension, and contractile state. Wall tension is related to ventricular volume (preload) and ventricular pressure. Contractility is related to the maximal rate of increase in systolic pressure. There is also a transmural gradient of wall tension, with greater tension in the subendocardium relative to subepicardium. Moreover, the basal oxygen demand is believed to be higher in the subendocardial region [59]. Major oxygen supply determinants include local perfusion and the amount of oxygen extraction from the blood. Moreover, oxygen extraction is influenced by oxygen content in the arterial blood, oxygen diffusion gradient, and blood flow velocity through the capillaries. At rest, oxygen extraction is near 75% and can rise to 90% under

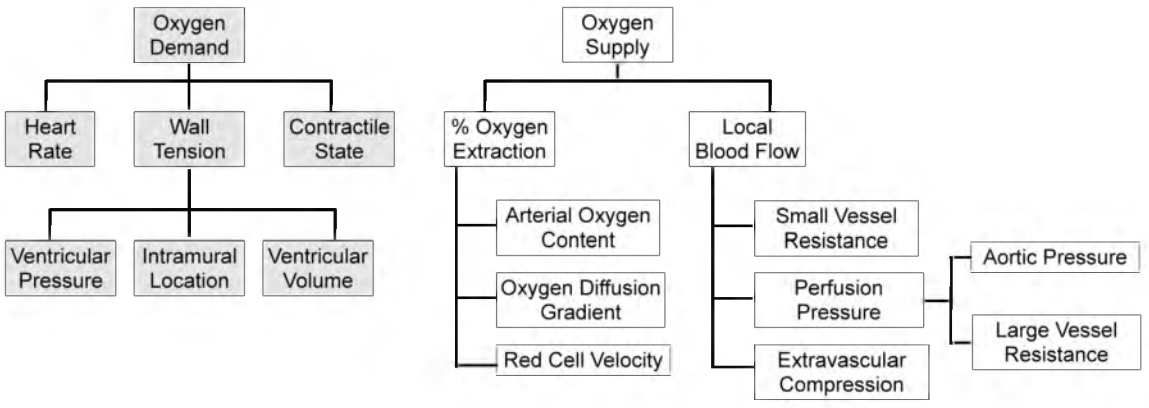

Fig. 2.22. Myocardial oxygen determinants: Major determinants of oxygen demand and supply to the heart.

stress conditions. Since the oxygen extraction is already high, any increase in metabolic demand must be met by a corresponding increase in coronary blood flow.

The heart relies primarily on continual resynthesis of mitochondrial ATP for its energy supply. At rest, the energy substrates include β oxidation of free fatty acids (60–70%) and metabolism of carbohydrates (30%) [1]. During exercise, oxidation of free fatty acids is inhibited, and carbohydrates become the primary mode for ATP production. The heart has reserves of high-energy phosphates (HEP) and phospocreatine (PCr), which can be used to generate ATP, but they can buffer the ATP levels for only a short period (15–30 seconds) in the absence of coronary blood flow [1]. Coronary flow is regulated variously by metabolic, mechanical, autonomic, and endothelial controls.

"Autoregulation" refers to the phenomenon in which a change in aortic pressure is met by the adjustment of coronary vascular resistance to ensure constant blood flow and is effective only in the range of 60–140 mmHg of systemic arterial pressure [1]. "Autoregulatory reserve" is a related term that refers to the maximal degree of vasodilation in the coronary perfusion bed and determines the perfusion pressures over which coronary flow is maintained. Thus, if a vascular bed is already maximally vasodilated, the capacity to autoregulate in the face of a further decrease in perfusion pressure is severely limited. Autoregulation is largely a local phenomenon mediated by myogenic tone (a change in tone in response to changes in pressure and flow) and metabolic means (washout of vasoactive metabolites such as adenosine) [1].

Most coronary flow occurs during diastole, when the perfusion pressure is greater than the intramyocardial pressure [60]. During ventricular systole, the intramyocardial tissue pressure gradient (decreasing towards the epicardium), through extravascular compression, causes a parallel gradient in systolic coronary vascular resistance [61]. Moreover, as the intramyocardial tissue pressure is greater than the coronary driving pressure, the coronary flow decreases and may cease in the subendocardium during systole. During ventricular diastole, the intramyocardial tissue pressure is similar across the myocardium, and the gradient in diastolic coronary vascular resistance exists (decreasing towards the endocardium) due to dilation of subendocardial coronary vessels [62]. The result is greater diastolic flow in the subendocardium over subepicardium. Thus, the subepicardium receives 90% of flow during systole and 10% during diastole. The midmyocardium receives an equal amount of blood flow in systole and diastole while the subendocardium is perfused primarily during diastole [1]. Moreover, the ratio of subendocardial flow to subepicardial flow is approximately 1.1:1, as the intrinsic coronary vascular resistance in the subendocardial arteries is lower.

2.3.4 Integrated Control of Cardiovascular Physiology

The autonomic nervous system (ANS) influences the smooth muscle tone of coronary arteries to modulate coronary flow, as shown in Fig. 2.23. The epicardial coronary arteries have both α-adrenergic (vasoconstriction) and β-adrenergic receptors (vasodilation) to mediate coronary flow. The α-adrenergic receptors mediate the release of norepinephrine (NE) during sympathetic stimulation, which can cause vasoconstriction of arteries. The stimulation of β_2-adrenergic receptors by circulating catecholamines results in coronary vasodilation. That said, the role of ANS in coronary flow regulation is often overshadowed by metabolic and mechanical factors [1].

An endothelium-dervied relaxing factor (EDRF) such as nitrous oxide (NO) is a powerful vasodilator and its release is triggered by a number of stress signals (e.g., hypoxia) and distending forces in the vascular wall [1].

The ANS influences vasomotor tone and cardiac function through its sympathetic (SNS) and parasympathetic (PNS) divisions to achieve an integrated and dynamic response, which entails integrating inputs from the cerebral cortex and specialized sensors (e.g., mechanoreceptors) into brain regions (hypothalamus, pons, medulla) and transmitting

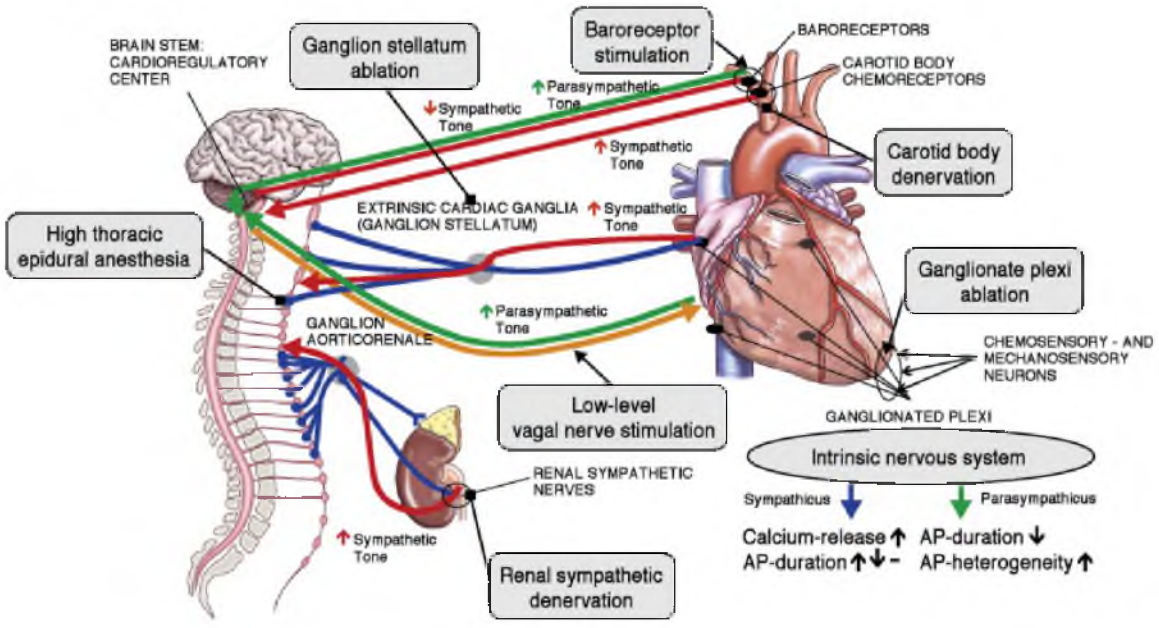

Fig. 2.23. Integrated control of cardiovascular physiology: Schematic of the CNS control. Reprinted with permission from American College of Cardiology Foundation. D. Linz, C. Ukena, F. Mahfoud, H. Neuberger, and M. Bohm, "Atrial autonomic innervation: A target for interventional anti arrhythmic therapy?" Elsevier (2014). *Journal of American College of Cardiology*, vol. 63(3), pp. 215-224, 2014.

efferent nerve impulses to the periphery over sympathetic and parasympathetic systems [1].

The parasympathetic system plays a relatively minor role in arterial pressure mediation, but an important role in modulating heart rate. The heart rate is maintained at a constant value (typically approximately 70 bpm in humans) via a continuous firing of the vagus nerve. Parasympathetic discharge increases potassium ion permeability in cardiac myocytes, thus increasing the threshold for depolarization to occur spontaneously in the SA node. As a result, the heart rate declines (negative chronotropic effect) and, with it, the cardiac output. This autonomic neural input predominates during sleep and other sedentary states, eliciting an increase in cardiac cycle time and therefore enabling the heart to expend less energy. Parasympathetic stimulation also slows conduction velocity (negative dromotropic effect) and decreases contractility (negative inotropic effect) although its impact on heart rate is much more potent.

Increased sympathetic activity increases heart rate by releasing norepinephrine, which causes a rise in the SA node depolarization rate (positive chronotropic effect). The increase in heart rate is due to an increase in activated calcium channels, which increases the speed at which depolarization occurs. This increased sympathetic outflow can be initiated by a large array of internal and external stimuli: exercise, increase in body temperature, trauma, or stress. Cardiac output is also increased with increased SNS activity by increasing stroke volume. The underlying mechanism for this increased SV is the enhanced cardiac myocyte contractility. Myocytes usually increase in length in proportion to their preload, and because they become more elongated, they also have the capability to shorten over a greater distance. This increased shortening leads to enhanced strength of contraction. The sympathetic excitation also facilitates a larger and more rapid calcium influx, which further augments the degree of overall contraction during systole. The time necessary for the heart to contract and relax fully decreases under sympathetic stimulation due to a larger proportion of the cardiac cycle that is made available for filling. Although an increase in heart rate makes the total duration of the cardiac cycle shorter, there is a decrease in the amount of time necessary for contraction of the heart. Thus, the heart is relaxed for a greater portion of the cycle, enabling enhanced filling to provide a greater volume of blood ejected for each contraction. Epinephrine also increases calcium influx and uptake by SR by stimulating the β receptors and thus acts a positive inotropic agent.

The stimulation and withdrawal of SNS activity are also powerful regulators for peripheral coronary circulation. Changes in blood supply to local tissue or organs are mediated by changes in resistance of peripheral vasculature in response to the need for blood elsewhere.

Control of the vascular peripheral resistance is achieved by varying the firing frequency with these sympathetic fibers. More specifically, postganglionic fibers release norepinephrine, which binds to α_1-adrenergic receptors within the smooth muscle cells in the arteriolar walls and causes an overall decrease in the diameter of arterioles (vasoconstriction). In contrast, lowering the basal tonic activity causes vasodilation since less norepinephrine is available for binding, causing the smooth muscle cells to relax. Sympathetic stimulation of a subset of fibers originating in the cerebral motor cortex releases epinephrine (instead of norepinephrine), which stimulates both α and β receptors. The effect of epinephrine at low concentrations is to produce vasodilation and at high concentrations is to induce vasoconstriction [1].

The arterial baroreceptor system regulates arterial pressure in the short term. The baroreceptors are primarily located in the walls of the aorta and carotid arteries. They sense both the magnitude and rate of stretch of arterial walls because of pressure fluctuations within the vessels. The afferent fibers projecting from the baroreceptors convey this information to the ANS, which in turn responds by either increasing or decreasing sympathetic or parasympathetic drive. The baroreceptor reflex functions as a negative feedback system, such that a decrease in arterial stretch induces an increased sympathetic discharge, resulting in raising the cardiac output. The increase in cardiac output increases the blood delivered to vessels containing baroreceptors, increasing arterial pressure, and, in turn, decreasing the tonic activity of these receptors. Homeostatic control of arterial pressure is managed because a decreased baroreceptor discharge rate causes a lower degree of sympathetic activity and results in cardiac slowing and a decrease in blood pressure. Long-term pressure regulation is not accomplished via baroreceptor input because of the adaptive nature of baroreceptors as described above. If the pressure in the aorta and carotid arteries remains elevated for sustained periods, the tonic firing rates will eventually return to resting values regardless of whether the pressure remains elevated. Long-term pressure regulation involves complex hormonal mechanisms administered by medullary cardiovascular centers.

2.4 Coronary Heart Disease (CHD) and Ischemia

Nearly 30% of deaths worldwide can be attributed to cardiovascular diseases [1]. Moreover, CHD afflicts nearly 13.7 million Americans, and the socioeconomic costs associated with CHD amounted to $165 billion dollars in 2009 [1].

CHD represents a spectrum of disease pathologies: chronic CHD, acute coronary syndromes (ACS), and sudden cardiac death. ACS represents all forms of myocardial ischemia

(e.g., atherosclerosis, coronary thrombosis, vasospasm) and myocardial infarctiona. Although CHD is typically attributed to coronary arterial disease (CAD) [63], other causes (e.g., congenital defects) can also precipitate an ACS event [1].

Myocardial ischemia is defined as an imbalance between the supply of oxygenated blood and the oxygen requirements of the heart [3], as shown in Fig. 2.24. The degree of imbalance between blood supply and demand varies and is qualified accordingly as mild, moderate, and severe [64]. Complete abolition of blood flow is termed "total ischemia." When myocardial ischemia is limited to a region of the heart and not the whole heart, the term "regional ischemia" is used. If the entire heart becomes ischemic (e.g., due to aortic stenosis), the term used is "global ischemia" [5].

A major component of ischemia is hypoxia, which refers to an imbalance between oxygen supply and oxygen requirements of the heart. In addition, ischemia is characterized by a reduction in the supply of metabolic substrates as well as a reduction in removal of catabolites. The onset of ischemia has immediate cellular consequences: metabolic (e.g., anaerobic glycolysis), structural (e.g., cell swelling), ionic (e.g., hyperkalemia), neurohumoral (e.g., release of catecholamines), electrical (e.g., rise in resting potential), and functional (e.g., contractile dysfunction) consequences.

Initially, cellular consequences of myocardial ischemia are reversible, but eventually damage occurs to critical subcellular organelles that is irreversible, which results in cellular necrosis, followed by an inflammatory response, macrophage removal of dead myocytes, and

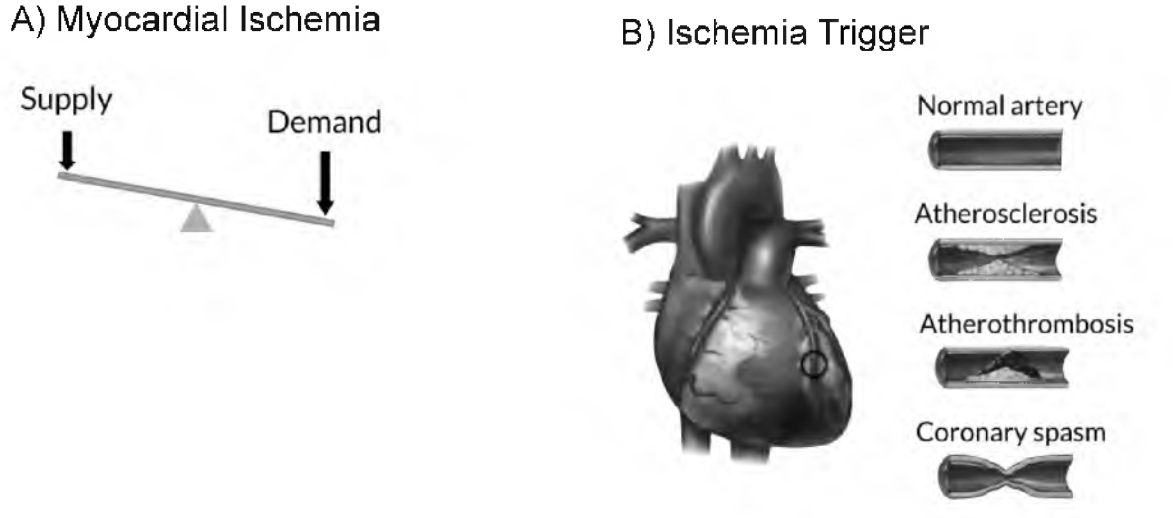

Fig. 2.24. Myocardial ischemia: (a) Schematic of supply and demand imbalance, (b) various ischemia triggers.

replacement by scar [5]. Restoration of blood flow (reperfusion) during the reversible phase of ischemia prevents cell death, and cellular structural, functional, and metabolic properties eventually recover. Conversely, reperfusion after cell death occurs often exacerbates the situation by causing cell swelling, massive calcium overload, disruption of the contractile apparatus, and damage to the microvasculature.

2.4.1 Definition and Classification

ACS includes all forms of acute myocardial ischemia (atherosclerosis, thrombosis, vasospasm, etc.), acute myocardial infarction including NSTEMI (non-ST segment elevated myocardial infarction) and STEMI (ST segment elevated myocardial infarction), and unstable angina.

2.4.1.1 Atherosclerosis, Coronary Thrombosis, Atherothrombosis

Atherosclerosis is a preexisting condition in the setting of ACS, described as a lipid-induced, inflammatory, systemic vascular disease leading to plaque formation [65]. Such plaque deposits typically form in locations associated with low shear stress (e.g., bifurcations, inner wall of curvatures) and regions with intimal thickenings [66]. They are heterogeneous in size and in their composition (fibrous tissue, necrotic lipid-rich core, foam cells, macrophages, and calcium deposits) [1].

Coronary thrombosis is the release of a free floating plaque (or "thrombus") in the vasculature, typically induced by plaque rupture [65] or plaque erosion [67]. When these thrombi eventually lodge in a vessel narrowing, they cause obstruction of coronary blood flow to the affected region and trigger the onset of myocardial ischemia and acute coronary syndrome (ACS). Atherothrombosis is atherosclerosis superimposed with thrombosis and is associated with high-risk or vulnerable plaques.

2.4.1.2 Angina Pectoris

Angina pectoris (chest pain) is characterized by a crushing, burning, or squeezing type of discomfort that may spread to the lower part of the neck and also radiate down the left arm. Typically, the pain lasts for 5–10 minutes and is attributed to the stimulation of sensory nerves surrounding the coronary arteries, possibly by adenosine [1]. In the clinical setting, angina pectoris is categorized as primary angina, secondary angina, unstable angina, or syndrome X.

Demand ischemia or effort induced angina is the result of increased metabolic demand

on the heart (e.g., due to exercise) and the inability of the coronary blood flow to keep up. It is also called *secondary angina* as ischemia is secondary to increased oxygen demand and is relieved when the patient stops exercising, leaves the stressful situation, or receives a vasodilator (e.g., nitroglycerin) [1].

Supply ischemia or primary angina is the result of a decrease in coronary flow (e.g., due to atherosclerosis or vasospasm) without a change in myocardial metabolic demand. Primary angina due to vasospasm is also called *variant angina* or *Prinzmetal angina*. The precise mechanism behind coronary vasospasm is not completely understood but is generally attributed to vasoconstrictors such as norepinephrine or epinephrin [1]. Primary angina can also be relieved through administration of vasodilators.

Unstable angina, also known as *preinfarction angina, intermediate coronary syndrome, and acute coronary insufficiency*, is manifested as a sudden worsening of chronic angina and may occur at rest or with exertion [1].

Syndrome X is a condition in which patients with angiographically normal coronary arteries test positive for ischemia during an exercise stress test and perfusion defects [1]. Although the exact mechanism behind this condition is not fully understood, it is commonly attributed to microvascular dysfunction [68].

Silent ischemia is a condition in which the patient with myocardial ischemia does not experience any chest pains. On the other hand, anginal pain can occur in the absence of ischemia, perhaps due to some form of gastrointestinal disorder.

2.4.1.3 Myocardial Infarction, STEMI, NSTEMI

Myocardial infarction refers to irreversible ischemia and results from severe and prolonged ischemia as a result of severe atherosclerosis or thrombosis. It is characterized by cell death.

NSTEMI or non-ST segment elevated myocardial infarction is a diagnosis of acute MI, in which the patient has chest pain and shows elevated levels of myonecrosis biomarkers such as troponin and creatine kinase myocardial band (CK-MB), but ST segment elevation or Q-waves indicative of myocardial infarction are not evident on the ECG [1].

STEMI or ST segment elevated myocardial infarction refers to the most severe manifestation of ACS and results in a manifestation of ST segment elevation and Q-waves on the ECG in addition to the presence of angina and elevated serum troponin and CK-MB levels [1].

2.4.2 Metabolic Consequences

In the absence of blood flow, the relatively small quantities of oxygen remaining in the capillary red blood cells (RBCs) get used up, and the decreasing tissue oxygen content is reflected in the appearance of cyanosis of the myocardium within the first 5–15 seconds of moderate to severe ischemia [5].

Without oxygen as the final electron receptor, oxidative mitochondrial metabolism is inhibited, and the glycogenolysis and anaerobic glycolysis are accelerated. However, this form of HEP production is inefficient as only two molecules of ADP can be phosphorylated per molecule of glucose converted to lactate. This amount is in contrast to 38 molecules of ATP created by complete oxidation of glucose to carbon dioxide and water [5]. In the end, anaerobic glycolysis can produce only about 7% of HEP needed by normal working myocardium [69].

Myocardial reserve stores of HEPs are limited and are sufficient for approximately 30 seconds of normal myocardial activity [4]. The contractile function is rapidly downregulated during ischemia. Even so, electrical activity and minimal mechanical activity use up the HEP reserves. Creatine phosphate is completely depleted within the first 3 minutes [70], and ATP content declines more slowly to about 35% of control by 15 minutes [71]. After 10 minutes of severe ischemia, declining ATP content is matched by declining levels of ADP [5]. Thus, there is rapid degradation of total adenosine nucleotide pool.

Severe ischemia also activates other forms of energy production, including lipid and protein metabolism, with diminishing returns. During ischemia, there is an accumulation of small quantities of fatty acids [72]; however, oxidation of fatty acids to carbon dioxide and water is again a mitochondrial process requiring oxygen. On the other hand, increased fatty acid and ampiphiles concentration in the plasma membrane, gap junction, and intracellular membranes of the SR and the mitochondria [73] has other detrimental cellular consequences: contractile dysfunction, inhibition of various enzymes, gap junction inhibition, and even cell membrane degradation [74]. Protein synthesis and protein degradation are energy-requiring processes and thus terribly inefficient [75].

Cessation of blood flow also implies nonremoval of catabolic waste products. There is a rapid accumulation of lactate (end product of anaerobic glycolysis), purines (breakdown of adenine nucleotides), and other catabolites [5]. Tissue acidosis increases rapidly as a result of several catabolic processes (e.g., glycolysis, lipolysis, and ATP hydrolysis), which has deleterious consequences, including inhibition of various metabolic pathways [76]. The inhibition of the metabolic pathways creates a cascading effect, including contractile

dysfunction, aggregation of nuclear chromatin, and formation of mitochondrial amorphous matrix densities [77].

Ischemia also increases the production of free radicals (e.g., superoxides), and their high reactive nature causes detrimental alterations in proteins, nucleic acids, and lipids [78]. They block most K^+ currents and activate SR Ca^{++} release channels, thus reducing AP upstroke and conduction velocity and increasing APD [4]. The activation of SR calcium release eventually triggers mitochondrial calcium overload and signals cell death.

2.4.3 Structural Consequences

During the first 15 minutes of severe ischemia (reversible phase), the principal ultrastructural changes include mild edema of the sarcoplasm, diminution of glycogen deposits, relaxation or stretching of myofibrils, and mild margination of nuclear chromatin [79]. In addition, mitochondria show loss of normal matrix granules and disorganization of cristae [80].

Longer periods of ischemic insult result in more marked changes. Nuclear chromatin is aggregated along the nuclear membrane, glycogen becomes severely depleted, mitochondrial swelling and loss of cristae become severely pronounced, and cell swelling is accentuated [81]. Amorphous densities develop within the matrix space of mitochondria and breaks in the plasmalemma of the sarcolemma appear, signaling the onset of irreversible phase of myocardial injury [64].

2.4.4 Ionic Consequences

Myocardial ischemia triggers changes in intracellular and extracellular concentrations of various ions: increases in extracellular K^+, intracellular Na^+, intracellular and extracellular H^+, intracellular Ca^{++}, and intracellular Mg^{++}.

2.4.4.1 Extracellular K^+ Accumulation

The onset of ischemia results in an increase in the extracellular K^+ concentration and occurs in three phases [82]. The initial phase begins within 20 seconds of the ischemia onset and lasts from 3 to 10 minutes, resulting in K^+ levels rising to 15 mM [83] (from approximately 4 mM), which is followed by a second phase (10–15 minute period), during which K^+ does not change or may actually decline slightly, which is attributed to the activation of the $Na^+ - K^+$ pump [5]. Following this plateau phase, K^+ rises again, but at a slower rate, which is believed to mark the transition to irreversible myocardial ischemia or cell necrosis. The rise in extracellular K^+ is attributed to shrinkage in the extracellular

space (ECS), inhibition of active K^+ influx, and an increase in passive K^+ efflux [4]. The shrinkage in ECS is due to osmotic movement of water into the capillaries. The K^+ influx is reduced due to partial inhibition of $Na^+ - K^+$ pump activity. The increased K^+ efflux is attributed to increased conductance due to the ionic currents $I_{KATP}, I_{KAA}, I_{KNa}$ and also to the existence of an inward leak current (I_{Na}, I_{NSC}, I_{Cl}) [4]

The increase in extracellular K^+ depolarizes the resting membrane, reduces the maximum rate of rise of the AP upstroke (V_{max}), lowers the AP amplitude and plateau potential, accelerates the slope of rapid repolarization, and in Purkinje fibers, decreases the rate of spontaneous diastolic depolarization [84]. The change in resting membrane potential is attributed to the change in the potassium equilibrium potential (E_K), and the change in V_{max} is due to inactivation of the rapid Na^+ inward current, which is dependent on the membrane potential at the onset of depolarization [5]. The increase in extracellular K^+ also delays the recovery of V_{max}, which prolongs the recovery of excitability [4].

Increasing extracellular K^+ has a biphasic effect on excitability and conduction. During the initial phase of K^+ efflux, the rising resting potential also decreases the threshold for excitability so that excitability and conduction are increased [4]. At higher levels of K^+, however, the rise in resting potential exceeds the threshold potential. Moreover, the slowing of V_{max} secondary to inactivation of Na^+ current becomes dominant, resulting in a decrease in excitability and a slowing of conduction [5].

If the blood flow is restored before the irreversible phase, the extracellular K^+ rapidly recovers to normal levels, but full recovery can take up to 60 minutes [64].

2.4.4.2 Intracellular and Extracellular Acidosis

There is also a fall in extracellular pH concomitant to rising extracellular K^+. However, the pH level falls continuously and without a plateau until the maximum level of 6.0 is reached and remains constant thereafter [85]. The fall can be attributed to increased production and the inability to remove the accumulating protons due to dysfunction of Na^+-H^+ exchanger, Na^+-HCO_3^- cotransport, and CO_2 removal [4].

Extracellular and intracellular acidosis impairs the functioning of most cell membrane channels, except I_{KATP} and I_{KAA}, by decreasing single channel conductance and reducing tissue oxygen, which leads to a rise in resting membrane potential [4]. Acidosis also results in a decrease in conduction velocity, a decrease in V_{max}, and an increase in internal longitudinal resistance, which collectively are responsible for cellular uncoupling and thus a slowing of conduction [5]. The prolongation of AP (due to slower recovery of Na^+ channels) and the occurrence of extra afterdepolarizations (EADs) that are thought to be responsible for

ectopic electrical activity are more likely to take place during reperfusion [4]. Recovery of pH is rapid (3–5 minutes), if blood flow is restored before irreversible injury sets in [4].

2.4.4.3 Intracellular Na^+ Accumulation

The intracellular Na^+ concentration nearly doubles (10 to 20 mM) due to impairment of the normal functioning of the Na^+-K^+ pump that uses ATP to transport Na^+ out of the cell [4]. Moreover, there is an increased influx of Na^+ via the Na^+ - H^+ exchanger and other inward leak currents: I_{Na}, I_{NSC}, and I_{Cl}. The accumulation of Na^+ is higher in the supepicardial cells compared to subendocardial cells [85]. Intracellular Na^+ accumulation reduces excitability due to hyperpolarization by triggering activation of multiple outward K^+ channels: I_{KNa}, I_{Ks}, and I_{KACh}. However, if blood flow is restored during the reversible phase, the intracellular Na^+ concentration is restored within 5 minutes [4].

2.4.4.4 Intracellular Ca^{++} Accumulation

Calcium is stored intracellularly in the SR and mitochondria, in addition to being available in the cytoplasm. There is an increase in systolic Ca^{++} that occurs within the first minutes of ischemia, and the mitochondrial Ca^{++} follows the systolic changes in cytosolic Ca^{++}. The increase in diastolic Ca^{++} is seen 10–20 minutes into the ischemic injury [4]. The increase in intracellular calcium can be attributed to the reduced ability to remove calcium through the Na^+-Ca^{++} exchanger (due to increased intracellular Na^+), reduced Ca^{++} uptake by the SR (through Ca^{++}-ATPase), an increase in inward leak current (activated by free radicals and mechanical stretch), and displacement by H^+ from the calcium binding sites (due to intracellular acidosis) [4].

An increase in cytosolic Ca^{++} modulates the number of channels, carriers, and enzymes and results in the shortening of APD (due to inactivation of I_{CaL}) and the occurrence of EAD, DAD, and arrhythmias upon reperfusion (due to premature SR release of calcium or increased conductance of leak currents) [4]. Depending on the severity and duration of the ischemic insult, the cytosolic Ca^{++} may normalize rapidly, fall to an intermediate level, and then eventually return to normal value or not recover at all and rather rise to more elevated levels, leading to cell death.

2.4.4.5 Intracellular Mg^{++} Accumulation

During ischemia, there is an increase in intracellular Mg^{++} due to ATP hydrolysis, to which Mg^{++} is bound, and also due to inefficient removal of Mg^{++} via Mg^{++}-ATPase and Na^+-Mg^{++} exchanger [4]. Increased intracellular Mg^{++} affects normal channel and

carrier function by its effect on phosphorylation, blocking of Na^+ and Ca^{++} channel pores, and by reducing outward K^+ currents through open channel block, thus triggering inward rectification [4]. The blocking of Ca^{++} channel pores has a protective effect by preventing mitochondrial calcium overload. Due to its effect on both Ca^{++} and K^+ channels, it may cause AP shortening or lengthening depending on which currents are most affected.

2.4.4.6 Activation of Stretch-Sensitive Channels

Stretch, whether induced by tension or an increase in volume (e.g., cell swelling), results in activation stretch-sensitive inward currents (I_{NSC}, I_{Cl}, I_{CaL}) and outward K^+ currents [4]. Cumulatively, these currents can result in depolarization or shortening of AP based on which currents are dominant. In any case, these changes are conducive to arrhythmias.

2.4.4.7 Increase in Tissue Resistivity

The onset of ischemia brings about an increase in tissue resistance: an increase in longitudinal extracellular resistance and longitudinal intracellular resistance [86]. This increase in resistance occurs in three phases. The first phase occurs immediately, resulting in an increase in extracellular resistance by 30%, and remains at that plateau level for approximately 5 minutes [87]. The second phase is characterized by a steady rise to nearly 160% of normal extracellular resistance and occurs over 10 minutes [87]. The third phase coincides with the irreversible phase (15–20 minutes after the onset of ischemia) and is characterized by an increase in intracellular resistance due to the closure of gap junctions. The increase in extracellular resistance is associated with cell swelling and shrinkage of extracellular space [88].

2.4.5 Neurohumoral Consequences

The onset of ischemia triggers the release of catecholamines in the systemic circulation and subsequently a delayed local release. α-receptor stimulation activates PKC phosphorylation that increases some K^+ currents (I_{Ks}, I_{KACh}, I_{KATP}, I_{KAA}) but decreases others (I_{to}, I_{Kur}, I_{K1}) [4]. It also causes a decrease in gap junction conductance, while potentiating the function of exchangers: Na^+-Ca^{++}, Na^+-K^+ and Na^+-H^+ exchangers [4]. The varied effect on K^+ currents can cause the cells to depolarize or hyperpolarize, whereas APD is increased due to its effect on the Na^+-Ca^{++} exchanger. If delayed afterdepolarizations (DADs) are already being caused by inward calcium leak, α-receptor stimulation increases the rate of occurrence. On the other hand, if DADs are being triggered by Na^+-K^+ pump

inhibition, the stimulating effect on the pump by α-receptor diminishes their incidence [4].

β- receptor stimulation activates most outward and inward cell membrane currents, gap junction channel conductance, and the SR calcium release channel [4], which leads to an increase in pacemaker activity (due to increased I_{CaL}) and increased AP amplitude (due to increased I_{Na}) and AP duration (due to increased I_{CaL}). In contractile cells, the AP amplitude is increased and the AP duration is shortened (stimulation of I_{KATP}). However, excessive β receptor activity can lead to calcium overload [4].

Adenosine and ACh release is enhanced during ischemia, and the effect is generally opposite to β-receptor stimulation. The gap junction conduction is reduced as are inward currents: I_{Ca}, I_{Cl}, and I_f [4]. On the other hand, I_{KACh} and I_{KATP} are enhanced. Cumulatively, these effects result in hyperpolarization, shortening of AP, reduced pacemaker activity, and inhibition of afterpolarizations (EAD and DAD) [4].

2.4.6 Electrical Consequences

The electrical consequences of ischemia that most influence tissue level behavior include a rise in resting potential, shortening of AP amplitude and duration, prolongation of ERP, a decrease in conduction velocity, and a change in excitability. Some of these changes also manifest on the ECG as changes in the morphology, amplitude, or polarity of various features: ST segment, T-wave, and the QRS complex. Moreover, ischemia also enables the development of arrhythmias.

2.4.6.1 ECG Changes

Fig. 2.25 summarizes the most important ischemia induced changes in the ECG. The rise in resting potential (due to increased K^+ efflux) causes a TQ segment shift [89]. The

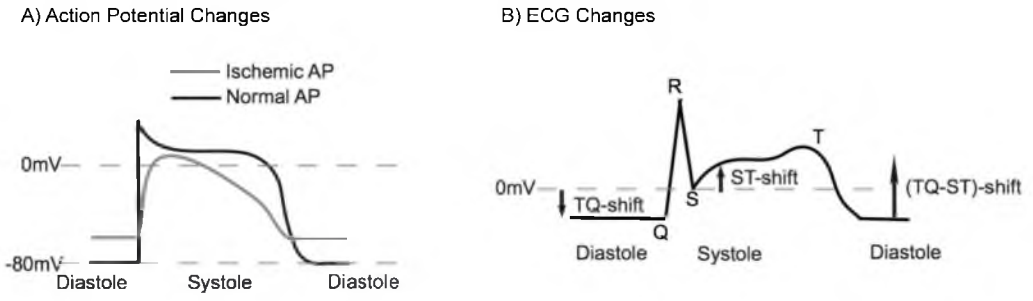

Fig. 2.25. Electrophysiological consequences of ischemia: (a) Change in action potential duration and amplitude, (b) corresponding changes on the ECG.

shortening of AP duration due to activation of I_{KATP} causes an ST segment shift [90]. The T-wave inversion is associated with reversal in transmural dispersion of repolarization due to shortening of the APD in the ischemic regions [91]. The slowing of conductance due to the fall in Na^+ and later an increase in longitudinal resistance corresponds to broadening of the QRS complex. The ERP is prolonged due to the slower recovery of inactivated Na^+ channels.

2.4.6.2 Arrhythmias

Arrhythmias require automacity, i.e., triggered activity (EAD or DAD), and a pathway for reentry, as shown in Fig. 2.26. During ischemia, automacity can be achieved in multiple ways: EAD and DAD (due to Ca^{++} overload and catecholamines release), excessive stretching of border zone cells, and activation of I_f in atrial and ventricular cells. The heterogeneity of ERP and slowed conduction also enhance the likelihood of there being a viable pathway for reentry during ischemia. Arrhythmias that occur during the first 30 minutes of ischemia typically fall into the category of are known as" Ia and Ib arrhythmias." [86] Phase Ia is initiated through intramural border zone reentry and evolves into multiple wavelets. Phase Ib mechanisms are believed to be associated with a combination of Ca^{++} overload, release of catecholamines, and increase in longitudinal resistance [4].

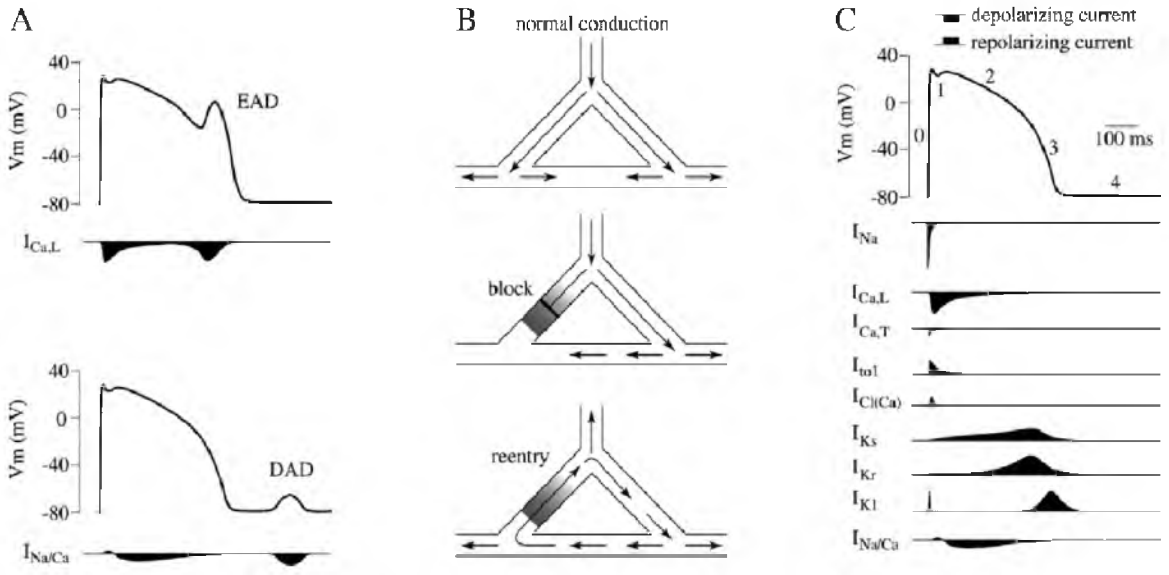

Fig. 2.26. Ischemia induced arrhythmias. Reprinted with permission from Oxford University Press. H. D. Den Ruijter, G. Berecki, T. Opthof, A. Verkerk, P. Zock, and R. Coronel, "Pro and anti arrhythmic properties of a diet rich in fish oil," *Cardiovascular Research*, vol. 73(2), pp. 316-325, 2007.

2.4.7 Functional Consequences

Myocardial ischemia is the consequence of an imbalance between blood flow to the heart and its metabolic requirements (heart rate, wall stress, contractility). Contractile dysfunction is one of the earliest functional consequences occurring within 5–10 seconds after the onset of ischemia [92]. Moreover, depending on the degree and duration of the ischemic injury, myocardial region affected, and the presence of collateral vessels from the adjacent vascular bed, ischemia has a variety of consequences: angina pectoris, myocardial stunning, myocardial hibernation, pre- or postconditioning, and under critical circumstances, myocardial infarction with subsequent heart failure [1].

2.4.7.1 Myocardial Stunning

Myocardial stunning refers to a prolonged and fully reversible myocardial dysfunction even after restoration of normal blood supply to the ischemic heart [1]. Myocardial stunning is generally attributed to the effect of reactive oxygen species (ROS) released during the first minutes of reperfusion and subsequent impairment of calcium handling in the affected myocytes [93].

2.4.7.2 Myocardial Hibernation

Myocardial hibernation refers to a chronic ventricular dysfunction in patients with chronic ischemic disease that becomes reversible after revascularization [94]. Myocardial hibernation is believed to result from a prolonged subacute or chronic state of myocardial ischemia that does not progress to necrosis but leads to a downregulation of myocardial metabolism and function to compensate for reduced coronary blood flow, thus achieving a new equilibrium [1].

2.4.7.3 Myocardial Preconditioning, Myocardial Postconditioning, Remote Preconditioning

Myocardial preconditioning refers to the phenomenon where brief episodes of ischemia produce a cardioprotective response during a subsequent longer episode of ischemia [95]. The ischemic preconditioning occurs in the two phases: acute ischemic preconditioning (first window) and delayed ischemic preconditioning (second window). The first window is characterized by the release of ischemia-stimulated mediators such as adenosine, opioids, etc., that activate the mitochondrial K_{ATP} channel, which prevents the opening of the mitochondrial permeability pore at reperfusion and thus prevents triggering apoptosis and necrosis. The acute phase of ischemic preconditioning is believed to last 60–120 minutes [96].

The second window is more persistent and is believed to last 3–4 days [96]. Myocardial post-conditioning refers to cardioprotective response due to brief periods of ischemia alternated with brief periods of reperfusion following lethal ischemia (e.g., infarction) [1]. Remote preconditioning refers to ischemia in one organ producing a protective response in another distal organ.

2.4.7.4 Myocardial Infarction (MI)

The irreversible phase of ischemia typically sets in 15–20 minutes following coronary occlusion and is marked by cell death that can be triggered by cell necrosis (physical disruption of sarcolemma) or cell apoptosis (programmed cell death) [9]. In the longer term (weeks to months and even years after the insult), the myocardium undergoes structural and functional remodeling to compensate for loss of cardiac muscle, which leads to scar formation and may eventually result in heart failure [1].

2.4.8 Diagnosis

Early and accurate detection of myocardial ischemia is an essential component of managing CHD. Various noninvasive (e.g., ECG, Echo, SPECT) and invasive diagnostic tools (e.g., angiography) are available for CAD detection. Moreover, treatment options vary from pharmacologic (e.g., nitrates) to revascularization (e.g., PCI, CABG) depending on the severity of the ischemia.

2.4.8.1 Patient History and Physical Examination

Past episodes of unstable angina or myocardial infarction, family history of premature atherosclerosis, and presence of CHD risk factors such as hypertension, diabetes, obesity, etc., provide valuable information and indicate a higher risk of ACS.

Chest pain or discomfort is a common manifestation of myocardial ischemia. The chest pain tends to radiate across the chest into the arms (left more than right) and neck, jaw, and back [1]. The pain lasts for 5–10 minutes and goes away after cessation of activity or with use of sublingual nitrates. The onset of shortness of breath, nausea, and vomiting during or after chest discomfort also suggests severe myocardial ischemia or myocardial infarction [1].

However, myocardial ischemia and myocardial infarction can manifest without chest pain. Such silent ischemia and even painless MI occur in up to 40% of CAD patients [1]. Moreover, chest pains are not specific to ACS and can be caused by other cardiac (e.g., pericarditis, mitral valve prolapse) and noncardiac events (e.g., anxiety, gastrointestinal

disorder) [1]. Finally, the description of pain is subjective and relies on the ability and willingness of the patient to share information.

2.4.8.2 Exercise ECG Stress Testing (ET)

Exercise stress testing is a noninvasive tool that uses exercise (e.g., running, biking) as the physiologic stress to monitor and evaluate the response of the cardiovascular system. The physiologic principle behind exercise testing is that total body oxygen uptake (VO_2) and myocardial oxygen uptake are distinct [1] and that patients experience significant shortfalls in myocardial oxygen supply before their total oxygen becomes critical. VO_2 is defined as the amount of oxygen extracted from inspired air as the body performs work and is estimated as the product of external work (cardiac output) and arteriovenous oxygen difference ($A - VO_2$). Since arteriovenous oxygen difference is approximately 15–17% at maximal exercise, VO_{2max} is then an indirect estimate of cardiac output [1]. Myocardial oxygen uptake is the amount of oxygen required only by the heart and is given as the product of heart rate and systolic blood pressure. During exercise, any unmet needs in cardiac demand can help identify abnormalities in myocardial perfusion and function such as myocardial ischemia. Moreover, ischemia produces changes in the body surface ECG (e.g., ST segment shifts, T-wave changes).

Exercise protocols either on a treadmill or a bicycle ergometer are designed to progressively ramp up speed and grade and last for 8–12 minutes [1]. The protocols are often individualized based on factors such as subject's physical abilities, age, and gender. The metabolic equivalent of the task (MET) is a commonly used metric for oxygen requirement of work rate during an exercise test. 1 MET is equated with the resting metabolic rate (3.5 mL of O_2/kg/min), and a MET value achieved from an exercise test is a multiple of resting metabolic rate, either measured directly through oxygen uptake or from maximal workload calculated using standard equations [97]. Typically, achieved maximal MET values less than 10 are associated with a poor prognosis [1].

ST segment depression on the ECG is typically the metric for exercise testing. The standard criterion for a positive test is 1 mm of horizontal or downsloping ST segment depression (in lead V_5) below the baseline or a further 1 mm if the baseline is already depressed [1], as shown in Fig. 2.27. ST segment elevation is indicative of severe transmural ischemia.

While ST segment depression is a marker of acute ischemia, it has a very poor ability to localize the size or extent of myocardial tissue that experiences ischemia. Moreover, ST segment depression in inferior leads (e.g., II, aVF) need not be indicative of myocardial

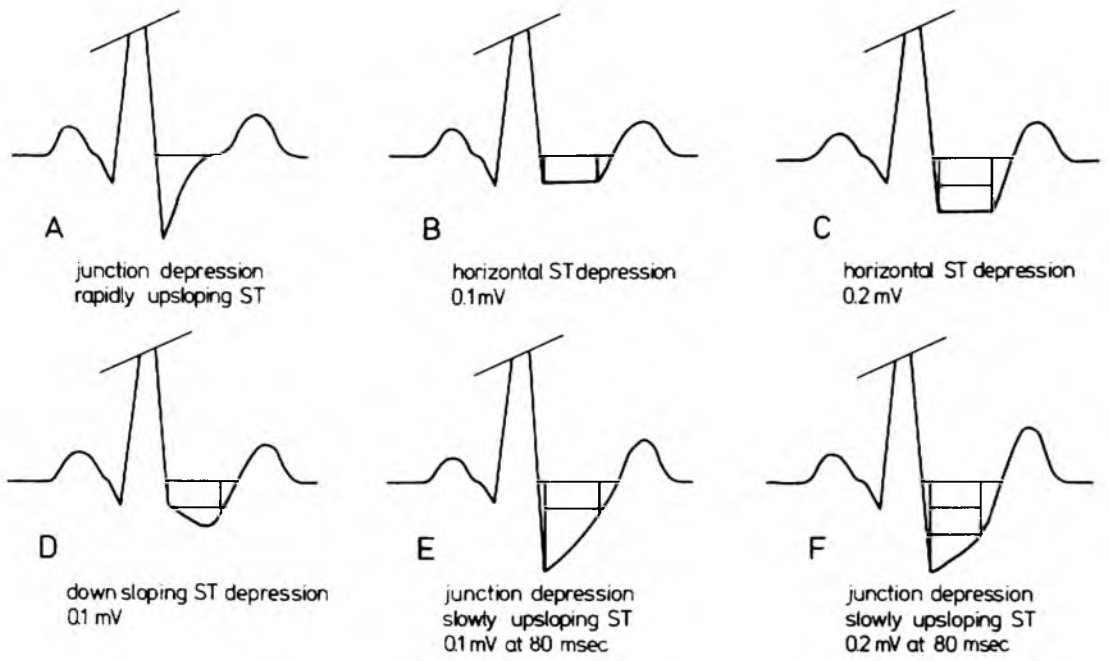

Fig. 2.27. ST segment depression: Patterns of ST segment depression during a stress test. Reprinted with permission from Wolters Kluwer Health, Inc. R. Rijncke, C. Ascoop, and J. Talmon,"Clinical significance of upsloping ST segments in exercise electrocardiography," *Circulation*, vol. 61(4), pp. 671-678, 1980.

ischemia, and the inclusion of these inferior leads can result in false positives [98]. Exercise-induced R-wave and S-wave amplitude changes are also not correlated with ischemia [1], further reducing specificity of this diagnostic test. Confusion can also arise because exercise-induced ST segment depression is not specific to myocardial ischemia and can also be attributed to left bundle branch block (LBBB), Wolff-Parkinson-White (WPW) syndrome, electronic pacemakers, and intraventricular conduction defects (IVCDs) [1]. As a result of these ambiguities, the mean sensitivity and mean specificity of ET to detect CAD remain at 68% and 77% [6], respectively.

2.4.8.3 Rest and Stress Echocardiography

Echocardiography refers to an evaluation of the myocardium with images produced by ultrasound and is also used for ischemia diagnosis. Images can be recorded through the chest wall (transthoracic echocardiography) or via a probe placed in the esophagus (trans-esophageal echocardiography). The primary application of echocardiography in patients with CHD is to detect the effects of myocardial ischemia and myocardial infarction on LV

structure and function [1]. The echocardiographic indicators of CAD include a reduction in systolic thickening, abnormal segmental wall motion during systole or diastole, alterations in acoustic properties of myocardium, and diminished regional blood flow (measured after intravenous echo contrast injection) [1].

The combination of stress testing and echocardiography (stress echocardiography) has become an important diagnostic tool for the detection of CAD. The technique is based on the concept that stress-induced ischemia will result in abnormalities of regional wall motion that can be identified by echocardiography. The location of wall motion abnormality can help identify the culprit coronary vessel(s), and the ratio of dyssynergic to normal myocardium can provide a quantitative assessment of LV ischemia [1]. Stress echocardiography is more sensitive and specific than ECG stress for detection of CAD [1]. However, high-quality ultrasound images can be difficult to acquire due to a poor signal to noise ratio. Moreover, considerable expertise is needed to acquire and to interpret the results.

In lieu of exercise stress testing, pharmacologic stress, which employs vasodilator agents (e.g., adenosine) or inotropic agents (e.g., dobutamine), can also be used. A vasodilator induces disproportionate and heterogenous myocardial perfusion, which can produce ischemia. On the other hand, an inotropic agent increases metabolic oxygen demand and thereby produces ischemia [99].

2.4.8.4 Myocardial Perfusion Imaging (MPI)

MPI with single photo emission computed tomography (SPECT) entails using a scintillation camera and an intravenous radiopharmaceutical (e.g., technetium -99m ^{99m}Tc) that is distributed to the heart in proportion to regional perfusion [1]. Since the radiopharmaceutical accumulates in the myocardium in proportion to regional blood flow, CAD can be detected by identifying a reduction in accumulation in a region supplied by a stenosed (at least 70%) vessel compared with a normal region during hyperemia [100]. The ability of SPECT MPI to assess hyperemic response is based on the degree of extraction of the tracer during its first pass through the myocardium. The amount of injected tracer in the heart at the time of imaging (net extraction) is proportional to that extracted by the myocardium (extraction fraction) and the amount retained at the time of imaging [101].

For exercise stress SPECT MPI, the tracer is injected at maximal stress and exercise is continued for an additional 1 minute of peak load [1]. Postexercise stress imaging commences usually 15 minutes to 2 hours after the stress injection to allow the patient to recover fully from stress, which prevents artifactual defects related to increased depth of respiration early

after stress [102]. The mean sensitivity and specificity for exercise SPECT MPI are reported at 87% and 73% [1], respectively.

2.4.8.5 Positron Emission Tomography (PET)

PET imaging can evaluate functions ranging from blood flow to biochemical reaction rates, substrate fluxes, and neuronal activity. For CAD detection, PET is used with pharmacologic stress agents such as adenosine and dipyridamole. Positron-emitting flow tracers ^{82}Rb and ^{13}N-ammonia are retained in the myocardium in proportion to blood flow so that the resulting images display the relative distribution of blood flow at rest and during hyperemia [1]. The images are interpreted visually and also using quantitative methods.

The mean sensitivity and specificity of PET are 87% and 100% [1], respectively, more specific than SPECT.

2.4.8.6 Coronary Artery Calcification Score (CACS)

An electron beam computed tomography (EBCT) scanner is employed to obtain high-resolution static images and to evaluate coronary artery calcification (CAC). The standard EBCT protocol is to acquire 40 consecutive images from the base of the heart to just below the carina [1].

A calcified lesion is defined as either two or three adjacent pixels of > 130 Hounsfield units (HU). In one common risk quantification scheme, each calcified lesion is then multiplied by a density factor and the total coronary artery calcium score (CACS) calculated as the sum of each calcified lesion in the four main coronary arteries over all the consecutive tomographic slices [1].

Coronary calcification is believed to begin early in life and is an actively regulated process occurring during atherosclerotic plaque development [103]. Although the absence of calcification does not exclude the presence of atherosclerotic plaque, calcification is not found in normal arteries. The mean sensitivity and specificity for detecting CAD using this combination of CT imaging and CACS scoring are reported at 97% and 39% [1], respectively.

2.4.8.7 Invasive Coronary Angiography

Coronary angiography remains the current gold standard for definitive CAD diagnosis. It entails vascular access to coronary arteries using catheterization and acquiring radiographic images of the vascular conduits and networks connected to internal structures (organs) [1].

Angiography provides an anatomic map of the site, severity, shape, and distribution of stenotic lesions, distal vessel size, intracoronary thrombus, diffuse atherosclerotic disease,

mass of myocardium served, an approximate index of coronary flow, and identification of collateral vessels [1]. The evaluation of a stenosis relates the percentage reduction in the diameter of a narrowed vessel to the adjacent unobstructed vessel and also includes the length of the stenosis (e.g., LAD proximal stenosis diameter 35%, long or short). Given the subjective nature of visual lesion assessment, there is variation in interpretations of lesions. Moreover, angiographic narrowing of 40–75% does not always correspond to abnormal physiology and myocardial ischemia [1].

2.4.8.8 Coronary Computed Tomography Angiography (CCTA)

CCTA relies on multidetector CT (MDCT) scanners to noninvasively detect coronary atherosclerosis approximating the invasive catheter-based coronary angiography. In addition, it can also provide information on plaque extent, distribution, location, and composition, in contrast to coronary angiography. The mean sensitivity and specificity for CCTA are 94% and 89% [104], respectively. CCTA with a high negative predictive value (99%) is a useful tool to exclude CAD in patients with a low pretest likelihood of disease [1]. CCTA also offers a time-efficient and cost-effective alternative to SPECT for initial evaluation of patients without known CAD.

The limitations of CCTA include decreased accuracy in patients with elevated heart rate (>90 BPM), irregular rhythm, extensive CACs, and an obese body type. The radiation exposure is two to four times that of invasive coronary angiography. The spatial and temporal resolution is also lower compared to coronary angiography.

2.4.8.9 Cardiac Magnetic Resonance (CMR)

The strength of CMR is its ability to evaluate pathological processes using several pulse sequences—each tuned to different biological properties—during a single examination [1]. Two main CMRI approaches to evaluating CAD are stress testing with imaging of myocardial contraction (e.g., dobutamine stimulation) or perfusion (e.g., adenosine stimulation). The dobutamine stress CMR is analogous to echocardiography and can be used to detect ischemic-induced wall abnormalities. However, there are logistical challenges to using this technique, including the potential for an ischemic event while the patient is inside the MRI scanner as well as distortion of the ECG by the magnetic field [1].

The adenosine stress CMR is the more commonly preferred approach for CAD assessment. Perfusion MRI has better spatial resolution than SPECT and does not subject the patient to ionizing radiation. Moreover, the examination time is 30–45 minutes versus 2–3

hours for SPECT [1]. The mean sensitivity and specificity for CMR are 85% and 81% [1], respectively. However, CMR is somewhat limited in patients with metallic hardware such as pacemakers.

2.4.9 Treatment

The treatment selection for patients with CHD is based on the magnitude of risk and severity of the ischemia. Treatment options include pharmacological, percutaneous, and surgical approaches, the primary goal of which is to reduce ischemia symptoms and prevent adverse and potentially fatal events such as acute MI and sudden cardiac death.

2.4.9.1 Pharmacologic Therapy

- **Anti-platelet therapy** is designed to prevent coronary thrombosis by inhibiting the production of thromboxane and includes agents such as aspirin, thienopyridines, and glycoprotein (GP) IIb/IIIa inhibitors [1].

- **Anticoagulation Therapy** is also designed to reduce the ability to form blood clots by targeting clotting factors and includes agents such as warfarin (vitamin K antagonist) and heparin [1].

- **Fibinolytic therapy** is focused on restoring blood flow by converting plasminogen to plasmin, which cleaves fibrin, resulting in clot dissolution. Streptokinase (SK), a tissue type plasminogen activator, is a commonly used fibrinolytic agent [1].

- **Lipid-lowering therapy** is geared toward reducing low-density lipoprotein (LDL) cholesterol production that is part of the plaque formation and includes agents such as 3-hydroxy-3-methylglutarly coenzyme reductase inhibitors (HMG-CoA), also called statins. Statins also have anti-inflammatory and antithrombotic properties [1].

- **β-adrenergic receptor antagonists** work by reducing heart rate, contractility, systemic arterial pressure, and LV wall stress, thereby reducing metabolic demand. Moreover, the slowing of heart rate also enables longer diastolic filling times, thus improving coronary blood flow. Propanolol is an example of a nonselective beta-blocker.

- **Calcium channel blockers** act as negative inotropic agents. They also lower systemic vascular resistance and mean arterial blood pressure to decrease LV afterload, thus reducing myocardial oxygen demand [1]. Diltiazem is an example of a nondihydropyridine calcium channel blocker.

- **Angiotensin-converting enzyme (ACE) Inhibitors** work by reducing the production of angiotensin II, thereby inducing vasodilation and lowering blood pressure, which in turn reduces myocardial oxygen demand. Ramipril is an example of an ACE inhibitor.

- **Organic nitrates** work by causing venodilation, which reduces end diastolic volume and pressure, leading to increased myocardial perfusion. Moreover, they also dilate epicardial coronary arteries to improve coronary blood flow and recruit coronary collaterals [1]. Nitroglycerin is a commonly used nitrate.

- **Ranolazine** is a sodium channel I_{Na} blocker and exerts an anti-anginal effect without affecting heart rate and blood pressure, by selectively inhibiting late sodium influx into myocytes, which leads to reduced contractility [105].

2.4.9.2 Coronary Artery Revascularization

For patients with an elevated risk profile and suitable coronary anatomy, revascularization with percutaneous coronary intervention (PCI) or coronary arterial bypass graft (CABG) surgery are possible procedures [106]. PCI is employed to restore coronary blood flow without open-heart surgery. Briefly, a balloon catheter is inserted into the culprit artery past the blockage and then inflated. The balloon inflation compresses the fatty tissue (plaque), thereby making the arterial lumen larger for improved coronary blood flow. In certain instances, tiny blades attached to the balloon can be used to break up the plaque (atherectomy). A tiny expandable metal coil (stent) is often placed in an opened area of the artery to provide structural support and help prevent the artery from narrowing or closing again. Moreover, these stents can be coated with medication (drug eluting stents) to help prevent scar tissue buildup inside the stent.

CABG entails taking a healthy artery or vein from one part of the body and connecting (grafting) it to the blocked coronary artery. The grafted artery (or vein) bypasses the blocked portion of the coronary artery and thereby creates a new route for the blood to flow.

2.4.10 Prevention

The goal of the preventative strategies is to affect modifiable CHD risk factors and thus reduce the incidence of preventable CHD, which is responsible for approximately 1.2 million myocardial infarctions and 500,000 deaths every year [107]. Common risk factors associated with CHD, physical inactivity, obesity, diabetes, hypertension, etc., can be behaviorally

modified and thus reduce the incidence of CHD [1]. Moreover, the slow progression of the disease allows for time to adopt preventative strategies, which can result in reduced CHD mortality. The CHD risk factor reduction guidelines are based on various clinical epidemiological studies and can be summarized into the "ABCDE" approach to preventative cardiology [108]. The abbreviation stands for **A**ssessment of CHD risk, antiplatelet and anticoagulant therapy, **B**lood pressure, **C**holesterol and cigarette smoking cessation, **D**iet and weight management and diabetes prevention and treatment, and **E**xercise. Treatment of patients with CHD is associated with high costs, and the patients often retain residual risk [1].

2.5 Literature Review

The study of cardiovascular diseases has been an active research area for over a century, as shown in Fig. 2.28. We provide here a summary review of literature relevant to myocardial ischemia research.

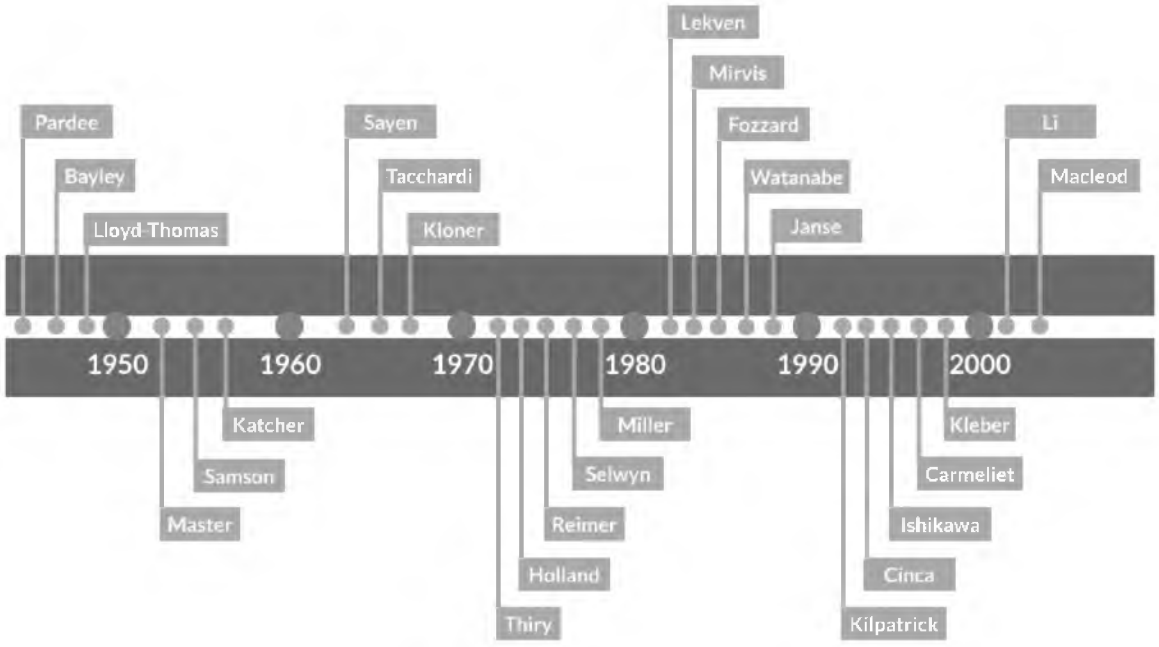

Fig. 2.28. Century of research: The timeline highlights major publications in myocardial ischemia research.

2.5.1 Pre-1950s

The term *angina pectoris* to describe chest pain due to coronary artery disease was coined in 1893 [109]. Moreover, Strascheskow later discovered that myocardial ischemia and myocardial infarction could occur without causing pain [109]. Collateral vessels were also discovered when postmortem studies on canine hearts revealed that coronary arteries were not end-arteries; rather they have many collateral connections at all levels of atria and ventricles [20].

The first ECG was recorded using a string galvanometer by Willem Einthoven in 1901. As the ECG became more widespread, changes in the ST segment were noted in patients with CAD [110]. Moreover, it also became evident that ECG morphology could be affected by heart position [111]. The two-step exercise tolerance test was introduced by Arthur Master to diagnose patients with ischemic heart disease in 1929 and served as the antecedent to the present-day exercise stress testing [112]. The ECG limb lead recordings with an inversion of T-wave or ST segment changes in leads I and II were accepted as standard markers for a positive diagnosis of ischemia, but the mechanisms behind the ECG changes were unresolved at the time [113].

DiPalma showed the presence of an intramyocardial pressure gradient from epicardial to endocardial regions [114], suggesting that the inner layers of the heart muscle are reached by arterial blood only in diastole, during which the local coronary pressure exceeds the local intramyocardial pressure.

The concept of "injury current" was introduced by Bayley in 1942 [115]. Accordingly, the ischemic "injured" area was considered electrically negative relative to the surrounding noninjured myocardium during diastole and positive during systole. The resulting potential difference gave rise to injury currents that produced ST segment shifts on the ECG, such that the injured area would be characterized by ST segment elevation on the surface, whereas the adjacent regions would be expected to exhibit ST segment depression. Moreover, ST segment depression was categorized into two types: reciprocal ST segment depression that overlay normal muscle remote from a large ischemic region and the other ST segment depression that could be found over the boundary physiologically impaired muscle and normal myocardium [116].

2.5.2 1950s - 1990s

The spatial orientation of myocardial fibers in the myocardial wall was characterized, as a well-ordered fiber continuum of interconnecting fibers with gradual changes in fiber angles from endocardium to epicardium [117]. It was noted that CAD led to an increase

in collaterals in both epicardial and endocardial regions, but the increase was greater in the subendocardial region [118]. Experimental studies on dogs suggested that immature collateral channels conductance is not maximal immediately after occlusion but increases with time [119].

The concept of acute coronary insufficiency (ACS) distinct from acute coronary occlusion (ACO) was well documented [120]. It was commonly accepted that ACS was associated with subendocardial ischemia and characterized by ST segment depression and T-wave inversion, whereas ACO was marked by ST segment elevation and Q-waves, signaling infarction spreading all the way to the pericardium. However, newer studies suggested that ACS can also produce transient and reversible ST segment elevation. Moreover, negative exercise tests or normal ECG did not preclude ACS [121]. It was also noted that induced tachycardia could produce ST segment depression [122].

The clinical treatments for angina pectoris included the use of vasodilators such as nitrites, beta-blockers such as propanolol, and newly introduced carotid sinus nerve electrical stimulation, which was shown to reduce heart rate by muting adrenergic discharges [123].

The field of vectorcardiography was established as a means to quantify abnormalities in ECG markers [124]. However, clinical studies suggested that ischemic ECG changes could also be affected by age as well as noncardiovascular disorders: pulmonary embolism, endocrine disorders, and acute infections among others [125]. The notion that atherosclerosis was a physiological aging process and thus irreversible was being discarded with the realization that it was a metabolic disease caused by accumulation of lipids, cholesterol, and lipoproteins and thus could be prevented or reversed. However, the exact pathogenesis was not understood [126].

Cellular electrophysiological studies using microelectrodes to record action potentials (AP) from strips of papillary muscle suggested that in the absence of coronary perfusion, the electrical changes included shortening of AP duration, followed by the progressive fall of the AP amplitude. These changes were attributed to shortening of the repolarization phase due to the rapid efflux of potassium (K^+) ions and impairment of Na/K pump due to changes in resting potential. Moreover, the falling resting potential was marked by similar changes in creatine phosphate and ATP [127].

Experimental studies conducted to measure epicardial electrograms using a wick electrode suggested that epicardial ECG changes were seen only in the presence of large ischemic regions, where coronary flow was reduced by at least 70% [128], and thus epicardial ST segment changes showed relative insensitivity as an index of acute regional ischemia.

However, intramyocardial electrograms were found to be sensitive to local ischemia [129].

Electrograms recorded using DC coupled amplifiers showed that ST segment elevation recorded by AC coupled amplifiers was the result of a combination of TQ segment shifts and true ST segment elevation. The TQ segment shifts were attributed to changes in the resting potential resulting from potassium efflux due to activation of KATP channels [90], whereas true ST segment elevation was attributed to changes in the AP amplitude [110]. Body surface potential maps were introduced as another tool to provide additional information not available on 12-lead ECG recordings [130]. Myocardial perfusion imaging (MPI) to track coronary blood flow was also demonstrated [131]. Moreover, atrial pacing as a means to induce ischemia in lieu of exercise was also noted [132].

Histological studies on canines by Jennings et al. suggested that the subendocardial layers in the left ventricle are more vulnerable to ischemia, since necrotic areas were more prevalent in the subendocardium relative to subepicardium [62]. Moreover, it was also noted that myocardial stress is maximal at the internal surface of the normal ventricle, implying that the subendocardial region requires more oxygen than subepicardium [133]. Studies investigating hemodynamic factors causing ischemia suggested that reduced coronary perfusion combined with elevated intramyocardial pressure reduced blood to inner layers of the heart, resulting in ischemia [114]. On the other hand, radioactive labeled blood studies suggested the accumulation of luminal blood in the inner layers of the ventricular myocardium by an ebb and flow into the sinusoids [134].

Studies on Purkinje fiber-myocardium junctions suggested the presence of low resistance intercellular connections, resulting in a flow of current during repolarization between neighboring cells [135]. Ischemia-reperfusion studies by Jennings suggested a reversible phase of ischemia of up to 18 minutes, if arterial flow was restored [136]. Electrophysiological responses to ischemia in canine model suggested that excitability was more depressed in the epicardium and papillary muscle tip than in the endocardium and Purkinje fibers, and was attributed to intrinsic differences in membrane responsiveness, in part due to the presence of Purkinje fibers in the subendocardial region [85]. Myocardial infarct studies in canines suggested that a narrow rim of subendocardium several cells thick survived extensive infarction [137]. Moreover, temporary occlusion experiments often yielded islands of necrotic cells interspersed with regions of surviving cells in the midmyocardium, suggesting a nonuniformity of ischemic injury [64].

During the early phase of occlusion in isolated rabbit hearts, the conduction delay was greater in the subepicaridum than in subendocardium, due to greater resistance of

subendocardial cells to effects of hypoxia, elevated potassium, and acidosis. Moreover, in the first 10 minutes of acute ischemia, an endocardial border zone of 40–60 cell layers existed where the transmembrane potentials were relatively little affected by ischemia [138].

Reimer et al. showed the progression of cell death following coronary occlusion in dogs as transmural wavefront from the subendocardium towards the subepicardium [9]. Steinberg et al. showed that in rat hearts ischemia resulted in discrete heterogeneous regions of anoxic tissue surrounded by normoxic region [139]. The ischemia border zone studies on pigs suggested that it was a mixture of normal and ischemic cells, characterized by an area with gradients in local blood flow, lactate content, HEP, and ST segment potentials [140]. Studies by Austin et al. suggested that even with global factors such as elevated diastolic ventricular pressure and reduced perfusion pressure placing subendocardium at risk of ischemia, there are islands of relatively greater vulnerability within the inner layers of the heart [141].

The protective effect of ischemic preconditioning was discovered, wherein brief ischemia episodes (1–2 minutes) in canines followed by a long LAD/LCX occlusion (40 minutes) delayed cell death and thus allowed greater salvage of the heart through reperfusion therapy [95]. The protective effect of preconditioning was attributed to a reduction in myocardial energy demand during ischemia, which reduced the rate of HEP utilization as well as the rate of anaerobic glycolysis [142]. It was noted that preconditioning was not an all or nothing phenomenon. A different magnitude of protection was induced based on the duration and number of preconditioning episodes [143].

Gradual reduction in myocardial blood flow in pigs produced a muted response in the metabolic markers of ischemia such as ATP content compared to sudden reduction in blood flow of 20–50%, which suggested a tightly regulated feedback or feed forward mechanism in maintaining a balance between oxygen demand and supply, such that the downregulation of metabolic energy requirements could almost keep pace with a gradual decline in coronary blood flow [144]. Moreover, the ATP was better maintained in demand ischemia than in supply ischemia for a given tissue receiving equal blood flow [145].

Ischemia studies on pigs by Holland noted that ischemic TQ and ST segment shifts were affected by the duration, size, and shape of the ischemic region as well as the location of the recording electrode. Moreover, the shape of the ischemic region was influenced by size, intraventricular pressure, wall tension, and location of anastomoses [10]. The spatial relationship between metabolites and epicardial electrocardiographic changes during reversible LAD ligation suggested that sites of ST segment elevation were associated with higher lactate concentrations and reduced HEP concentrations and thus could be construed

as reflecting transmural ischemia. However, isoelectric sites could reflect no ischemia or very mild ischemia [146].

The intramural ST segment changes were more sensitive than corresponding epicardial ST segment changes [147] to regional ischemia. Moreover, the epicardial ST segment shifts were more sensitive than precordial ST segment shifts [148]. There was a general nonlinear correlation between epicardial ST segment elevation and biochemical changes, regional myocardial blood flow (RMBF), and myocardial electrolyte alterations during the reversible phase of ischemia [149]. Endocardial and midmyocardial ST segment changes were more sensitive than epicardial ST segment changes and strongly correlated with changes in extracellular K and PCO2 [150]. The lack of clear correlation between ECG ST segment to the site of occlusion was attributed to the presence or absence of collateral circulation, individual differences in coronary vasculature, heart position in relation to electrode locations, and the distance from the heart to the electrodes [151]. Studies by Li et al. on sheep ischemia model suggested that distributions of epicardial potentials either from LCX or LAD ischemia source were similar. Moreover, ischemic epicardial ST segment depression was attributed to injury current flowing along the lateral boundary of subendocardial ischemia [152]. However, the inability of epicardial ST segment depression to localize nontransmural ischemia could not be explained [153].

2.5.3 2000s - Present

Studies by our group using a canine ischemia model showed that heart rate also influences epicardial potential distribution. Moreover, induced demand and supply ischemia produced differing epicardial potential distribution patterns for the same level of ischemic stress [154]. In related studies, Shome et al. [155] used canine ischemia model studies to suggest that epicardial and transmural potential distribution during demand ischemia arose from complex sources, such that a severe demand ischemia evoked heterogeneous transmural potential distribution, which influenced the epicardial potential distribution pattern. Moreover, the epicardial potential distribution reflected the local fiber orientation at the ischemic boundary [156].

Our research builds on the work done by these researchers and many others as they contributed to the cumulative knowledge on myocardial ischemia. Specifically, this dissertation seeks to characterize the complex bioelectric sources of acute myocardial ischemia, how they evolve spatio-temporally, and the sensitivity of epicardial electrical markers to detect these ischemic sources.

CHAPTER 3

DESIGN OF EXPERIMENTS

This chapter provides details on the research methodology as well as the rationale behind the choices made including selection of animal species, experimental setup, and study protocols. Moreover, a description of data acquisition, data processing, and data visualization pipeline is also included as shown in Fig. 3.1, which will provide the context for interpreting the results from the research.

3.1 Animal Models

The animal models used for these studies included both canines and swines. Each species has certain attributes that make it relevant. Canines have relatively well-developed coronary collateral vasculature compared to swines and humans [157]. Indeed, humans

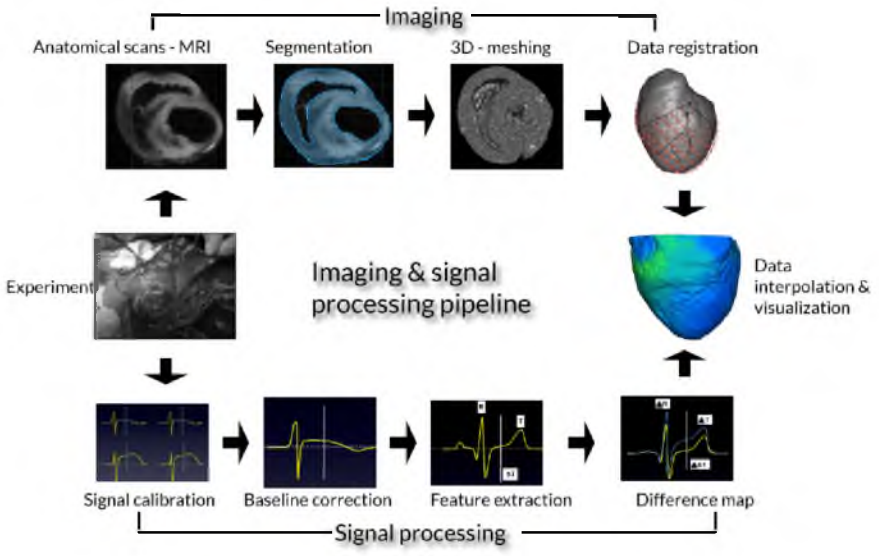

Fig. 3.1. Image and signal processing pipeline: The figure shows workflow from data acquisition to data processing and finally data visualization.

have few collaterals during the early phase of CAD [18]. Thus, swines, with their sparse collateral vasculature, are an appropriate animal model for ischemia research. On the other hand, patients with chronic CHD develop a more extensive network of collateral circulation as an adaptive response [18] so that canines represent a more relevant model. Given that no one animal model can entirely mimic human pathophysiology, we used both the animal models to study and characterize myocardial ischemia. All studies were approved by the Institutional Animal Care and Use Committee at the University of Utah and conformed to the Guide for Care and Use of Laboratory Animals.

3.2 Experimental Setups

Most ischemia studies were conducted in anesthetized animals in in situ, open-chest preparations, which have a number of advantages over alternatives. First this preparation involves opening the chest cavity through a midsternal incision and thus provides ready access to the heart. This generous access to the heart provides the ability to acquire electrical signals from the epicardium by means of multielectrode sock electrodes, as well as the intramural regions by means of electrodes embedded in thin, flexible needles. This configuration allows a high and controllable degree of spatial resolution, which is not possible with a closed-chest model. A second advantage of this extensive access to the heart is that the site and extent of ischemia can be varied and more finely controlled compared to the closed-chest preparation. Third, the preparation provides flexible options for controlling coronary blood flow, for example a hydraulic occluder or a glass or plastic cannula, as described in more detail in a later section. Achieving coronary flow control in a closed-chest preparation is more difficult and less precise.

The open-chest preparation also has some disadvantages, however. There is trauma associated with surgical preparation that would not arise in the closed-chest model [158]. This trauma can also lead to elevated ST segments and thus confound the interpretation of ischemia-induced changes. A final disadvantage of the open chest preparation is that it requires extensive anesthesia, which reports suggest may influence the response of the tissue to occlusion [159].

The left anterior descending (LAD) coronary artery was used to produce regional ischemia as it has been shown that LAD occlusion produces greater impairment of global LV function than LCX occlusion especially in humans and swines [18].

3.2.1 In Situ Setup

In this setup, a midsternal thorocotomy allowed direct access to the heart for recording epicardial potentials from the entire surface of both ventricles and capturing intramural potentials from the anterior aspects of the right and left ventricles. The animals were anesthetized by bolus injection of sodium pentobarbital (30 mg/kg) for canines or isoflurane gas (1–3% inhalant to effect) for pigs, followed by maintenance doses administered as needed.

After the thorocotomy, the heart was suspended in a pericardial cradle. Ventilation was room air mixed with oxygen adjusted to maintain physiological blood gas parameters and pH. A heated and automatically monitored table ensured physiological body temperature and insulation, and monitoring maintained stable cavity temperature to minimize any thermally induced repolarization changes. A pacing clip attached to the right atrial appendage provided control of heart rate above the intrinsic rate for each animal.

A suitable left anterior descending (LAD) segment was then dissected and freed from the underlying tissue. The flow through the dissected LAD was regulated using either a hydraulic occluder, a cannula inserted into the vessel and connected by hose to a blood pump, or a snare, as shown in Fig. 3.2.

A heat exchanger ensured that the perfused blood was maintained at physiological temperatures. A measurement of coronary flow and intrinsic heart rate at the start of each experiment determined default resting values.

3.2.2 Isolated Heart Perfused by Support Animal

Some studies were conducted by removing the entire heart from a donor animal and maintaining its blood supply, which is a modified version of the Langendorff prepara-

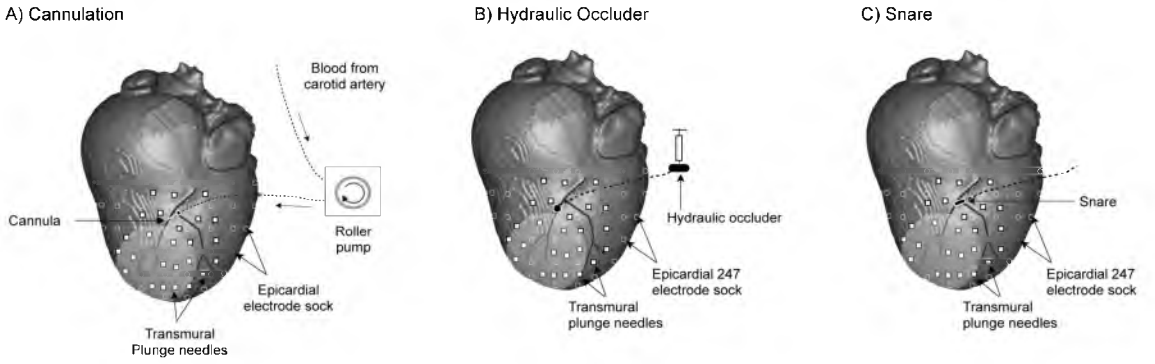

Fig. 3.2. In situ preparation: Panel A highlights cannula setup. Panel B shows hydraulic occluder setup. Panel C shows the total occlusion snare setup.

tion [160, 154], as shown in Fig. 3.3. This preparation has been successful using dogs only for both the donor and support animals.

Once extracted and connected to a support animal, the isolated heart was suspended in a torso tank filled with electrolyte composed of NaCl (1.35 gm/l) and sucrose (89 gm/l) (adjusted for isotonicity and a bulk conductivity of 500 Ωcm).

3.3 Study Protocols

The study protocol was designed to simulate two forms of acute ischemia: 1) a stress test with pacing as a surrogate for exercise and 2) episodes of reduced coronary perfusion to simulate coronary artery disease. Mirvis et al. have shown that tachycardia increases oxygen demand that is unaffected by mode of tachycardia induction such as exercise or pacing [161]. Similarly, by combining elevated heart rate and reduced coronary perfusion in different protocols, we were able to simulate both of what are known as "demand" and "supply" types of ischemia.

For demand ischemia, characterized by progressively elevating metabolic demand under stable perfusion conditions, the coronary perfusion was held constant and the pacing rate was increased in a stepwise manner in increments of the pacing interval of 30–50 milliseconds.

For supply ischemia, in which demand is stable but blood supply is reduced, ischemia was induced by keeping the pacing rate constant and decreasing the perfusion rate in steps of 7–10 ml/min for the cannulated LAD and steps of 25% perfusion deficit when using the

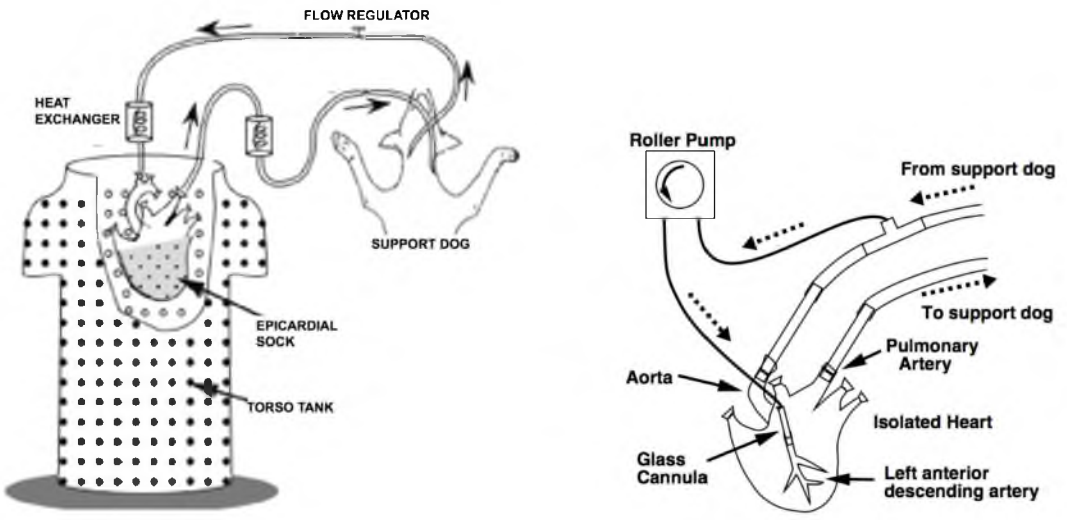

Fig. 3.3. Isolated heart preparation: The figure shows the schematic of the isolated heart perfused by a support animal.

hydraulic occluder, as shown in Fig. 3.4.

Each resulting ischemic episode lasted 2–10 minutes, depending on the protocol, the intrinsic heart rate and coronary flow values of the animal, and the maximum heart rates tolerated. Each experiment consisted of four to six such episodes separated by recovery periods of approximately 25–30 minutes.

3.4 Data Acquisition

Data acquisition included recording of bioelectric signals from epicardial and intramural regions of the heart as well as geometric information through imaging and mechanical digitization of electrode locations. If the experimental setup included a torso tank, we also acquired electrical recordings from the torso surface and the location of the heart within the torso tank. In addition, we collected blood gases, pH, and electrolyte information during the experiment.

3.4.1 Time Signal Acquisition

Epicardial potentials were recorded from the surfaces of both ventricles using a 247-electrode flexible sock array, the construction of which is described elsewhere [162]. Briefly, a nylon stocking material (sock) was placed on a plaster of paris mold of a representative heart. The 247 electrode locations were marked on the sock with an approximate mean interelectrode spacing of 8 mm. The electrodes (0.003 inch insulated silver wire) were sewn

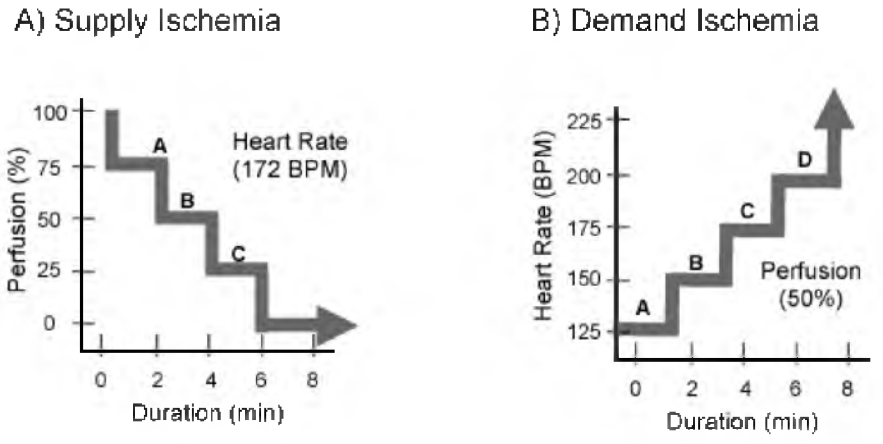

Fig. 3.4. Study protocol. By altering either heart rate or perfusion rate in regularly spaced increments and for set durations (typically 2 minutes), we were able to simulate both supply (Panel A) and demand (Panel B) forms of ischemia.

into the sock at the marked locations. Finally, a tiny section of the insulation in the wire was removed to expose the recording electrode.

Up to 26 fiberglass needles, each carrying 10 electrodes along its length spaced at 1.5 mm, were used to record intramural potentials, as shown in Fig. 3.5. These small and flexible plunge needles [163] were constructed to create less tissue injury and therefore more sensitive measurements than previous electrodes with metal shafts. The plunge needles were inserted into the ventricles in and around the region presumably perfused by the cannulated or occluded LAD, taking care to avoid injuring the epicardial arteries. The spacing between needles within the epicardial region they covered did not exceed 10 mm. The perfused region was identified before insertion by stopping blood flow through the LAD for 45 seconds and recording the resulting epicardial potentials. Localized ST segment elevations were considered indications of nearby ischemia.

The potentials from sock and needle electrodes were recorded using a custom acquisition system permitting simultaneous acquisition of 1024 channels at 1 kHz sampling rate and 12 bit resolution [164]. Briefly, the acquisition system consisted of multiplexers, interface circuitry, and a personal computer (PC) hosting a custom software written in Labview (Na-

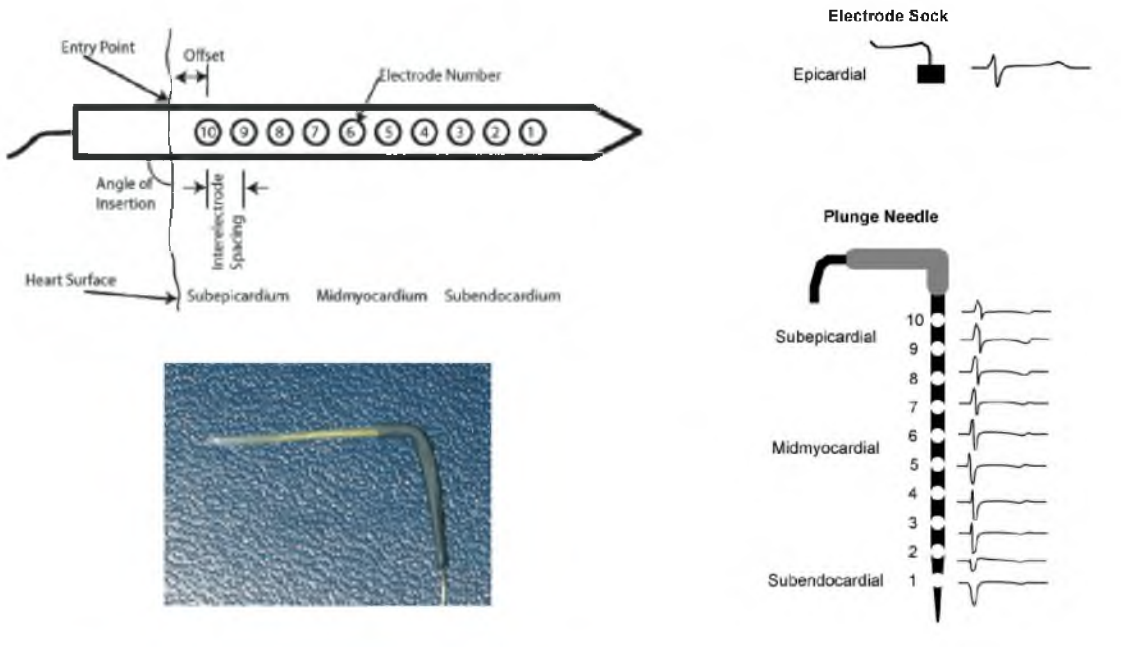

Fig. 3.5. Intramural electrodes and recording electrograms: Left hand panels show the needle electrodes used for intramyocardial electrodes and the right hand panels show sample electrograms recorded from the cardiac surface (upper panel) and intramurally (lower panel) using sock and plunge needle electrodes, respectively.

tional Instruments) that managed the hardware and allowed continuous signal acquisition for up to 30 minutes. A band pass filter with cutoff frequencies at 0.03 and 500 Hz avoided both DC potentials and aliasing. A single limb lead was used as a remote reference for all the unipolar signals recorded from the sock and needle electrodes in the in situ preparations. Electrical recordings as were taken for typically 3 seconds every 15–30 seconds during the ischemic episode as well as during the recovery period.

3.4.2 Image Acquisition

Following each experiment, the heart was excised and scanned with a 7-tesla MRI scanner (Bruker, Inc., Billerica, MA). Anatomical scans were generated using two pulse sequences: fast imaging with steady precession (FISP) and fast low angle shot imagine (FLASH). The pulse sequence parameters used were, as shown in Table 3.1. The FISP scans were selected for higher contrast, whereas FLASH scans were chosen for a higher signal to noise ratio, as shown in Fig. 3.6.

Table 3.1. FISP and FLASH pulse sequence parameters.

Parameters	**FISP**	**Flash**
Echo Time (TE)	5 ms	5 ms
Repetition Time (TR)	10 ms	36.2 ms
Flip Angle (α)	59.5°	30°
Field of View (FOV)	80 mm	80 mm
Spatial Resolution	0.32 mm	0.32 mm

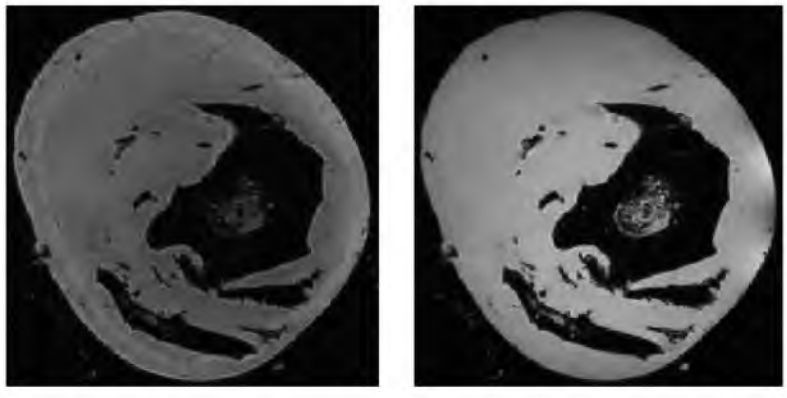

Fig. 3.6. Anatomical scans: The figure shows a slice from the FISP (left) and FLASH scan (right).

3.4.3 Registration Data Acquisition

At the end of the experiment, the locations of preselected sock electrodes and all the plunge needles on the cardiac surface were digitally recorded using a Microscribe three-dimensional digitizer (Solution Technologies, Inc., Oella, MD). In addition, landmark sites including the location of the occlusion site, distribution of major epicardial coronary arteries, and the outline of the myocardial shape were also captured using the digitizer. Once the locations of the plunge needles were recorded, they were replaced with plastic spacers, as shown in Fig. 3.7. These spacers not only prevented closure of the tissue holes created by the needles, but also were visualized in the acquired anatomical MRI scans, thus providing information for electrode location (described in a later section).

3.5 Data Processing

Data processing entailed basic signal conditioning and extraction of relevant features (e.g., ST40% potentials, T-peak, etc.) from the epicardial and intramural electrograms, segmentation of the myocardium and the plunge needle locations from the anatomical scans, and geometry processing that included generating tetrahedral volume meshes from the heart segmentation and eventual spatial and functional mapping (registration) of the sock and plunge needle electrodes to the volume mesh.

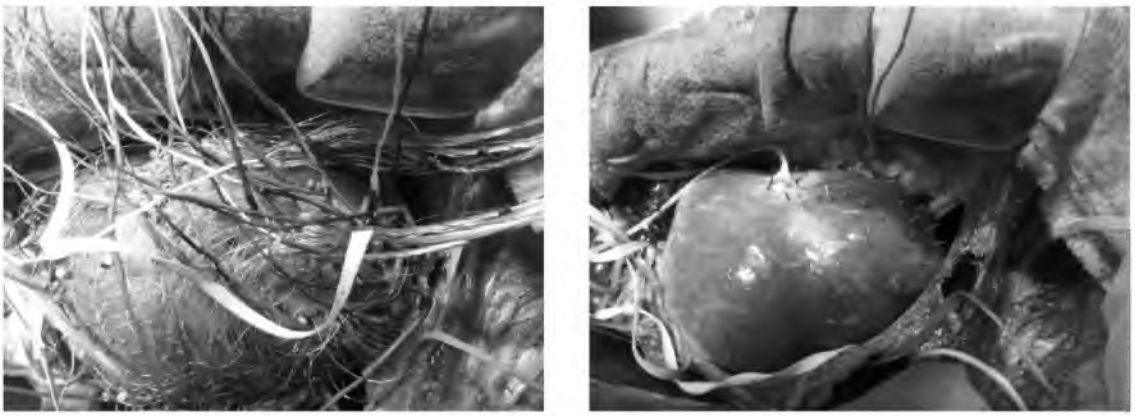

Fig. 3.7. Plunge needle locations: The left image shows the plunge needles in place immediately after an experiment and, in the right panel after the digitization process, when they have been replaced by plastic spacers.

3.5.1 Time Signal Processing

The electrograms recorded during the study were processed in Matmap, a custom MATLAB-based signal processing program developed in our laboratory. The signals were first calibrated and the gain adjusted and their baselines corrected. Calibration entailed first acquiring a reference signal for each of the 1024 input channels on the acquisition system. The reference signal was a sine wave of set amplitude(s), which was then used to extract a correction factor to be applied to all the recorded signals, resulting in a gain adjustment.

Baseline drifts that naturally occur during recording of biosignals were corrected by selecting two points along the assumed isoelectric portion of the electrogram (e.g., QT segment) and drawing a straight line between these points. This line set the baseline for the electrograms and was then subtracted from the recorded signals.

Poor quality signals from sock and needle electrodes, for example, due to incomplete contact with the tissue, were discarded. Electrograms recorded from needle electrodes near the tip that were without positive Q-wave deflection were identified as cavity electrodes and also discarded.

The global root mean squared (RMS) signal computed from the electrograms at all the sock and needle electrode was used to identify the J-point and T-peak time instants, as shown in Fig. 3.8. Subsequently, features such as ST40%, T-peak, QRS amplitude, etc., were extracted from the electrograms. The value of potentials at 40% of the ST segment between the J-point and the peak of the T-wave (ST40%) provided the metric for local ischemia. The peak amplitude of the T-wave also served as a T-wave marker.

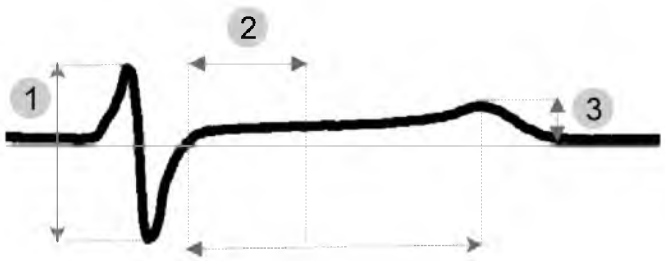

Fig. 3.8. Basic signal processing: The figure shows the features extracted from a sample recorded electrogram.

3.5.2 Image Processing (Segmentation)

Segmentation is a process of identifying regions of interest (e.g., ventricles, atria) from a given set of image scans and creating what is known as a "mask label" that assigns each voxel with a particular region a label associated with that region, as shown in Fig. 3.9. The anatomical MRI scans of the heart were segmented to identify the atria, ventricles, and locations of plunge needles using Seg3D [165]. Briefly, this entailed first smoothing the images using either median [166] and Gaussian anisotropic filters [167] to remove noise (e.g., speckle noise), while also trying to preserve edge information. Next, the filtered images were thresholded (based on interactively setting the range of intensity values) to identify atria, ventricles, and plunge needles. Finally, the selected regions were manually edited as needed to capture appropriate anatomical details.

3.5.3 Geometry Processing

The geometry processing pipeline included generating a volume mesh based on the segmentation and registering the location of the sock and needle electrodes to this mesh, which allowed for generating a subject specific spatial and functional map of electrical potentials. We generated volume meshes (with tetrahedral elements) derived from the segmentation of the anatomical MRI scans, as shown in Fig. 3.10. The mesh was generated using a meshing software called BioMesh3D [168].

Registration refers to transformation of two or more sets of spatially organized datasets into a given coordinate space [169]. We employed a feature-based registration technique, in which landmarks (e.g., plunge needle locations, epicardial coronary arteries, etc.) identified (and digitized) at the end of the experiment were aligned with those from the anatomical MRI scans and the corresponding volume mesh, as shown in Fig. 3.11. The alignment of

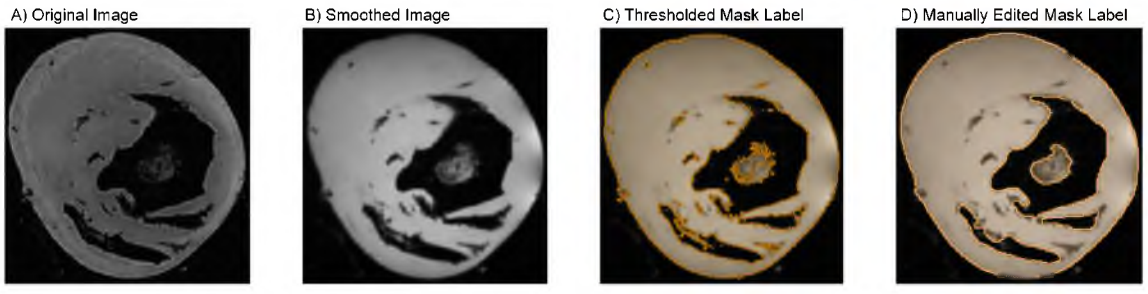

Fig. 3.9. Image processing: a) Original image scan, (b) smoothed image, (c) thresholded image mask label, (d) manually edited mask label.

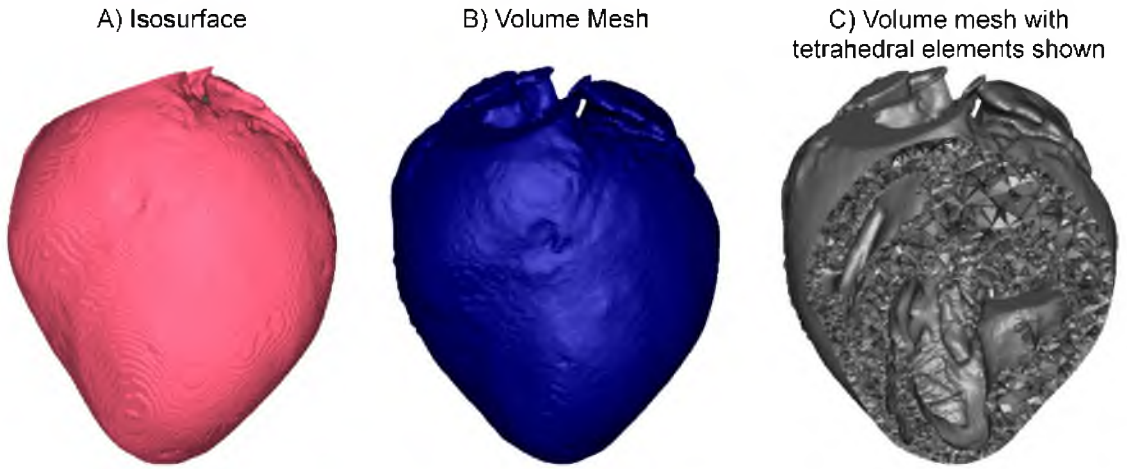

Fig. 3.10. Volume meshing: Panel A shows the isosurface of the heart based on the segmentation. Panel B shows the volume mesh generated from the segmentation using BioMesh3D software. Panel C shows the tetrahedral elements of the volume mesh.

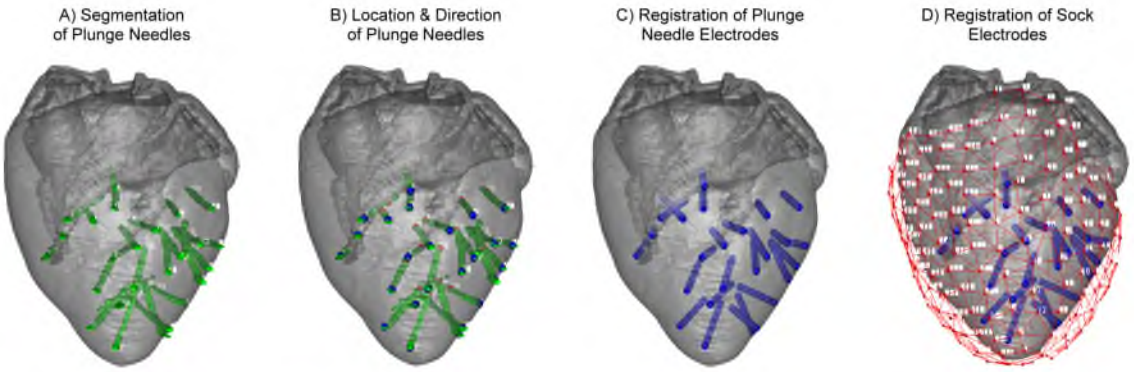

Fig. 3.11. Geometry processing: a) Segmentation of the plunge needles, (b) captured location and direction of entry of the plunge needles, (c) needle electrodes registered to the mesh, (d) sock electrodes registered to the mesh.

landmarks included both rigid and linear transformations [170], as well as scaling and morphing of the geometry with nonlinear transformations [171], depending on the registration requirements.

3.6 Data Visualization

We generated volume maps using SCIRun, which entailed interpolating the potential distributions throughout the LV wall using the radial basis function (RBF) approximation, which generated surface maps from intramural potentials by cutting planes through the

volume and evaluating the potential distribution at a given snapshot in time. Moreover, we could also isolate the ischemic regions, while making the rest of the heart volume semitransparent and track the spatio-temporal evolution, as shown, for example, in Fig. 3.12. The top row shows the intramural two-dimensional map and the bottom row shows an intramural three-dimensional map of the ST40% potential distribution. The colored region shows the sampled perfusion bed, whereas the gray region shows the rest of the heart region that was not sampled.

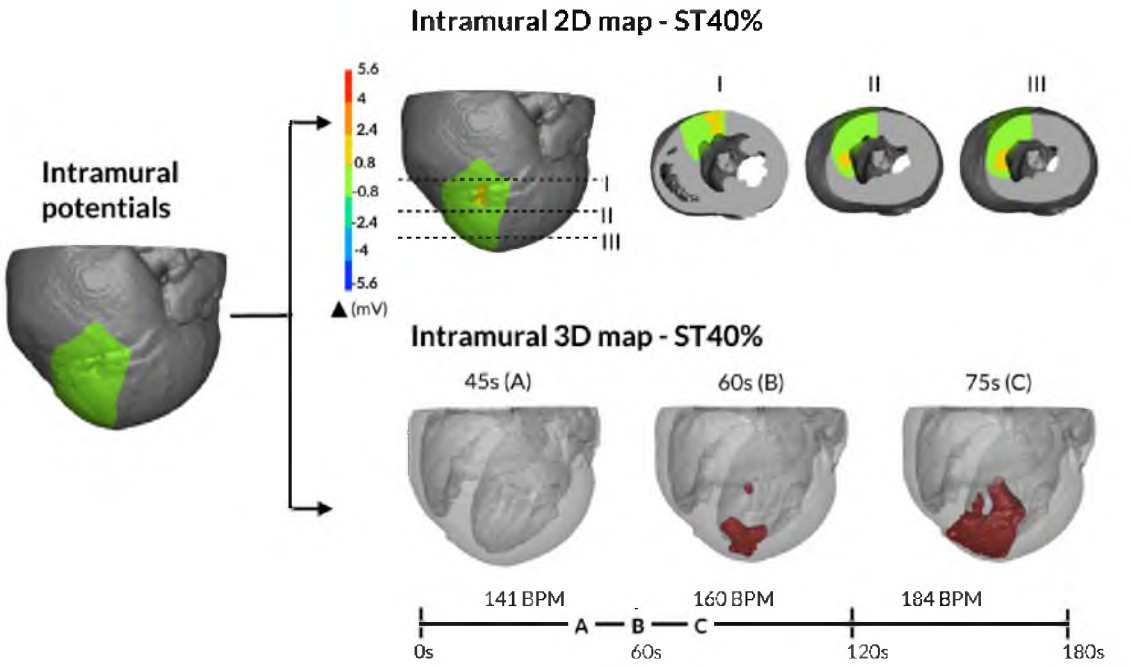

Fig. 3.12. Data visualization: The top row shows the intramural two-dimensional map and the bottom row shows an intramural three-dimensional map of the ST40% potential distribution.

CHAPTER 4

SPATIAL ORGANIZATION OF MYOCARDIAL ISCHEMIA

The goal of the first study was to evaluate the conventionally held mechanisms for nontransmural ischemia. The following research has been submitted to the *Journal of Electrocardiology.*

4.1 Abstract

Myocardial ischemia is a pathological condition initiated by supply and demand imbalance of the blood to the heart. Previous studies suggest that ischemia originates in the subendocardium, i.e., that nontransmural ischemia is limited to the subendocardium. By contrast, we hypothesized that acute myocardial ischemia is not limited to the subendocardium and sought to document its spatial distribution in an animal preparation. The goal of these experiments was to investigate the spatial organization of ischemia and its relationship to the resulting shifts in ST segment potentials during short episodes of acute ischemia.

We conducted acute ischemia studies in open-chest canines (N=19) and swines (N=10), which entailed creating carefully controlled ischemia using demand or supply ischemia protocols and recording intramyocardial and epicardial potentials. Elevation of the potentials at 40% of the ST segment between the J-point and the peak of the T-wave (ST40%) provided the metric for local ischemia. The threshold for ischemic ST segment elevations was defined as two standard deviations away from the baseline values.

Acute ischemia was characterized by pockets of ST-segment elevated regions variously distributed in the subepicardial, midmyocardial, and subendocardial regions in 79% of canine and 67% of swine ischemic episodes ($p < 0.05$).

Our findings suggest that the spatial distribution of acute ischemia is a complex phenomenon spread throughout the myocardial wall and is not limited to the subendocardium.

4.2 Introduction

Despite a century of research and practice, the clinical accuracy of the electrocardiogram (ECG) to detect and localize myocardial ischemia remains less than satisfactory [172]. Myocardial ischemia occurs when the heart does not receive adequate oxygen-rich blood to keep up with its metabolic requirements, and severe ischemia can lead to myocardial infarction and life-threatening arrhythmias. Early and accurate detection is therefore an essential component of managing this condition. In the emergency room (ER), a resting 12-lead ECG is often recorded in patients with symptoms of angina (chest pain). However, such a single resting ECG is normal in up to 50% of patients with chronic, stable angina [1]. Far from static, ischemia is known to be a dynamic condition that reflects a changing imbalance between blood supply and metabolic demand. This dynamic behavior presents diagnostic challenges and encourages continuous monitoring, which is feasible only with a technique like the ECG. Outside the emergency room, it is natural that examination of the ECG under physical stress conditions, or exercise testing (ET), has long been in widespread clinical use. However, ET is characterized by poor sensitivity (68%) and specificity (77%) [1], limiting its diagnostic usefulness. Due to the extremely high incidence of ischemia and the many practical and economical advantages of ECG based testing, any improvements in this technique and the interpretation of the data it gathers will have a profound impact on clinical practice.

The most common clinical ECG marker for myocardial ischemia detection is the ST segment, that portion of the ECG time signal that lies between the QRS complex and the T-wave. Changes in the ST segment can occur within 15–30 seconds after the onset of ischemia [173] and hence represent one of the earliest markers of the condition. The ST segment represents the period when the ventricles are depolarized, i.e., the ventricular action potentials are all in the plateau phase. In a healthy heart, this means that all regions of the ventricles have approximately the same transmembrane potential and that this phase of the normal ECG is isoelectric. However, the ST segment potential can shift above (ST segment elevation) or below (ST segment depression) the baseline during myocardial ischemia, depending on the flow of what are known as "injury currents." These currents are the result of voltage gradients between normal and ischemic regions, gradients that arise because of differences between the action potentials of ischemic and normal cells that include localized shortening, diminishing amplitude, and a decrease (more positive value) in resting membrane potential. The resulting injury currents can produce an ST segment *elevation* in an extracellular or body-surface electrode if they are directed *towards* the

recording electrode or ST segment *depression* if they are directed *away* from the electrode.

Classic electrocardiographic theory builds on these biophysically sound concepts with additional assumptions about the spatial distribution of healthy and ischemic tissues; however, these assumptions may be too simplified to explain both experimental and clinical observations. The historical basis for many of these assumptions lies in postmortem examinations of infarcted hearts [174, 175] under the additional assumption that the location and extent of eventual scar and infarct zones match approximately the ischemic regions that arise acutely following onset of ischemia. Careful experimental evaluation of these assumptions has become possible only recently with the development of flexible multielectrode needles [163] that can capture extracellular potentials throughout the ventricular wall. Previous studies of acute ischemia were instead based on measured potentials only from the epicardial and endocardial surfaces [176, 177, 138, 178]. While surface potentials are a reflection of intramyocardial events, it is only possible to *infer* the underlying bioelectric sources rather than measure them directly.

From these early experiments have come several elements that now make up the prevailing putative explanation for clinical observations of ST segments during acute ischemia. Central to this explanation of the spatial dynamics of ischemia is the assumption that at low grades of perfusion deficit, myocardial ischemia is localized to the subendocardium (innermost region of the heart wall) [173]. Justification for this assertion includes the notion that this region has the highest metabolic demand and is the most distal perfusion zone and hence most vulnerable [173]. Moreover, with increased stress, ischemia was thought to progress over time uniformly towards the epicardium (outermost region), eventually becoming transmural (spanning the full thickness of the heart wall). According to this theory, ischemia localized to the subendocardium would generate injury currents flowing away from the epicardial or body-surface electrodes toward the localized subendocardial ischemic region. Thus ST segment depression is thought to indicate subendocardial ischemia. Moreover, transmural ischemia would then produce injury currents flowing towards the recording electrodes located above the affected region of the heart, resulting in ST segment elevations. Many decades of clinical practice and experimental studies have shown that, indeed, superficial leads with ST segment elevation can be linked spatially to the region of ischemia and thus provide a means to localize transmural ischemia from the body surface. However, the same is not true of the ability of ST segment depression to locate nontransmural ischemia [179, 180, 152].

Preliminary results from our group using intramyocardial recordings do not support the

assertion that nontransmural ischemia arises only in the subendocardium [181, 182] and have motivated a comprehensive evaluation of the spatial distribution of acute ischemia based on high-resolution measurements under a range of conditions. Our goal in this study was to evaluate the conventional mechanisms for nontransmural ischemia using intramural electrodes to measure three-dimensional potential distributions in the ventricles of animals exposed to acute ischemia. We conducted a series of 29 separate experiments under a range of acute ischemia conditions using two different in situ animal models. To interpret the resulting electrograms, we assumed that localized ischemia causes localized elevations in the extracardiac ST segment potentials. We measured three-dimensional surface and transmural potential distributions under study protocols that altered both the local coronary supply and global metabolic demand.

4.3 Methods

4.3.1 Experimental Preparation

The goal of these experiments was to detect the three-dimensional distribution of ischemia-induced shifts in ST segment potentials during the acute phase of short episodes of ischemia created by reduced coronary flow and an increased rate of contraction. We performed experiments on open-chest, intact canines and swines using multipolar intramural needle electrodes and epicardial surface electrodes. Study subjects included 29 animals: 19 purpose bred dogs and 10 adult mini pigs, following the approval from the Institutional Animal Care and Use Committee at University of Utah and conforming to the Guide for the Care and Use of Laboratory Animals (NIH Pub. No 85-23, Revised 1996).

An open-chest preparation following midsternal thorocotomy allowed direct access to the heart for recording epicardial potentials from the entire surface of both ventricles and transmural potentials from the anterior aspects of the right and left ventricles. The animal was anesthetized by bolus injection of sodium pentobarbital (30 mg/kg) for canines or isoflurane gas (1–3% inhalant to effect) for pigs, followed by maintenance doses administered as needed. After the thorocotomy, the heart was suspended in a pericardial cradle. Ventilation was with room air mixed with oxygen adjusted to maintain physiological blood gas parameters and pH. A heated and automatically monitored heating table ensured physiological body temperature, and insulation and monitoring maintained stable cavity temperature to minimize any thermally induced repolarization changes. A pacing clip attached to the right atrial appendage provided control of heart rate above the intrinsic rate for each animal.

A suitable left anterior descending (LAD) segment was then dissected and freed from the underlying tissue. For one set of experiments in which we regulated the coronary flow progressively, the LAD was cannulated and perfused by the blood from one of the carotid arteries with flow rates controlled by a digital pump. In a second set of experiments, we circled the LAD using a snare that we closed completely to create ischemic episodes. In a third set of experiments, we circled the LAD using a hydraulic occluder and used it to regulate coronary flow. In this third approach, calibration of the fluid volume injected into the occluder enabled us to perform graded reductions in coronary perfusion. A heat exchanger ensured that the perfused blood was maintained at physiological temperatures. A measurement of coronary flow and intrinsic heart rate at the start of each experiment determined default resting values.

4.3.2 Experimental Protocols and Data Acquisition

The study protocol was designed to simulate two forms of acute ischemia: 1) a stress test with pacing as a surrogate for exercise and 2) episodes of reduced coronary perfusion to simulate coronary artery disease. Mirvis et al. have shown that tachycardia increases oxygen demand that is unaffected by mode of tachycardia induction, such as exercise or pacing [161]. Similarly, by combining elevated heart rate and reduced coronary perfusion in different protocols, we were able to simulate both of what are known as "demand" and "supply" types of ischemia. For demand ischemia, characterized by progressively elevating metabolic demand under stable perfusion conditions, the coronary perfusion was held constant and the pacing rate was increased in a stepwise manner in increments of the pacing interval of 30–50 milliseconds. Supply ischemia, in which demand is stable but blood supply is progressively reduced, was induced by keeping the pacing rate constant and decreasing the perfusion rate in steps of 7–10 ml/min for the cannulated LAD and steps of 25% perfusion deficit when using the hydraulic occluder. Each resulting ischemic episode lasted 2–10 minutes depending on the protocol, the intrinsic values of resting heart rate and coronary flow of each animal, and the maximum heart rates tolerated. Each experiment consisted of four to six such episodes separated by recovery periods (at intrinsic heart rates and perfusion) of approximately 25–30 minutes. Electrical recordings (described in detail below) were taken for 3 seconds every 15–30 seconds during the ischemic episode as well as during the recovery period. Fig. 4.1 contains a schematic of the animal preparation.

Epicardial potentials were recorded from the surfaces of both the ventricles using a 247-electrode flexible sock array, the construction of which is described elsewhere [162]. In addition, up to 26 flexible fiberglass needles [163], each carrying 10 electrodes along

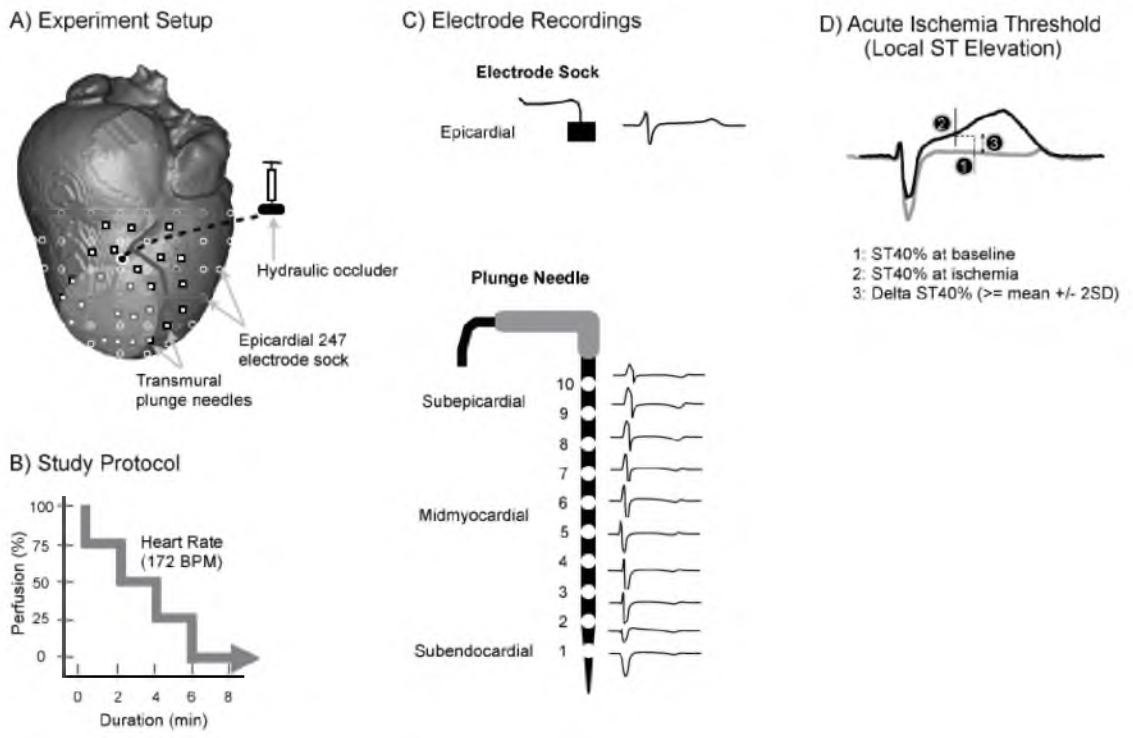

Fig. 4.1. Experiment setup: (a) Experiment setup, (b) sample study protocol, (c) sample epicardial and intramural electrograms, (d) ischemia threshold based on localized ST40% potential.

its length, spaced at 1.5 mm, were inserted into the ventricles in and around the region presumably perfused by the cannulated or occluded LAD, taking care to avoid injuring the epicardial arteries. The spacing between needles within the epicardial region they covered did not exceed 10 mm. The perfused region was identified before insertion by stopping blood flow through the LAD for 45 seconds and recording the resulting epicardial potentials. Localized ST segment elevations were considered indications of nearby ischemia. The potentials from sock and needle electrodes were recorded using a custom acquisition system permitting simultaneous acquisition of 1024 channels at 1 kHz sampling rate [164]. A single limb lead was used as a remote reference for all the unipolar signals recorded from the sock and needle electrodes.

4.3.3 Postexperiment Imaging and Signal Processing

The electrograms recorded during the study were processed in Matmap, a custom MATLAB-based signal processing program developed in our laboratory. The signals were first calibrated and gain adjusted and their baselines corrected. Poor quality signals from

sock and needle electrodes, for example, due to incomplete contact with the tissue, were discarded. Electrograms recorded from needle electrodes near the tip without positive Q-wave deflection were identified as cavity electrodes and also discarded. At the end of the experiment, the locations of preselected sock electrodes and all the plunge needles on the cardiac surface were digitally recorded using a Microscribe three-dimensional digitizer (Solution Technologies, Inc., Oella, MD). Interactive visualization of the resulting spatio-temporal maps of cardiac potentials was by means of *map3d* [183]. Following each experiment, the heart was excised and scanned with a 7-tesla MRI scanner (Bruker, Inc., Billerica, MA). The resulting image sets were segmented to identify the atria and ventricles using Seg3D [165], and the segmentations became the basis of a volumetric tetrahedral mesh created using SCIRun. The digitized sock and needle electrodes were then registered to this mesh geometry and visualized in SCIRun. Additional visualization and analysis were performed by interpolating potentials on parallel cutting planes regularly spaced through the volume. We differentiated between subendocardial, midmyocardial, and subepicardial regions, as defined by 0–30%, 30–70%, and 70–100% of the distance along those electrodes of each transmural plunge needle that were within the myocardium.

Elevation of the value of the potentials at 40% of the ST segment between the J-point and the peak of the T-wave (ST40%) provided the metric for local ischemia. The global root mean squared (RMS) signal computed from all the sock and needle electrode electrograms was used to identify J-point and T-peak fiducials. To minimize the effects of signal noise, we first computed the average of 10 potential values around the ST40% time instant. In addition, to minimize the influence of beat to beat fluctuations, we further averaged the ST40% values from three consecutive beats for each electrode site. The results from initial experiments indicated the need to normalize ST segment changes from control recordings taken before each intervention. All ST40% values within the same intervention were evaluated relative to these control values. We also defined a threshold for ischemic ST segment elevations from these normalized ST40% potentials as two standard deviations away from the baseline values.

4.3.4 Statistical Analysis

A chi-square test of goodness-of-fit was performed to determine whether the spatial distribution of acute ischemia—subendocardial, and distributed—were equally preferred. Statistical significance was set at alpha <0.05.

4.4 Results

In the experiments, we found examples of ischemia distributed over most of the ventricular wall. We show here three representative examples of ischemia measured in the subendocardium, the midwall, and the subepicardium together with statistical summaries of relative frequency of occurrence across all 29 experiments.

Fig. 4.2 highlights data from a canine study of supply ischemia in which acute ischemia was distributed in multiple, separate regions across the ventricular wall, all within the same ischemic intervention. Panel A shows the intramural ischemic volume and associated

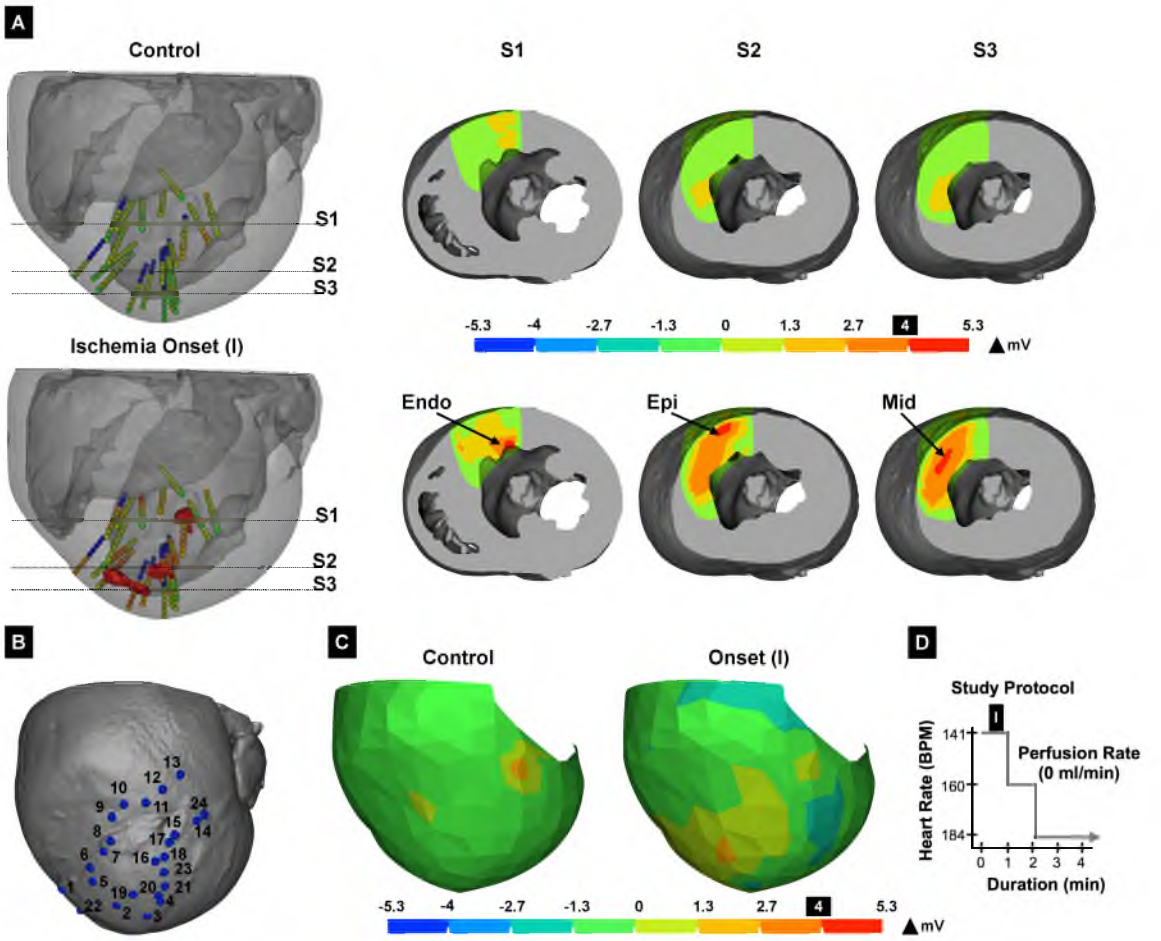

Fig. 4.2. Ventricular response to demand ischemia: Panel A shows the intramural ischemic volume and potential distributions across three slices. The locations of ST segment elevated regions are highlighted in red in the volume and the axial slices through the ST segment elevated regions in the subendocardium (S1), subepicardium (S2), and midwall (S3) regions, respectively. Panel B shows the canine heart with plunge needle locations. Panel C displays the corresponding epicardial ST40% potential difference map. Panel D shows the study protocol.

potentials at three axial slices, marked "S1" "S2," and "S3" under control conditions and at the onset of ischemia, which occurred 30 seconds into the intervention. The onset of ischemia was characterized by three ST segment elevated regions (in red) exceeding the threshold of two standard deviations from baseline (4 mV). The subsequent columns show the location of the ischemic regions in the subendocardium (S1), subepicardium (S2), and midwall (S3) regions, respectively. Panel B shows a rendering of the ventricles of this canine heart with locations of the plunge needles. Panel C displays the epicardial ST40% potential difference map at control and the onset of ischemia, which was nontransmural at this stage and showed no meaningful ST-segment shifts on the epicardial surface. The threshold for the epicardial ST40% marker was also at 4 mV corresponding to two standard deviations from baseline conditions. Panel D shows the study protocol: a sequence of demand ischemia with zero perfusion (no flow) through the LAD and increasing the heart rate from 150 to 200 BPM at 1 minute intervals.

Fig. 4.3 highlights data from another canine study during supply ischemia in which

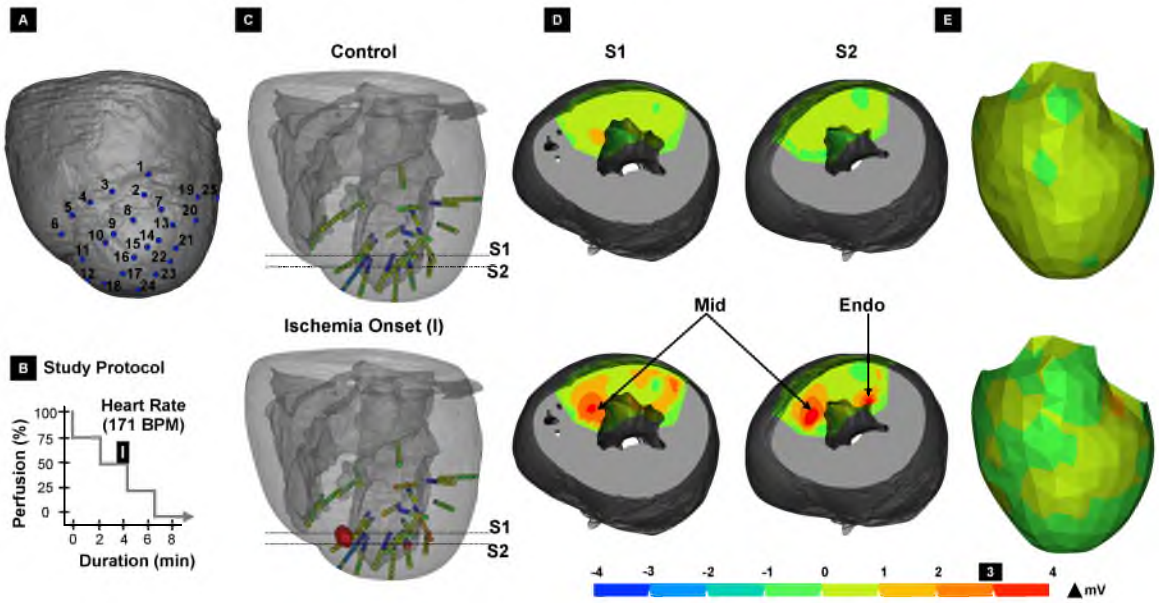

Fig. 4.3. Ventricular response to supply ischemia: Panel A shows the canine heart with plunge needle locations. Panel B shows the study protocol. Panel C and Panel D show the intramural ischemic volume and potential distributions across two slices, S1 and S2. The locations of ST segment elevated regions are highlighted in red in the volume and the axial slices through the ST segment elevated regions in the midwall (S1) and subendocardial (S2) regions, respectively. Panel E displays the corresponding epicardial ST40% potential difference map.

acute ischemia was also distributed in multiple, separate regions across the ventricular wall. Panel A shows a rendering of the ventricles of this canine heart with locations of the plunge needles. Panel B shows the study protocol: a sequence of supply ischemia with maintained heart rate at 171 BPM and decreasing the LAD perfusion from 100% to 0% at 2-minute intervals. Panel C shows the intramural ischemic volume and associated potentials at two axial slices, marked "S1," and "S2" under control conditions and at the onset of ischemia, which occurred at 50% reduction in LAD perfusion. The onset of ischemia was characterized by two ST segment elevated regions (in red) exceeding the threshold of two standard deviations from baseline (3 mV). Panel D shows the location of the ischemic regions in the midwall (S1) and subendocardial (S2) regions, respectively. Panel E displays the epicardial ST40% potential difference map at control and the onset of ischemia, which being nontransmural at this stage, is not yet localized on the epicardial surface maps. As in the previous figure, there is no apparent change in epicardial ST-segment potential at this early phase of ischemia. The threshold for the epicardial ST40% marker was also 3 mV, corresponding to two standard deviations from baseline conditions.

Fig. 4.4 shows an example of a single zone of acute ischemia localized in the midwall for a swine subject. Panel A shows a rendering of the swine heart with locations of the plunge needles. Panel B shows the intramural ischemic volume and associated potentials at the axial slice, marked "S1" under control conditions and at the onset of ischemia, which occurred at 50% reduction in LAD perfusion. The onset of ischemia was characterized by an ST segment elevated region (in red) exceeding the threshold of two standard deviations from baseline (3 mV). Panel C shows the location of the ischemic regions in the midwall (S1). Panel E displays the epicardial ST40% potential difference map at control and the onset of ischemia. The threshold for the epicardial ST40% marker was also at 3 mV, corresponding to two standard deviations from baseline conditions. Panel E shows the study protocol: a sequence of supply ischemia with maintained heart rate at 133 BPM and decreasing the LAD perfusion from 100% to 0% at 2-minute intervals.

We conducted acute ischemia studies on 29 animals (19 animals and 100 episodes in canines and 10 animals and 36 episodes in swines). For canines, 81% (81 out of 100), and in case of swines, 92% (33 out of 36) of episodes included ischemic regions in the subendocardial region. In addition, 75% of canine (75 out of 100), and 64% of swine (23 out of 36) episodes included ischemic regions in the midwall region. The subepicardium was least often represented with only 21% of canine (21 out of 100) and 22% of swine (8 out of 36) episodes including ischemia in this region. Furthermore, 64% (64 out of 100) of

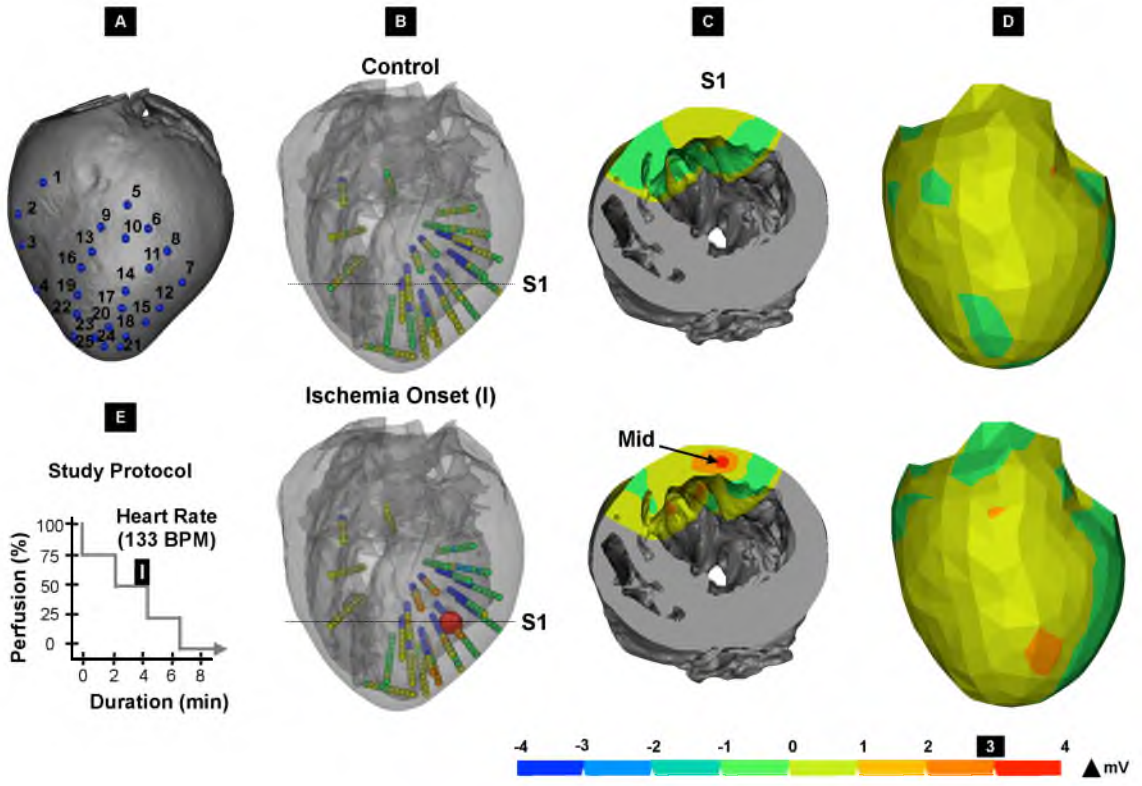

Fig. 4.4. A single ischemic zone in the midmyocardium of a pig study: Panel A shows the swine heart with plunge needle locations. Panel B and Panel C show the intramural ischemic volume and potential distributions across the axial slice (S1). The locations of ST segment elevated regions are highlighted in red in the volume and the axial slice through the ST segment elevated regions in the midwall (S1) region. Panel D displays the corresponding epicardial ST40% potential difference map. Panel E shows the study protocol.

canine, and 56% (20 out of 36) of swine episodes included ischemic regions that overlapped both subendocardial and midwall regions. Moreover, 21% of canine (21 out of 100) and only 0.02% of swine (1 out of 36) episodes resulted in ischemic regions overlapping both midwall and subepicardial regions. Figure 4.5 shows the statistical summary of the spatial organization of acute ischemic episodes resulting from the study. The upper histogram shows the relative frequency of occurrence of episodes in subendocardial, midwall and subepicardial regions as well as the overlapping regions (subendocardial and midwall, midwall and subepicardial) across the two species. The second row of the figure contains a different form of summary that indicates the number of episodes that included ischemia in the subendocardium or that spanned subendocardial and midmyocardial (blue bars) compared to those that included ischemia distributed through the ventricles. The distributed group comprised the remaining episodes, i.e., that resulted in ischemia that included at least one

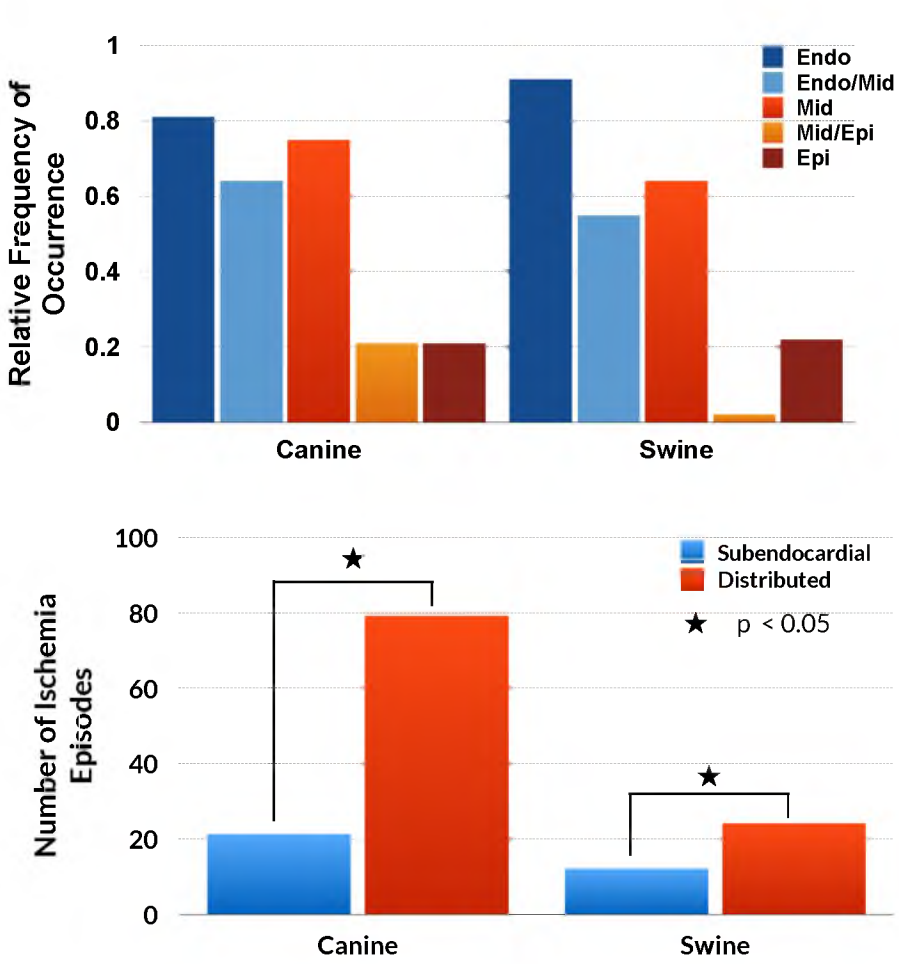

Fig. 4.5. Statistical summary of ischemia distribution across all studies: The histograms (upper row) quantify the relative frequency of occurrence of acute ischemia in each of the three defined regions of the ventricular wall as well as the two overlapping regions. The figures captures a total of 100 episodes of ischemia in dogs and 36 in pigs. The lower row contains a histogram of the distribution of the number of episodes that were localized to the subendocardium (blue) compared to those that included locations distributed across the ventricles (red).

region in midwall, subepicardial, or overlapping both midwall and subepicardial regions. For canines, 79% of episodes (X2 (1, N=100) = 33.64, $p < 0.05$), and for swines, 67% of episodes (X2 (1, N=36) = 4, $p < 0.05$), produced ischemia distributed across the ventricular wall.

4.5 Discussion

The aim of this study was to evaluate the conventionally held assumptions about nontransmural ischemia using intramural electrodes to measure three-dimensional potential

distributions in the ventricles of animals exposed to acute ischemia. To that end, we conducted a series of in situ experiments on canine and swine subjects and profiled the resulting intramural and epicardial potentials. We captured the spatial distribution of the electrocardiographic response acute myocardial ischemia under staged conditions of both supply and demand forms of the condition in both dogs and pigs. The consistent finding was that under any of these conditions and species, acute ischemia originated not only in the subendocardium but throughout the ventricular wall, i.e., in the subendocardium, midmyocardium, or the subepicardium. The most important conclusion from this study is that the electrical response of the heart to acute ischemic stress is not localized to the subendocardium, thus calling into doubt a major tenet of electrocardiography and the conventional explanation for primary ST segment depression.

Our choice of animal species follows the example of many past studies of ischemia and cardiac electrophysiology. Neither species is a perfect match to humans and so has strengths and weaknesses as an experimental model. Dogs have a conduction system more similar to that of humans [184], while it is the swine coronary vascular system that is more similar to that of humans [184]. The collateral circulation is more extensive in dogs compared to pigs, whereas the human collateral network falls somewhere between those two species [184]. Hence it is all the more meaningful that the results were consistent across both animal models, suggesting a fundamental mechanistic truth.

The study protocol was designed to simulate exercise testing or the very initial phase of a coronary spasm or myocardial infarct and thus focused on the most acute phase of ischemia. We designed the duration of ischemic episodes (2–10 minutes) to be within what is considered the reversible range [64], i.e., a level of insult from which the heart would recover fully in a short time. To allow sufficient recovery between ischemic episodes, we followed each ischemic episode by 25–30 minutes of recovery. Jennings et al. have shown that such a recovery period is enough to restore normal ATP production and achieve reversal of changes in cellular ultrastructure [64]. The use of plunge needle electrodes to record intramural potentials resulted in some tissue trauma, which resolved quickly with little myocardial scarring or LV dysfunction [185].

The findings of this study depend on the assumption that local shifts in extracellular ST segment potentials can be detected with sufficient spatial resolution and that they reflect nearby ischemia. While an indirect marker of what is fundamentally a perfusion deficit, intramural extracellular ST segment potentials have been shown to be a sensitive marker for ischemia [129, 150] and correlate well with regional blood flow [147] and local gas tension

measurements [186]. Moreover, the spatial resolution of our intramural recordings was 1.5 mm along each needle and 10 mm between neighboring needles, thus enabling a precise enough identification of intramural ischemia at the several millimeter scale we measured it.

There is some evidence in the literature to support the possibility that ischemia would occur first in subendocardial zones. For example, some studies speculate that the subendocardium is the region most vulnerable to ischemia due to transmural gradients in regional blood flow [187, 188, 189, 152], and others suggest the existence of intramyocardial pressure gradients [190, 191, 60] and greater metabolic stress [192, 64, 193]. Our results, however, do not support the resulting hypothesized consequences, none of which have actually been supported by measurements of three-dimensional parameters such as our studies describe.

Ours is not the only study to suggest heterogeneity of the ischemic response within the endocardium [139, 194, 85, 138, 195, 141, 196]. Steenbergen et al. [139] used NADH fluorescence photography in their rat model studies to show that ischemia produced by gradual reduction in coronary flow resulted in heterogeneous areas of anoxic tissue and attributed this response to intrinsic properties of arterioles. Gilmour et al. [85] studied the transmembrane potentials in a canine ischemia model to suggest that epicardial and papillary muscle excitability is more easily depressed during ischemia compared to endocardium, which is more responsive due to contact with the Purkinje fibers that provide continued electrical stimulation. Wilensky et al. [138] investigated transmembrane potentials in a rabbit model and suggested that during the first 10 minutes of ischemia, an endocardium rim layer, 60 cells deep (approximately 600 μ), remains unaffected by ischemia and may be attributed to multiple factors including diffusion of oxygen and nutrients from the cavity, blood transport via luminal vessels towards the subendocardial tissue, electrical coupling with Purkinje fibers, and greater resistance of subendocardial cells to effects of hypoxia, elevated extracellular potassium, and acidosis. Austin et al. [141], based on measurements of canine regional blood flow, suggested spatial heterogeneity of myocardial perfusion within the endocardium, resulting in islands of viable subendocardial tissue due to differences in local metabolic demand secondary to differences in regional function. Leshnower et al. [196], in an irreversible ischemia study on sheep, found that the midmyocardium was most vulnerable to ischemia and the subendocardium was most resistant. Even if there remains uncertainly as to specific mechanisms, there is emerging agreement from our and other findings calling into doubt the prevailing notion that the onset of ischemia is limited to the subendocardium. Ours remains the first to measure the electric potentials responsible for the ECG and thus capture the consequences of acute ischemia that are likely to be

clinically meaningful.

Our study suggests that acute ischemia arises throughout the myocardium, with no clear link between the type of ischemic insult and the location of electrocardiographic response. The experiment protocol was designed to induce reversible ischemic injury and measure localized ST segment potentials to determine the spatial distribution of early ischemia. Moreover, we benefited from the most detailed and comprehensive electrical measurements reported to date: a 247-electrode sock array to record epicardial potentials and up to 260 needle electrodes to measure intramural potentials, thus providing a high degree of three-dimensional spatial resolution. Additionally, the plunge needle electrodes were finer than previously available, creating less tissue injury, and therefore more sensitive measurements than possible in previous studies.

The clinical accuracy of the electrocardiogram (ECG) to detect and localize myocardial ischemia remains less than satisfactory [172], and our findings suggest possible mechanisms for this poor performance. ECG leads that show ST segment elevation provide a means of localizing transmural ischemia from the body surface and are a well-known clinical marker of infarction [197]. However, the ability of ST segment depression to locate ischemia is considerably less specific [179]. Acute ischemia studies with animal models have shown that even on the cardiac surface (epicardium), ST segment changes have poor sensitivity [150]. Our studies have shown that acute ischemia is not localized in the endocardium, rather, it arises throughout the myocardial wall. It is possible then that the superposition of these discrete ischemic sources may attenuate or neutralize resulting injury currents, limiting the ability of the epicardial electrograms to detect and localize nontransmural ischemia. Indeed, our data suggest that nontransmural ischemia is often undetected on the epicardial surface, especially using the ST segment as a marker. The consequences of this ambiguity on the body-surface ECG remain unexplored but are likely to be even less predictive than the more proximal and spatially resolved epicardial potentials.

4.6 Conclusion

In summary, our results suggest a complex electrocardiographic response to acute ischemia characterized by heterogeneous distribution of ST segment elevated regions across the myocardial wall. Understanding the spatial and temporal nature of these underlying bioelectric sources may provide future insights into ways to localize ischemia from the cardiac surface and may impact how we interpret potentials measured on the body surface. A possible approach we have also begun to evaluate successfully is to identify other electrical

markers (T-wave, QRS complex, etc.) in combination with ST segment that could improve the ability to detect and localize the extent of myocardial injury [198]. At a minimum, the spatial heterogeneity of the ischemic response that we have documented suggests a need to refine the current electrocardiographic model of ischemia.

CHAPTER 5

SPATIO-TEMPORAL EVOLUTION OF ACUTE MYOCARDIAL ISCHEMIA

The goal of this study goal was to evaluate whether acute myocardial ischemia follows a pattern of spatial and temporal evolution similar to that seen in myocardial infarction. The following research has been submitted to the *Journal of Electrocardiology*.

5.1 Abstract

We hypothesize that the spatio-temporal evolution of acute myocardial ischemia is more complex than the wavefront phenomenon of ischemic cell death during myocardial infarction. The goal of these experiments was to investigate the spatio-temporal progression of ischemia-induced shifts in ST segment potentials during short episodes of acute ischemia.

We conducted acute ischemia studies in an open-chest canine model, by creating finely controlled demand or supply ischemic episodes, and recording intramyocardial and epicardial potentials. The shape and size of the ischemic regions were tracked and shape analysis done by computing singular value decomposition (SVD) to determine the direction of maximal variation. A chi-square test of goodness-of-fit was also performed to determine whether the three directions of expansion—circumferential, longitudinal, and radial—were equally preferred.

During the early stages of acute ischemia development, the multiple and distinct ischemic regions grew in all three directions (radial, circumferential, and longitudinal), with more rapid expansion in the circumferential direction ($p < 0.05$). With increased stress, these regions continued to grow and eventually merged into one another, in the extreme becoming transmural.

Our findings suggest that the spatial and temporal progression of acute myocardial ischemia is more complex than the transmural wavefront phenomenon of myocardial infarction.

5.2 Introduction

Clinical performance of an electrocardiogram (ECG) to localize and detect the extent of myocardial ischemia remains less than satisfactory [172]. Myocardial ischemia occurs when the heart does not receive enough oxygen-rich blood to keep up with its metabolic requirements. Severe ischemia can lead to a heart attack and life-threatening arrhythmias so that early and accurate detection is an essential component of managing this condition. In the emergency room (ER), a resting 12-lead ECG is often recorded in patients with symptoms of angina (chest pain). However, the resting ECG is normal in up to 50% of the patients [1] with chronic stable angina. Moreover, myocardial ischemia occurs in approximately 70% of the patients [1] without angina. Exercise ECG stress testing (ET) has also been in widespread clinical use in the detection of myocardial ischemia. However, ET is characterized by poor sensitivity (68%) [1] and specificity (77%) [1], limiting its diagnostic efficacy.

The most common clinical ECG marker for myocardial ischemia detection is the ST segment. The changes in the ST segment can occur within 15–30 seconds after the onset of ischemia [173] and hence represent one of the earliest ECG markers of myocardial ischemia. The ST segment connects the QRS complex (ventricular depolarization) and the T-wave (ventricular repolarization) and represents the period when the ventricles are depolarized. It is isoelectric in a normal ECG. However, it can shift above (ST segment elevation) or below (ST segment depression) the baseline during myocardial ischemia depending on the flow of injury currents. These currents are the result of voltage gradients between normal and ischemic regions. In particular, the potential difference is caused by the electrical changes that occur in ischemic cells: localized shortening of action potential, diminishing amplitude of action potential, and a localized decrease in resting membrane potential. The resulting injury currents produce an ST segment elevation, if they are moving toward the recording electrode, and ST segment depression, if they are moving away from the electrode.

Classic electrocardiographic theory does not account for the clinical error rates. In clinical settings, ST segment elevation is closely related to the region of ischemia; however, ST segment depression's ability to locate nontransmural ischemia remains unclear [179]. Ischemia is known to be a dynamic condition that reflects the changing imbalance between blood supply and metabolic demand. The literature suggests that cell death (necrosis) during a myocardial infarction progresses transmurally as a wavefront from the inner (endocardium) surface and towards the outer (epicardium) surface [9]. Our goal in this study was to evaluate whether acute myocardial ischemia follows a similar pattern of spatial and

temporal evolution.

We hypothesized that ischemia progression is a more complex phenomenon than previously believed. To validate our hypothesis, we conducted a series of acute ischemia canine model studies under the assumption that localized ischemia causes localized ST segment changes. In particular, we measured three-dimensional surface and transmural potential distributions under study protocols that varied both local coronary supply and global metabolic demand.

5.3 Methods

5.3.1 Experimental Preparation

The goal of these experiments was to investigate the spatio-temporal progression of ischemia-induced shifts in ST segment potentials during short episodes of ischemia created by reduced coronary flow and increased rate of contraction. To this end, we performed experiments on open-chest, intact canines using multipolar intramural needle electrodes and surface electrodes. This study was performed in 19 animals including 8 mongrel dogs and 11 purpose bred dogs, following approval from the Institutional Animal Care and Use Committee at University of Utah and conformed to Guide for the Care and Use of Laboratory Animals (NIH Pub. No 85-23, Revised 1996).

An open-chest preparation following midsternal thorocotomy allowed easy access to the heart for recording epicardial and transmural electrical potentials. The animal was anesthetized by bolus injection of isofluorane gas (1–3% inhalant to effect), followed by maintenance doses administered as needed. After the thorocotomy, the heart was suspended in the pericardial cradle. A suitable left anterior descending (LAD) segment was dissected and freed from the underlying tissue. The coronary flow was regulated using a hydraulic occluder (Access Technologies Inc) placed around the dissected segment of the left anterior descending artery. Calibration of the fluid volume injected enabled us to perform graded, reproducible reductions in coronary perfusion. A pacing clip was attached to the right atrial appendage to control heart rate. The animal was ventilated with room air mixed with oxygen, and regular monitoring of blood gas parameters and pH ensured adequate ventilation. Core temperature was continuously monitored and stabilized by a heated table, and the cavity temperature was monitored and maintained by insulating the open chest. A measurement of coronary flow and intrinsic heart rate at the start of each experiment determined default resting values.

The study protocol was designed to simulate two forms of acute ischemia: 1) Demand ischemia, as would arise, for example, during a stress test with pacing as a surrogate for

exercise and 2) supply ischemia, through episodes of reduced coronary perfusion to simulate spasm or other transient reduction in coronary artery flow. It has been shown that tachycardia increases oxygen demand and is unaffected by mode of tachycardia induction such as exercise or pacing [199]. To create demand ischemia, we progressively elevated metabolic demand (by reducing the pacing interval stepwise in 30–50 milliseconds increments) under stable (often below normal) perfusion conditions. Supply ischemia was induced by keeping the pacing rate constant (but often elevated) and decreasing the perfusion in steps of 25% of normal.

Fig. 5.1 contains a schematic of the animal preparation. The experiment setup including the cartoon of the hydraulic occluder, 247-electrode epicardial sock, and 25 plunge needles is shown in Panel A of the figure. An example study protocol (supply ischemia) can be seen in Panel B. Sample epicardial and intramural electrograms recorded during the experiments are shown in Panel C. The threshold for localized ST40% potential elevation is calculated as shown in Panel D.

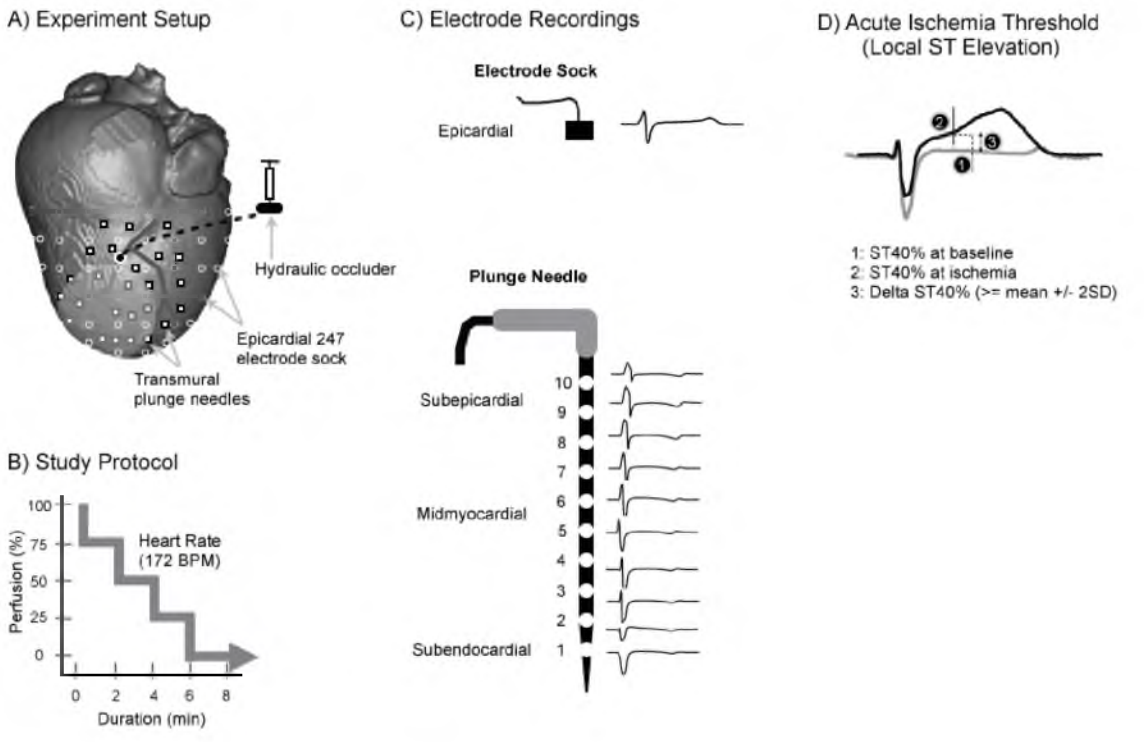

Fig. 5.1. Experiment setup: (a) Experiment setup, (b) sample study protocol, (c) sample epicardial and intramural electrograms, (d) ischemia threshold based on localized ST40% potential.

5.3.2 Experimental Protocols and Data Acquisition

Each resulting ischemic episode was 8–10 minutes in duration depending on the protocol, the intrinsic values of the animal, and the maximum heart rates tolerated. Each experiment consisted of four to six such episodes and the recovery period (at intrinsic heart rates and perfusion) between episodes was approximately 25–30 minutes. Electrical recordings were taken for 3 seconds every 15 seconds during the ischemic episode, as well as during the recovery period.

Epicardial potentials were recorded from the surfaces of both ventricles using a 247-electrode flexible sock array [162]. In addition, 25 flexible fiberglass needles [163], each carrying 10 electrodes along its length spaced at approximately 1.5 mm, were inserted into the left ventricle (LV) in and around the region presumably perfused by the occluded LAD, taking care to avoid injuring the epicardial arteries. The spacing between needles within the epicardial region they covered did not exceed 1 cm. The perfused region was identified by stopping blood flow for 45 seconds and recording the resulting epicardial potentials. Localized ST segment elevations in the needle electrograms were considered indications of nearby ischemia. The potentials from sock and needle electrodes were recorded using a custom acquisition system [164] permitting simultaneous recordings of 1024 channels at 1 KHz sampling rate. A single limb lead was used as a remote reference for all the unipolar signals recorded from the sock and needle electrodes.

At the end of the experiment, the locations of preselected sock electrodes and all the plunge needles on the cardiac surface were digitally recorded using a Microscribe three-dimensional digitizer (Microscribe Inc, Oella, Maryland). Interactive visualization of the resulting spatio-temporal maps of cardiac potentials was by means of SCIRun.

5.3.3 Postexperiment Imaging and Signal Processing

Following each experiment, the anatomical MRI scans of the excised heart were segmented to identify the atria and ventricles using the Seg3D [165] program, and the segmentations became the basis of a volumetric tetrahedral mesh created using BioMesh3D [168]. The digitized sock and needle electrodes were then registered to this mesh geometry and visualized in SCIRun. Visualization of the three-dimensional potential distributions within the heart in SCIRun required interpolation of the potential distribution for which we used a radial basis function (RBF) approximation.

The electrograms recorded during the study were processed in Matmap, a custom signal processing software. The signals were first calibrated and gain adjusted followed by baseline correction. Poor quality signals from sock and needle electrodes, perhaps due to bad contact,

were discarded. Electrograms recorded from needle electrodes without positive Q-wave deflection were identified as cavity electrodes and also discarded. The global root mean squared (RMS) signal computed from the electrograms at all the sock and needle electrode were used to identify the J-point and T-peak time instants. The value of potentials at 40% of the ST segment between the J-point and the peak of the T-wave (ST40%) provided the metric for local ischemia.

To minimize the effects of signal noise, an average of 10 potential values around the ST40% was taken. In addition, to minimize beat to beat fluctuations, the average of ST40% of five consecutive beats was computed. A key step in the signal processing was determining the regions of the heart that showed electrical indications of ischemia. For this, we computed potential differences between ST segment potentials (ST40%) recording during each ischemic episode relative to immediately preischemia controls. We defined a threshold for ischemic ST segment elevations in the resulting difference maps as two standard deviations from control values.

5.3.4 Statistical Analysis

Ischemic regions during an episode were characterized by local ST40% potentials exceeding the threshold value. The shape, size, and volume of these ischemic regions were tracked through the duration of the episode. Computing the singular value decomposition (SVD) of ischemic regions enabled us to determine the direction of maximal expansion.

Fig. 5.2 shows the SVD approach to the analysis of spatio-temporal progression of ischemia. The first column shows a representative heart with an initial ischemic region (blue) and the same ischemic region (red) expanded as a result of increased stress. The next three columns show the result of SVD on the two regions to identify the directions of the variation. The first singular vector correlates with the direction of maximal variation. The second and the third singular vectors map to the direction of the second and third most variation, respectively. For the sample case, the direction of maximal variation was circumferential, followed by longitudinal and then radial.

A chi-square test of goodness-of-fit was performed to determine whether the three directions of expansion—circumferential, longitudinal, and radial—were equally preferred. Statistical significance was set at alpha <0.05.

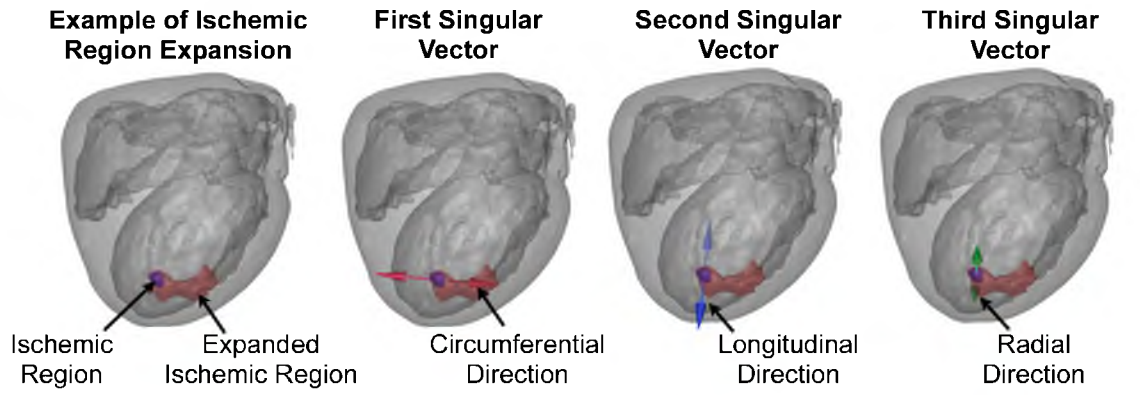

Fig. 5.2. Singular value decomposition (SVD) of the ischemic region expansion into first, second, and third singular vectors.

5.4 Results

For this study, we conducted 19 experiments in which there were 100 episodes of supply (50) and demand ischemia (50). All animals participated in the study. We show here representative data from supply ischemia and also demand ischemia experiments, depicting the spatial and temporal evolution of intramural and epicardial ST40% potential changes during acute ischemia.

Fig. 5.3 highlights data from one of the canine supply ischemia studies designed to induce graded reduction in LAD perfusion at a maintained heart rate of 171 BPM. The first row shows the subject-specific heart with location of plunge needle electrodes, the study protocol, and a table of the computed volumetric size of the ischemic regions at the specified instances (A, B, C, and D) during the ischemic episode. The threshold for epicardial and intramural markers was at 3 mV (ST40%), corresponding to two standard deviations from control conditions. The second row shows the volumetric (three-dimensional) intramural ST40% potential difference map and the plunge needle electrodes at control and at the corresponding time points, from which we computed the size of the intramural regions exceeding the ischemic threshold. The onset of ischemia when the perfusion was reduced to 25% (A) was characterized by two distinct regions. With continued stress (B), these regions expanded in size in all three directions—circumferentially, radially, and longitudinally. Moreover, an additional region appeared. The shapes of the ischemic regions suggested faster expansion circumferentially relative to the other two directions. At time point C, the regions had not only further expanded but two of them had merged together. With increased stress (0% perfusion) at time point D, these regions merged to become one transmural

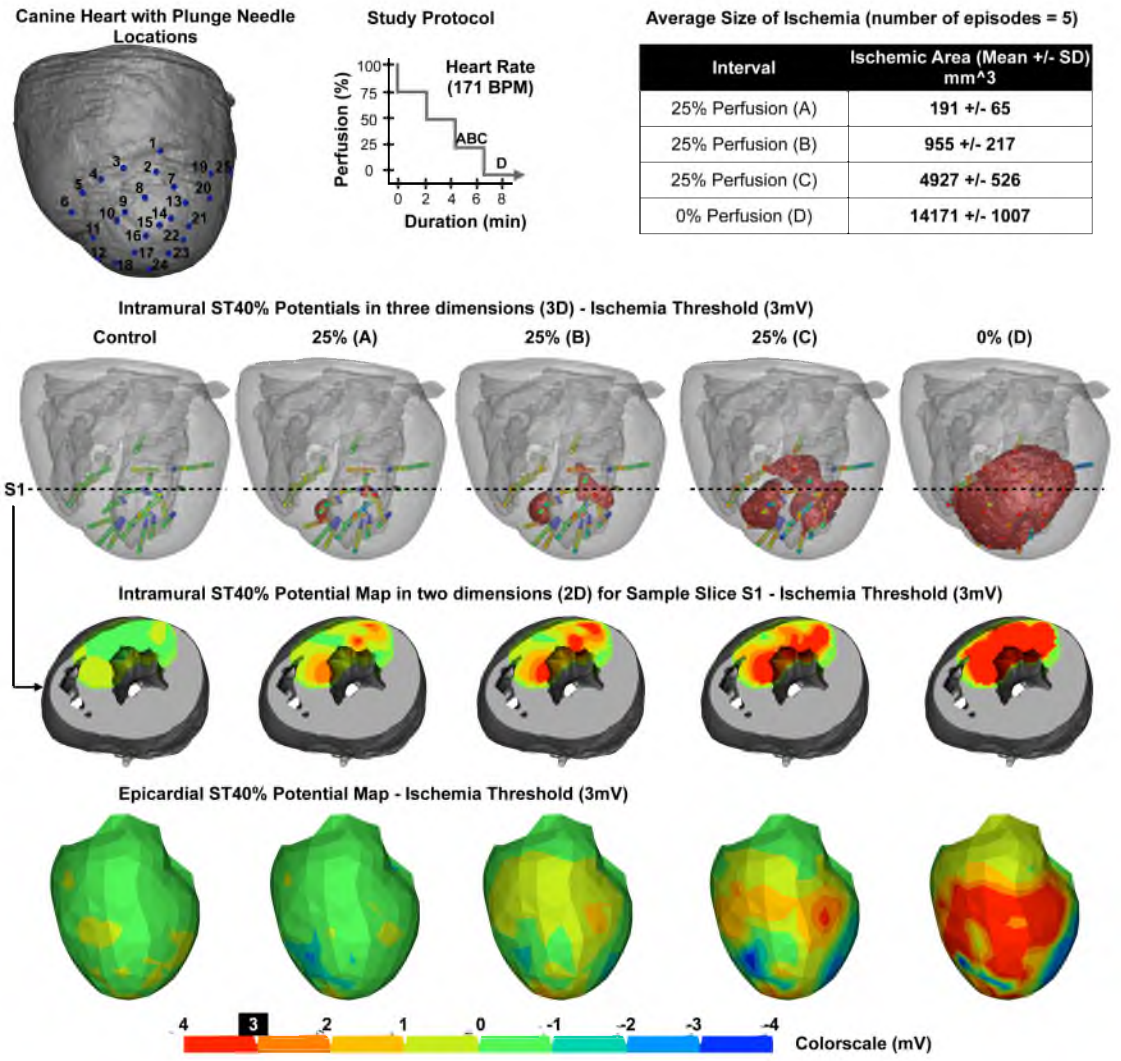

Fig. 5.3. Canine supply ischemia: The first row displays the heart location, plunge needle locations, study protocol, and a table of computed volumetric size of ischemic regions. The second row shows the volumetric intramural ST40% potential difference map. The third row displays the surface intramural ST40% potential difference map. The fourth row shows the epicardial ST40% potential difference map.

region. The third row displays a sample slice in two dimensions (surface) of the intramural ST40% potential difference map corresponding to the described behavior. The fourth row shows the equivalent epicardial ST40% potential difference map. The transmural nature of ischemic regions is captured on the epicardial surface at time point D.

Fig. 5.4 highlights data from one of the canine demand ischemia studies designed to induce graded increased in heart rate at perfusion reduced to no flow. The first row shows the subject-specific heart with location of plunge needle electrodes, the study protocol, and a

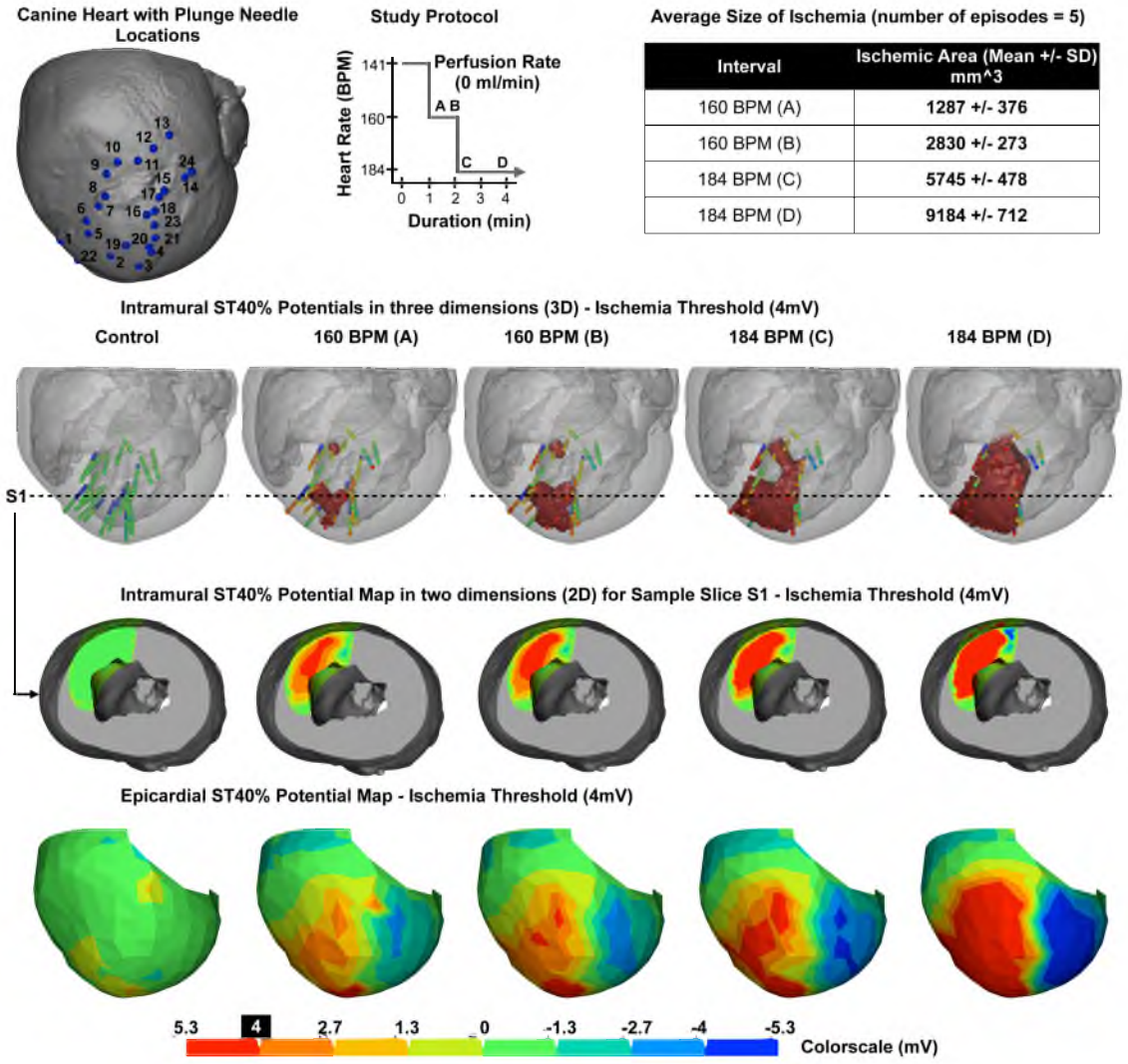

Fig. 5.4. Canine demand ischemia: The first row displays the heart location, plunge needle locations, study protocol, and a table of computed volumetric size of ischemic regions. The second row shows the volumetric intramural ST40% potential difference map. The third row displays the surface intramural ST40% potential difference map. The fourth row shows the epicardial ST40% potential difference map.

table of the computed volumetric size of the ischemic regions at the specified instances (A, B, C, and D) during the ischemic episode. The threshold for epicardial and intramural markers was at 4 mV (ST40%), corresponding to two standard deviations from control conditions. The second row shows the volumetric (three-dimensional) intramural ST40% potential difference map and the plunge needle electrodes at control and at the corresponding time points. The onset of ischemia when the heart rate was increased to 160 BPM (A) was

characterized by two distinct regions. With continued stress (B), these regions expanded in size in all three directions. With increased heart rate to 184 BPM at time point C and D, the regions had expanded and merged together. The third row displays a sample slice in two dimensions (surface) of the intramural ST40% potential difference map. The fourth row shows the corresponding epicardial ST40% potential difference map.

Fig. 5.5 displays the summary information from the 19 animal experiments. The bar graph represents three groups of ischemic regions based on their size (1000, 2000, or 3000 mm^3) and the direction of maximal expansion based on SVD analysis of their shapes. The right top panel shows the three directions, and the table below shows the results of the chi-square test of goodness-of-fit for each group. During the early stages of ischemia characterized by smaller ischemic regions, preference for the three directions was not equally distributed, with faster expansion seen circumferentially, X2 (2, N=19) = 8.00, $p < 0.05$.

5.5 Discussion

The aim of this study was to evaluate whether the spatio-temporal progression of acute ischemia was comparable to the transmural wavefront phenomenon seen in myocardial infarction. To that end, we conducted a series of acute ischemia in situ experiments on canines and characterized the resulting intramural and epicardial potentials. As seen in Fig. 5.3 and Fig. 5.4, we demonstrated that acute ischemia is characterized by multiple distinct regions that with increased stress expand in all three directions and eventually merge, in the extreme

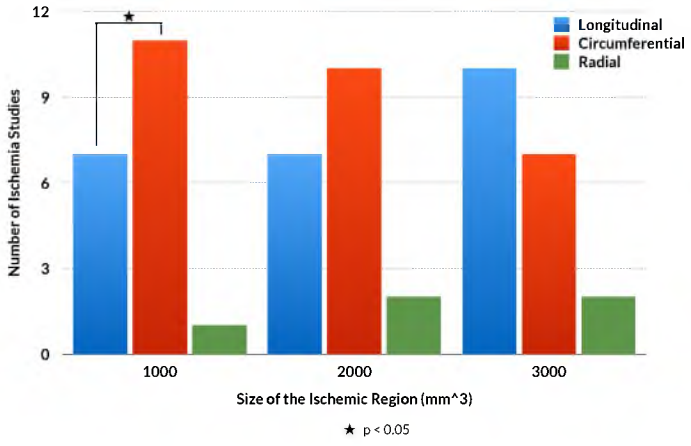

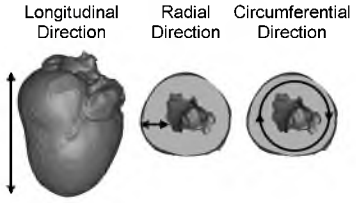

Chi-square test of goodness-of-fit (DF = 2, N = 19)

Group	X^2	P-value
1000	8.00	**p < 0.05**
2000	5.16	p > 0.05
3000	5.16	p > 0.05

Fig. 5.5. Study summary: The bar graph displays the summary results from the study. The right top panel shows the three directions of expansion. The table shows the results of chi-square test of goodness-of-fit.

becoming transmural. Moreover, in the early stages, the expansion of ischemic regions is faster in the circumferential direction relative to the radial and longitudinal directions. The main finding of this study is that spatial and temporal progression of acute ischemia does not follow the pattern documented for myocardial infarction.

The findings of this study depend on the assumption that local shifts in extracellular ST segment potentials can be detected with sufficient spatial resolution and that they reflect the underlying ischemia. The intramural extracellular ST segment potentials have been shown to be a sensitive marker for ischemia and correlate well with regional blood flow [150, 147, 186]. Moreover, with the spatial resolution of our intramural recordings, which was 1.5 mm along the axial direction (the recording needle shaft) and approximately 10 mm along the longitudinal direction (between adjacent needles), the resulting identification of intramural ischemia is precise enough for comparison with nearby epicardial potentials recorded from a high-resolution epicardial sock electrode.

To our knowledge, this is the first study to characterize the spatio-temporal progression of acute myocardial ischemia. Reimer et al., in their pioneering study on canine models, measured regional blood flow using microspheres and showed that irreversible ischemic injury characterized by necrosis progresses as a transmural wavefront from subendocardium to epicardium. Other studies have also reported that ischemia is detected in the subendocardial zone earlier than on the epicardial surface [152, 187]. It would be reasonable to construe that myocardial ischemia would display similar spatio-temporal evolution as myocardial infarction, expanding radially from subendocardium towards the epicardium. Our results, however, do not support this interpretation as none of the studies have been supported by measurements of three-dimensional parameters such as our studies describe.

Our study suggests that spatio-temporal progression of acute ischemia is characterized by distinct regions that expand in all directions and with increased stress eventually merge to become transmural. Moreover, in the early stages of ischemia development, the expansion is more rapid in the circumferential direction. This behavior makes sense, if one takes the geometry of the myocytes into consideration. Cardiomyocytes have elongated shapes with a shorter width (10–40 microns) than length (50–200 microns) [22]. Thus, for the same number of ischemic myocytes stacked radially and circumferentially, the shape of the resulting ischemic region would be larger in the circumferential direction. During the later stages of development, these merge to become larger regions, and the resulting shapes along the longitudinal and circumferential directions suggest a possible correlation with the orientation of myocardial fibers. The more rapid expansion of ischemia along the

circumferential and longitudinal directions as opposed to radially could also be tied back to the anisotropic and syncytial nature of the cardiac tissue. Indeed, studies have shown that in both the intracellular space and the interstitial space, conductivity is higher along the fiber direction than in the transverse direction [200]. Although ischemia expansion in the radial direction has the shortest distance to cover to reach the epicardium, the electrical anisotropy of the cardiac tissue, myocardial fiber orientation, and the shape of the individual cardiomyocytes all appear to play a role in faster expansion in the other two directions.

Of critical importance is the question of how these results might translate to the body surface, where ST segment changes certainly arise during ischemia but have yet to be linked precisely to the degree of intramural ischemia, as in this study. The clinical model of myocardial ischemia used for ECG-based diagnosis is tied to the expectation that spatio-temporal evolution of myocardial ischemia follows the myocardial infarction progression pattern. Our studies indicate that acute ischemia exhibits a more dynamic behavior with multiple ischemic regions across the ventricular wall that expand in all directions and eventually merge to become transmural. Thus, the current clinical model of ischemia may not be completely accurate and could be part of the problem with indeterminate results and false negatives routinely observed in the emergency room and during ET. We believe that the findings from this study may provide future insights into ways to localize ischemia from the cardiac surface and may impact how we interpret potentials measured on the body surface. A possible approach we have also begun to evaluate successfully is to identify other electrical markers (T-wave, QRS complex, etc.) in combination with the ST segment that could improve the ability to detect and localize the extent of myocardial injury [198].

5.6 Conclusion

In summary, our findings show that the spatial and temporal evolution of acute ischemia is characterized by multiple distinct regions that expand in all three directions, with maximal expansion in the circumferential direction, especially in the early stages of ischemic development. Furthermore, with increased stress, these regions continue to expand and eventually merge into one another, and in the extreme become transmural. These findings also point to the possibility of the combination of microvasculature distribution and cardiac fiber orientation affecting the shape, size, and location of the ischemic regions, a topic of ongoing research. In conclusion, the spatio-temporal progression of acute ischemia is a more complex phenomenon than previously believed and necessitates refining the current electrocardiographic model of ischemia.

CHAPTER 6

EPICARDIAL SENSITIVITY TO MYOCARDIAL ISCHEMIA

Our goal in this study was to evaluate whether electrical markers other than the ST segment changes are visible during acute ischemia and thus could improve diagnosis and localization. The following research was published in the *Journal of Electrocardiology* [198] and has been adapted for reprint with their permission.[1]

6.1 Abstract

We hypothesize that electrocardiographic measurements from the intramyocardial space contain more sensitive markers of ischemia than those detectable on the epicardium. The goal of this study was to evaluate different electrical markers for their potential to detect the earliest phases of acute myocardial ischemia.

We conducted acute ischemia studies in open-chest animals, by creating finely controlled demand or supply ischemic episodes and recording intramyocardial and epicardial potentials.

Under the conditions of mild perfusion deficit, acute ischemia induced changes in the T-wave that were larger and could be detected earlier on the epicardial surface than ST segment changes.

Our findings indicate that in the setting of very acute ischemia, epicardial T-waves have higher sensitivity to mild degrees of acute ischemia than epicardial ST segment potentials. These results suggest that changes in the T-wave shape may augment shifts in ST segments to improve ECG-based localization of ischemia.

---

[1] Adapted from *Journal of Electrocardiology*, vol. 47(6), K. Aras, B. Burton, D. Swenson, and R. MacLeod, "Sensitivity of epicardial electrical markers to acute ischemia detection," pp. 836-841, 2014, with permission from Elsevier.

6.2 Introduction

Despite a century of research and practice, the clinical accuracy of the electrocardiogram (ECG) to detect and localize myocardial ischemia remains less than satisfactory [172]. Myocardial ischemia occurs when the heart does not receive adequate oxygen-rich blood to keep up with its metabolic requirements, and severe ischemia can lead to myocardial infarction and life-threatening arrhythmias. Early and accurate detection is an essential component of managing this condition. Ischemia is known to be a dynamic condition that reflects a changing imbalance between blood supply and metabolic demand so that it is natural that examination under physical stress conditions or exercise testing (ET) is in widespread clinical use. However, ET is characterized by poor sensitivity (68%) and specificity (77%) [1], limiting its diagnostic usefulness.

The most common clinical ECG marker for myocardial ischemia detection is the ST segment, that portion of the ECG time signal that lies between the QRS and the T-wave. The ST segment represents approximately the period when the ventricles are depolarized, i.e., the ventricular action potentials are all in the plateau phase and in a healthy heart have approximately the same transmembrane potential. As a result, this phase is approximately isoelectric in a normal ECG. Changes in the ST segment arise in response to spatial heterogeneity of plateau potential and can occur within 15–30 seconds after the onset of ischemia [173], and hence are considered one of the earliest markers of the condition.

The mechanism for the ST segment potential shifting above (ST segment elevation) or below (ST segment depression) the baseline during myocardial ischemia is the flow of what are known as "injury currents." These currents are the result of voltage gradients between normal and ischemic regions that occur because of reduced amplitude and duration of ischemia action potentials. Changes in the action potentials can affect not only the ST segments but also the morphology of other electrical features of the ECG including the QRS complex [201, 202] and the T-wave [203, 202].

ECG leads that show ST segment elevation are spatially linked to the region of ischemia and thus provide a means of localizing transmural ischemia from the body surface. However, the ability of ST segment depression to locate ischemia is considered much less specific [179, 202]. ST segment depression is seen in patients with acute occlusion of the left circumflex artery (LCx) in leads V2-V3 and is an effect of ischemia in the free (postero) lateral wall. Moreover, patients with demand ischemia during exercise testing (ET) paradoxically show maximum ST segment depression in lead V5. Acute ischemia studies with animal models have shown that even on the cardiac surface (epicardium), ST segment changes have poor

sensitivity [150]. Thus, the ST segment, by itself, is not a reliable index of ischemia.

Our goal in this study was to evaluate whether electrical markers other than the ST segment changes are visible during acute ischemia and thus could improve diagnosis and localization. To this end, we conducted a series of acute ischemia studies on animal models to measure epicardial surface and three-dimensional, transmural potential distributions while varying both local coronary supply and global metabolic demand.

6.3 Methods

6.3.1 Experimental Preparation

The goal of these experiments was to evaluate ischemia-induced changes in epicardial electrical markers during the acute phase of short episodes of ischemia created by reduced coronary flow or increased heart rate. To this end, we performed experiments on 10 open-chest, intact swines using multipolar intramural needle electrodes and epicardial surface electrodes, following the approval of the Institutional Animal Care and Use Committee at University of Utah and conforming to the Guide for the Care and Use of Laboratory Animals (NIH Pub. No 85-23, Revised 1996).

An open-chest preparation following midsternal thorocotomy allowed direct access to the heart for recording epicardial and transmural electrical potentials. The animal was anesthetized by bolus injection of isofluorane gas (1–3% inhalant to effect), followed by maintenance doses administered as needed. After the thorocotomy, the heart was suspended in a pericardial cradle. A suitable left anterior descending (LAD) segment was then dissected and freed from the underlying tissue. The coronary flow was regulated using a hydraulic occluder (Access Technologies Inc) placed around the dissected segment of the left anterior descending artery. Calibration of the fluid volume injected enabled us to perform graded, reproducible reductions in coronary perfusion. The study protocol was designed to simulate two forms of acute ischemia: 1) Demand ischemia, as would arise, for example, during a stress test with pacing as a surrogate for exercise, and 2) supply ischemia, through episodes of reduced coronary perfusion to simulate spasm or other transient reduction in coronary artery flow. To create demand ischemia, we progressively elevated metabolic demand (by reducing pacing interval stepwise in 30–50 milliseconds increments) under stable (often below normal) perfusion conditions. Supply ischemia was induced by keeping the pacing rate constant (but often elevated) and decreasing the perfusion in steps of 25% of normal.

Fig. 6.1 contains a schematic of the animal preparation. The experiment setup including the cartoon of the hydraulic occluder, 247-epicardial electrode sock, and 25 plunge needles is shown in Panel A of the figure. An example study protocol (supply ischemia) can be seen

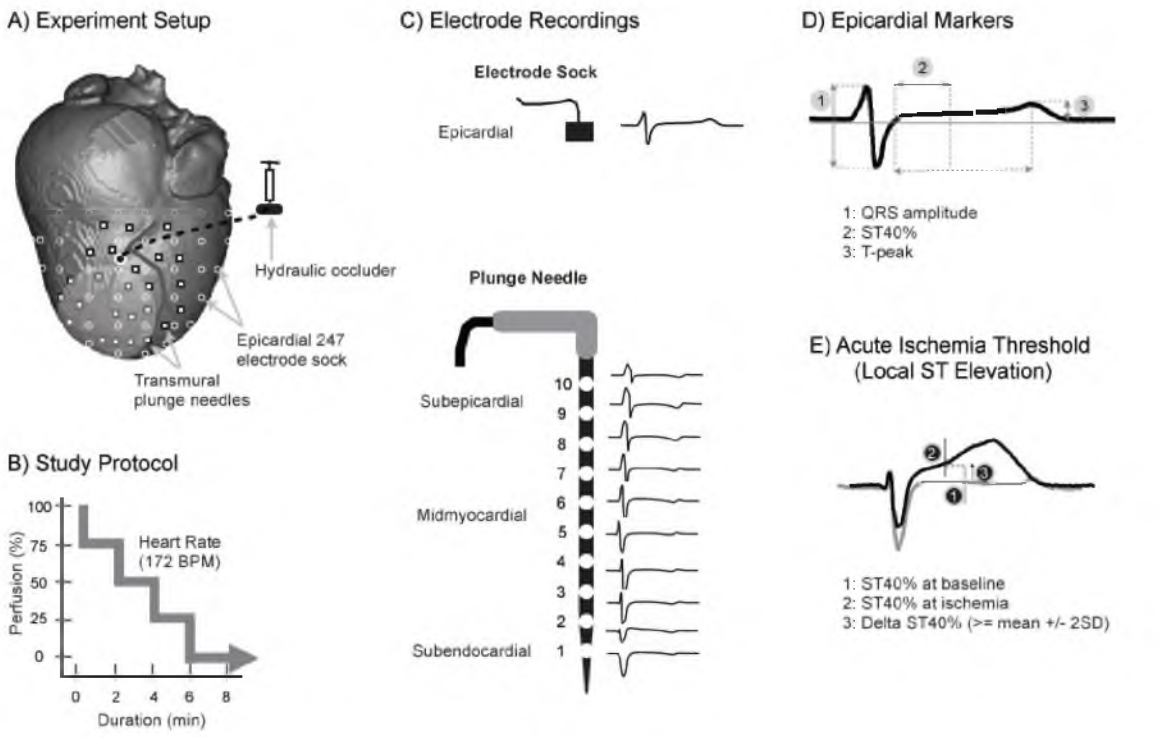

Fig. 6.1. A schematic of the animal preparation. The experiment setup including the cartoon of the hydraulic occluder, 247-epicardial electrode sock and 25 plunge needles shown in Panel A of the figure. An example study protocol (supply ischemia) can be seen in Panel B. Sample epicardial and intramural electrograms recorded during the experiments are shown in Panel C. Panel D shows epicardial electrical markers extracted for analysis. The threshold for localized ST40% potential elevation is calculated as shown in Panel E.

in Panel B. Sample epicardial and intramural electrograms recorded during the experiments are shown in Panel C. Panel D shows epicardial electrical markers extracted for analysis. The threshold for localized ST40% potential elevation is calculated as shown in Panel E.

6.3.2 Experimental Protocols and Data Acquisition

Each resulting ischemic episode was 8–10 minutes in duration depending on the protocol, the intrinsic values of the animal, and the maximum heart rates tolerated. Each experiment consisted of four to six such episodes and the recovery period (at intrinsic heart rates and perfusion) between episodes was approximately 25–30 minutes. Electrical recordings were taken for 3 seconds every 15 seconds during the ischemic episode, as well as during the recovery period.

Epicardial potentials were recorded from the surfaces of both ventricles using a 247-electrode flexible sock array [162]. In addition, 25 flexible fiberglass needles [163], each

carrying 10 electrodes along its length spaced at approximately 1.5 mm, were inserted into the left ventricle (LV) in and around the region presumably perfused by the occluded LAD, taking care to avoid injuring the epicardial arteries. The spacing between needles within the epicardial region they covered did not exceed 1 cm. Localized ST segment elevations in the needle electrograms were considered indications of nearby ischemia and served as the gold standard for the presence and location of ischemic regions. The potentials from sock and needle electrodes were recorded using a custom acquisition system [164].

At the end of the experiment, the locations of preselected sock electrodes and all the plunge needles on the cardiac surface were digitally recorded using a Microscribe three-dimensional digitizer (Microscribe Inc, Oella, Maryland). Interactive visualization of the resulting spatio-temporal maps of cardiac potentials was by means of SCIRun.

6.3.3 Postexperiment Imaging and Signal Processing

Following each experiment, the anatomical MRI scans of the excised heart were segmented to identify the atria and ventricles using the Seg3D [165] program, and the segmentations became the basis of a volumetric tetrahedral mesh created using BioMesh3D [168]. The digitized sock and needle electrodes were then registered to this mesh geometry and visualized in SCIRun.

The global root mean squared (RMS) signal computed from the electrograms at all the sock and needle electrodes were used to identify the J-point and T-peak time instants. The value of potentials at 40% of the ST segment between the J-point and the peak of the T-wave (ST40%) provided the metric for local ischemia. The peak amplitude of the T-wave also served as a T-wave marker. Other markers evaluated in this study included the peak to peak amplitude of the QRS complex and the R-wave amplitudes.

A key step in the signal processing was determining the regions of the heart that showed electrical indications of ischemia. For this, we computed potential differences between ST segment potentials (ST40%) recording during each ischemic episode relative to immediately preischemia controls. We defined a threshold for ischemic ST segment elevations in the resulting difference maps as two standard deviations from control values.

6.3.4 Statistical Analysis

True positive (TP) was defined as the number of sock electrodes that correctly detected the underlying intramural ST segment potentials above a threshold. False negative (FN) was defined as the number of sock electrodes that identified the underlying intramural ST segment potentials above the threshold as normal. True negative (TN) was defined as

the number of sock electrodes that correctly identified intramural ST segment potentials below the threshold. False positive (FP) was defined as the number of sock electrodes that identified the underlying intramural ST segment potentials below the threshold as ischemic. From these values, we computed sensitivity as (TP/(TP+FN)) and specificity as (TN/(TN+FP)) of the epicardial electrical markers.

The receiver operating characteristic (ROC) curves were calculated for the three epicardial markers: ST40%, T-wave, and R-wave. The area under the curve (AUC) was used as the metric for performance comparison. A one-way between subjects ANOVA was conducted with post hoc comparisons using the Tukey HSD (Honest Significance Difference) to evaluate the performance of ST40%, T-wave, and R-wave markers under demand ischemia, and supply ischemia conditions. Statistical significance was set at alpha <0.05.

6.4 Results

For this study, we conducted 10 experiments in which there were 44 episodes of supply (22) and demand ischemia (22). All animals participated in the study, and we rejected data from 12 episodes because of animal preparation degradation during the course of the experiment, resulting in ischemia persisting at control conditions. We show here representative data from only the supply ischemia experiments, depicting the spatial and temporal progression of epicardial ST segment and T-wave changes during acute ischemia.

Fig. 6.2 highlights data from one of the swine ischemia studies designed to induce a graded decrease in LAD perfusion at a maintained heart rate of 172 BPM (supply ischemia).

The figure includes electrograms recorded from one plunge needle and the overlying epicardial sock electrode with the locations of the plunge needle and the sock electrode shown in Panel A. Panel B shows the study protocol, and Panel C shows examples of epicardial and intramural electrograms recorded at control and during an acute ischemia episode at the designated stages of perfusion deficit. At 75% perfusion (A), changes in the intramural electrograms included elevated and upright T-waves and to a smaller extent changes in the QRS and ST segment. On the epicardial surface, there were corresponding changes only in the T-wave, which became elevated and upright. At 50% reduction (B), there were additional, progressive changes in all markers from the intramural electrograms, whereas on the epicardial surface, the electrogram displayed only slightly elevated ST segments in addition to the progressively elevated T-wave. At 25% perfusion (C), the epicardial electrode displayed elevated R-wave, ST segment, and T-wave, matching transmural ischemic conditions represented by the underlying plunge needle electrograms but delayed in their time of onset. Thus, the first changes seen anywhere on the epicardium

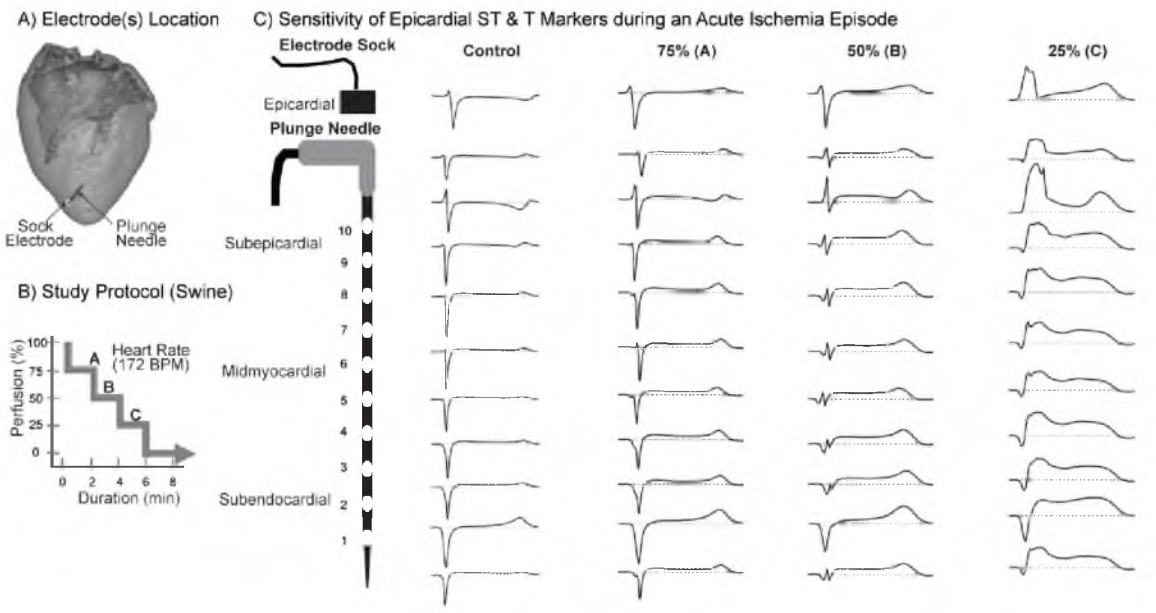

Fig. 6.2. Data from one of the swine ischemia studies designed to induced graded decrease in LAD perfusion at a maintained heart rate of 172 BPM (supply ischemia). The figure includes electrograms recorded from one plunge needle and the overlying epicardial sock electrode with locations of the plunge needle and the sock electrode shown in Panel A. Panel B shows the study protocol while Panel C shows examples of epicardial and intramural electrograms recorded at control and during acute ischemia episode at the designated stages of perfusion deficit.

were in the T-waves, subsequently followed, under conditions of increased ischemic load, by corresponding ST segment and R-wave changes. This progression in the appearance of changes in electrograms was not dependent on time but rather on the extent of ischemia induced by progressive reduction in coronary perfusion levels.

Fig. 6.3 highlights data from the same swine study, and includes spatio-temporal progression for epicardial and intramural electrograms.

The locations of the sock and the plunge needle electrodes, as well as the study protocol are seen in Panel A. Panel B highlights the corresponding epicardial ST40% and T-wave potential difference maps at control and at different perfusion rates. The thresholds for the epicardial markers were 1.5 mV (ST40%) and 3 mV (T-wave), respectively, corresponding to two standard deviations from baseline conditions. At 75% perfusion (A), there was diffused epicardial ST segment elevation over the anterior apical region, but sharp T-wave elevation on the anterior apical and midregions. At 50% perfusion (B), there was a marked increase in the size of the elevated T-wave regions on the epicardial surface. Moreover, the ST segment potential map displayed the first sharply elevated regions in the mid— and apical region. At

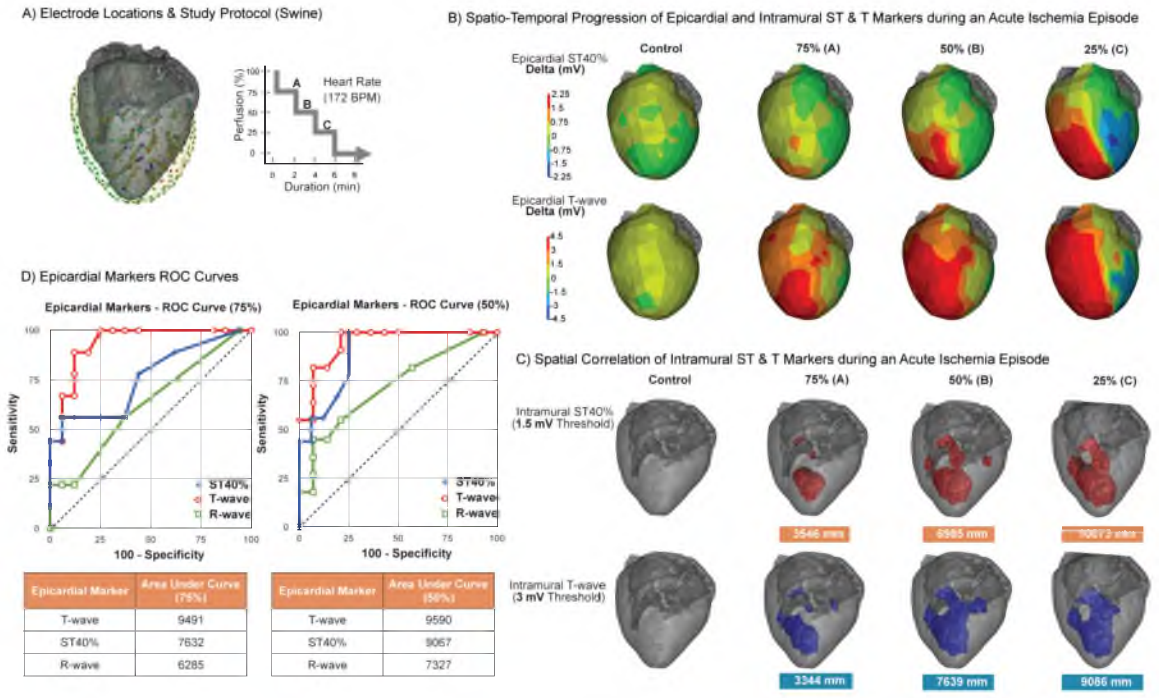

Fig. 6.3. Data from the same swine study, and spatio-temporal progression for epicardial and intramural electrograms. The locations of the sock and the plunge needle electrodes, as well as the study protocol are seen in Panel A. Panel B highlights the corresponding epicardial ST40% and T-wave potential difference maps at control and at different perfusion rates. The thresholds for epicardial markers were 1.5 mV (ST40%) and 3 mV (T-wave), respectively, corresponding to two standard deviations (SDs) from baseline conditions.

25% perfusion (C), there was a progressive increase in the elevated T-wave regions and to a lesser extent in the ST segment elevated regions on the epicardial surface. Panel C highlights the corresponding intramural ST40% and T-wave difference maps within the volume of the ventricle at the corresponding time points, from which it was possible to compute the size of the intramural regions exceeding the respective thresholds. There is a strong spatial correlation seen between the T-wave and ST segment potentials at the intramural level and also on the epicardial surface. Panel D displays the receiver operating characteristics (ROC) curves for the three most sensitive epicardial markers (ST40%, T-wave, R-wave) at 75% and 50% perfusion, relative to intramural ST segment elevations documented in Panel C. At 75% perfusion (mild acute ischemia), the epicardial T-wave marker consistently showed higher sensitivity at similar values of FPR, when compared to ST40% and R-wave epicardial markers. At 50% perfusion (moderate acute ischemia), the predictive value of epicardial T-wave and ST40% became comparable. Even so, the epicardial T-wave exhibited slightly higher sensitivity compared to ST40% at similar FPR values.

Fig. 6.4 shows the statistical summary of the epicardial sensitivity of electrical markers to acute ischemia detection from the studies on 10 swine animals. To summarize all the supply ischemia episodes, under the conditions of mild perfusion deficit (>50% perfusion), the area under the ROC curve was 0.83 +/- 0.03 for the T-wave, 0.60 +/- 0.07 for the ST40%, and 0.55 +/- 0.01 for the R-wave, respectively. The T-wave performed better than both ST40% and R-wave ($p < 0.05$) under mild perfusion deficit conditions. There was no statistical significance in the performance of ST40% and T-wave markers under moderate and severe perfusion deficit conditions.

For all the demand ischemia episodes, under the conditions of moderately elevated heart rates (172 BPM), the area under the ROC curve was 0.85 +/- 0.02 for the T-wave, 0.56 +/- 0.04 for the ST40%, and 0.33 +/- 0.03 for the R-wave, respectively. The T-wave performed better than both ST40% and R-wave ($p < 0.05$) under both moderate (172 BPM) and high heart rate (200 BPM) demand ischemia conditions.

6.5 Discussion

The aim of this study was to evaluate the sensitivity and specificity of epicardial electrical markers of acute ischemia relative to markers derived from intramural electrograms. To that end, we conducted a series of acute ischemia in situ experiments on swines and profiled the resulting intramural and epicardial potentials. As seen in Fig. 6.2, Fig. 6.3, and Fig. 6.4 we demonstrated that early in the development of acute ischemia, while the intramural electrograms were characterized by shortening of QRS potentials and elevation of T-wave and ST segment potentials, the corresponding epicardial electrograms showed changes only

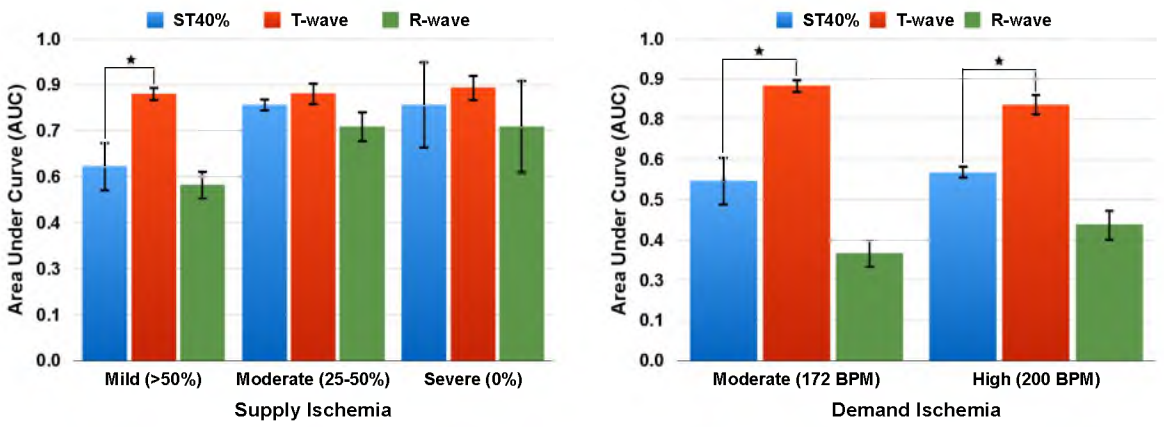

Fig. 6.4. Statistical summary of epicardial electrical markers to acute ischemia detection from the studies on 10 swine animals.

in the T-wave morphology. As the severity of acute ischemia increased, the epicardial electrograms eventually showed ST segment shifts and changes in the QRS morphology. The key finding from this study is that the epicardial T-wave is a more sensitive index of acute ischemia than epicardial ST segment changes, especially in the early stages of acute ischemia development.

The findings of this study depend on the assumption that local shifts in extracellular ST segment potentials can be detected with sufficient spatial resolution and that they reflect the underlying ischemia. Intramural extracellular ST segment potentials, an indirect marker of what is fundamentally a perfusion deficit, have been shown to be sensitive markers for ischemia and correlate well with regional blood flow [150]. Moreover, the spatial resolution of our intramural recordings, which was 1.5 mm along the axial direction (the recording needle shaft) and approximately 10 mm along the longitudinal direction (between adjacent needles), has never been achieved in any previously reported study to our knowledge. The resulting identification of intramural ischemia is therefore precise enough for comparison with nearby epicardial potentials recorded from a high-resolution epicardial sock electrode.

While our results are suggestive of new metrics for evaluating acute ischemia, they are based on epicardial and not body-surface potentials. Poor sensitivity of standard ECG stems, at least in part, from the fact that the magnitude of body surface potentials varies inversely with the distance between the recording leads and the heart [204]. Thus, the body surface electrodes, even those placed over the ischemic zone, would be expected to record lower ST segment deviation than cardiac surface electrodes placed near the ischemic area. The rational of our approach is that while good performance of an epicardial marker is no guarantee of similar results on the body surface, any useful body surface marker must perform at least as well on the epicardium. Moreover, an open-chest preparation, combined with intramural measurements, provides unparalleled documentation of the electrical consequences of ischemia and thus a robust ground truth for any more remote marker.

Within this framework, our results show that, even on the epicardial surface, the ST segment by itself has poor sensitivity during the early development of acute ischemia that does not extend to the epicardial wall, i.e., nontransmural acute ischemia. Several other groups have described the limited sensitivity of the epicardial ST segment to acute ischemia [150, 189]. For example, Smith et al. [189] reported that epicardial ST segment elevation implied ischemic injury; however, lack of ST segment elevation did not exclude the possibility of ischemia being present. Our results are consistent with these reports and suggest that the epicardial ST segment has high specificity but low sensitivity to

acute ischemia especially under mild perfusion (75%) deficit conditions. These results also suggest that performance based on body surface ECGs will likely be even worse under these conditions.

Previously described, ischemia-induced changes in the T-wave include the inverted T-wave turning shallow, flat, or upright [205]. These changes are attributed to shortening of the action potential duration in the ischemic cells, which reverses the direction of normal transmural potential gradients between the endocardium and the epicardium. Our results showed that the changes in epicardial T-waves were highly sensitive to low levels of acute ischemia. Moreover, the epicardial T-wave changes showed strong spatial correlation to ischemia-induced changes in the intramural T-wave and ST segment potentials. Miller et al. [206] have suggested that during repolarization (T-wave), the energy consuming process (Na+/K+ -ATPase) required to restore resting potential of the cell is likely to suffer from ischemia-induced hypoxia. As a result, this phase of the action potential might be expected to be more sensitive than others to the reduction in perfusion and energy substrate supply. Our results support these studies.

Of critical importance is the question of how these results might translate to the body surface, where ST segment and T-wave changes certainly arise during ischemia but have yet to be linked precisely to the degree of intramural ischemia, as in this study. It should be noted that our studies were, by design, focused on the early development of ischemia as characterized by the degree of perfusion and on measurements performed during this very acute phase. This restriction may limit translation to the broad clinical setting, as patients with acute supply ischemia are not likely to have their ECG recorded during the first few minutes of the ischemic episode. However, during exercise testing or other acute ischemic events, e.g., during surgery, our findings are likely to be, once again, relevant.

6.6 Conclusions

In summary, our results show that in the setting of very acute ischemia, epicardial T-waves have higher sensitivity to mild degrees of acute ischemia than epicardial ST segment potentials. Epicardial QRS potentials show even less sensitivity to mild ischemia than the ST segments and thus are likely to have very limited ability to localize the spatial extent or degree of myocardial ischemia. These results suggest the possibility of combining epicardial ST segment and T-wave markers to provide a more reliable index of acute ischemia than either in isolation, a topic of ongoing research.

CHAPTER 7

CONCLUSIONS AND FUTURE WORK

The research goal of this project on bioelectric source characterization of acute myocardial ischemia was to seek a better understanding of the electrical sources of ischemia. Motivation for this approach is the persistent lack of accuracy of current ECG based methods for ischemia evaluation. Rather than performing research on improved signal analysis or image reconstruction approaches our central goal was to capture with high spatial and temporal resolution the structure, location, organization and dynamic development of acute ischemia. Specifically, we asked three questions. First, where are these ischemic sources located? Second, how do they evolve? Third, how does the electrical data we collect relate to this ischemic sources? In this chapter, we summarize key findings and outline research ideas that could drive future research in this area.

7.1 Conclusions

Despite a century of research and practice, the clinical accuracy of the electrocardiogram (ECG) to detect and localize myocardial ischemia remains less than satisfactory [172]. Myocardial ischemia occurs when the heart does not receive adequate oxygen-rich blood to keep up with its metabolic requirements, and severe ischemia can lead to myocardial infarction and life-threatening arrhythmias. Early and accurate detection is an essential component of managing this condition.

The most common clinical ECG marker for myocardial ischemia detection is the ST segment, that portion of the ECG time signal that lies between the QRS complex and the T-wave. Changes in the ST segment can occur within 15–30 seconds after the onset of ischemia [173] and hence represent one of the earliest markers of the condition. The ST segment connects the QRS complex (ventricular depolarization) and the T-wave (ventricular repolarization) and represents the period when the ventricles are depolarized, i.e., the ventricular action potentials are all in the plateau phase and thus in a healthy heart have approximately the same transmembrane potential. As a result of the spatially homogeneous

transmembrane potentials, this phase of the normal ECG is isoelectric. However, the ST segment potential can shift above (ST segment elevation) or below (ST segment depression) the baseline during myocardial ischemia depending on the flow of what are known as "injury currents." These currents are the result of voltage gradients between normal and ischemic regions, gradients that arise because of changes that occur in the action potentials of ischemic cells: localized shortening, diminishing amplitude, and a decrease (more positive value) in resting membrane potential. The resulting injury currents can produce an ST segment elevation in an extracellular or body-surface electrode if they are directed toward the recording electrode or ST segment depression if they are directed away from the electrode.

Ischemia is known to be a dynamic condition that reflects a changing imbalance between blood supply and metabolic demand so that it is natural that examination under physical stress conditions or exercise testing (ET) is in widespread clinical use. However, ET is characterized by poor sensitivity (68%) and specificity (77%) [1], limiting its diagnostic usefulness and providing the motivation to address some gaps in our understanding of myocardial ischemia and its ECG signature. The goal of this research was to characterize the bioelectric sources of acute myocardial ischemia through a series of acute ischemia studies using high-resolution mapping of cardiac potentials on both canine and swine models.

The current literature suggests that myocardial ischemia originates from the subendocardium. However, studies done in the past have relied on measurements primarily on the epicardial and endocardial surfaces. Moreover, intramural measurements have been limited by sparse spatial resolution. Despite widespread use, the link, especially quantitatively, between the direction and extent of ST segment shifts and the putative ischemia is equivocal and thus the cause of persistent clinical error.

The aim of the first study was to evaluate the conventionally held mechanisms for nontransmural ischemia using intramural electrodes to measure three-dimensional potential distributions in the ventricles of animals exposed to acute ischemia. To that end, we conducted a series of demand and supply ischemia in situ experiments on canine and swine models and profiled the resulting intramural and epicardial potentials.

We benefited from the most detailed and comprehensive electrical measurements reported to date: a 247-electrode sock array to record epicardial potentials and up to 260 needle electrodes to measure intramural potentials, thus providing a high degree of three-dimensional spatial resolution. Additionally, the plunge needle electrodes were finer than previously available, creating less tissue injury and therefore more sensitive measurements

compared to previous studies.

We demonstrated that the electrocardiographic response of acute myocardial ischemia originated throughout the ventricular wall, i.e., in the subendocardium, midmyocardium, or the subepicardium under various conditions. The most important finding from this study is that the electrical response of the heart to acute ischemic stress is not localized in the subendocardium. Nor is there a clear link between the type of ischemic insult and the location of electrocardiographic response.

Understanding the spatial and temporal nature of these underlying bioelectric sources may provide future insights into ways to localize ischemia from the cardiac surface and may impact how we interpret potentials measured on the body surface. At a minimum, the spatial heterogeneity of the ischemic response that we have documented suggests the need to refine the current electrocardiographic model of ischemia.

The results from the first study provided the motivation for the second study, which was to profile the spatio-temporal evolution of acute myocardial ischemia. The literature suggests that cell death (necrosis) during a myocardial infarction progresses transmurally as a wavefront from the inner (endocardium) surface and toward the outer (epicardium) surface [9].

Our goal in the second study was to evaluate whether acute myocardial ischemia follows a pattern of spatial and temporal evolution similar to that seen in myocardial infarction. To that end, we conducted a series of acute ischemia in situ experiments on canines and characterized the resulting intramural and epicardial potentials. Our findings show that the spatial and temporal evolution of acute ischemia is characterized by multiple distinct regions that expand in all three directions, with maximal expansion in the circumferential direction, especially in the early stages of ischemic development. Furthermore, with increased stress, these regions continue to expand and eventually merge into one another, and in the extreme become transmural. These findings also point to the possibility of the combination of microvasculature distribution and cardiac fiber orientation affecting the shape, size, and location of the ischemic regions.

The implication of our findings is that the clinical model of ischemia used for ECG-based diagnosis may not be completely accurate and could be part of the problem, resulting in indeterminate results and false negatives routinely observed in the emergency room and during ET. The data generated in this study strongly suggest that the spatio-temporal progression of acute myocardial ischemia is a complex phenomenon. Based on these findings, we suggest an alternative model of spatio-temporal evolution of acute myocardial ischemia,

as shown in Fig. 7.1. We suggest that ischemia is not localized in the endocardium. Moreover, it is characterized by multiple regions distributed across the ventricular wall. These regions expand in all directions with increased stress. Moreover, they often merge together and in the extreme become transmural.

ECG leads that show ST segment elevation are spatially linked to the region of ischemia and thus provide a means of localizing transmural ischemia from the body surface. However, the ability of ST segment depression to locate ischemia is considered much less specific [203, 206]. ST segment depression is seen in patients with acute occlusion of the left circumflex artery (LCx) in leads V2-V3 and is an effect of ischemia in the free (postero) lateral wall. Moreover, patients with demand ischemia during exercise testing (ET) paradoxically show maximum ST segment depression in lead V5. Acute ischemia studies with animal models have shown that even on the cardiac surface (epicardium), ST segment changes have poor sensitivity [179]. Thus, the ST segment, by itself, is not a reliable index of ischemia.

The aim of the third study was to evaluate the sensitivity and specificity of epicardial electrical markers of acute ischemia relative to markers derived from intramural electrograms. To that end, we conducted a series of acute ischemia in situ experiments on swines and profiled the resulting intramural and epicardial potentials. We demonstrated that early in the development of acute ischemia, while the intramural electrograms was characterized by shortening of QRS potentials and elevation of T-wave and ST segment potentials, the corresponding epicardial electrograms showed changes only in the T-wave morphology. As the severity of acute ischemia increased, the epicardial electrograms eventually showed ST segment shifts and changes in the QRS morphology. The key finding from this study is that the epicardial T-wave is a more sensitive index of acute ischemia than epicardial ST segment changes, especially in the early stages of acute ischemia development. Epicardial QRS potentials show even less sensitivity to mild ischemia than the ST segments and thus are likely to have a very limited ability to localize the spatial extent or degree of myocardial ischemia. These results suggest the possibility of combining epicardial ST segment and T-wave markers to provide a more reliable index of acute ischemia than either in isolation.

7.2 Future Work

This dissertation sought to understand the bioelectric sources of acute myocardial ischemia relative to how they arise, evolve, and manifest on the epicardial surface. The results from the three studies have provided new information that contributes to our knowledge of acute myocardial ischemia and its ECG signature. Even so, there is much we do not

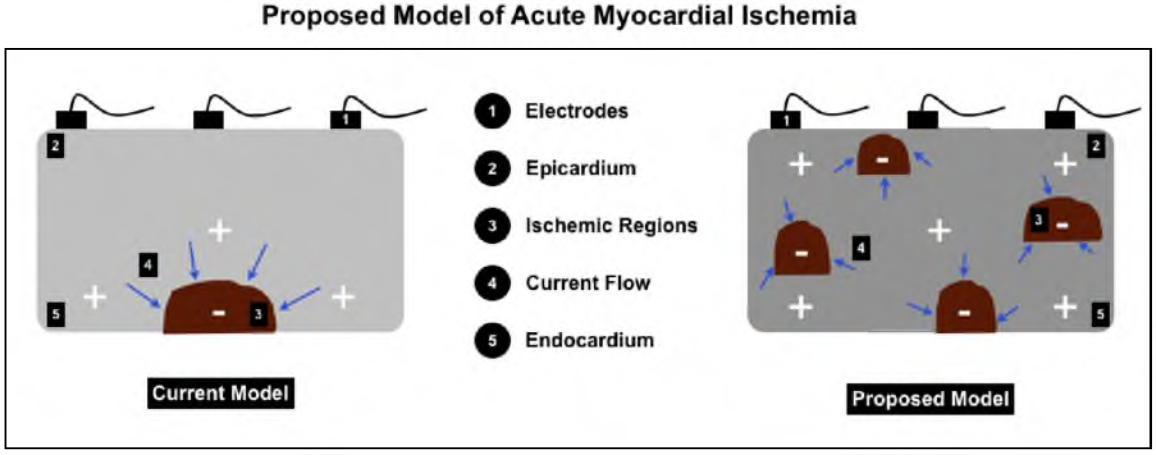

Fig. 7.1. Current and proposed model of acute myocardial ischemia. The proposed model suggests multiple ischemic regions distributed across the ventricular wall that expand in all three directions with increased stress. Moreover, they often merge together and in the extreme become transmural.

yet understand. In addition, the results from our studies have provoked new questions that merit further investigation. The following sections identify some of these questions and suggest potential studies that could help answer them. To achieve symmetry, we have organized the future work into three categories mapping to the three studies from the dissertation.

7.2.1 Spatial Organization of Ischemia

The aim of the first study was to evaluate the conventionally held mechanisms for nontransmural ischemia originating in the subendocardial region. The most important finding from this study was that the electrical response of the heart to acute ischemic stress results in distributed ischemia arising throughout the myocardial wall. However, the biophysical basis for distributed ischemia remains a matter of speculation. In addition, ancillary research questions that merit further exploration are briefly described below.

7.2.1.1 Demand Ischemia Versus Supply Ischemia

We conducted ischemia studies to simulate two forms of acute ischemia: a stress test with pacing as a surrogate for exercise, also called demand ischemia, and episodes of reduced coronary perfusion to simulate coronary artery disease, also called supply ischemia. Our research focused on understanding where the acute sources of ischemia arise when induced by demand or supply ischemia. An extension of this study would be to investigate if

demand and supply ischemia interventions conducted on the same animal would produce acute ischemia in similar locations.

7.2.1.2 Ischemic Preconditioning

Myocardial preconditioning refers to the phenomenon where brief episodes of ischemia produce a cardioprotective response during a subsequent longer episode of ischemia [95]. Our studies were designed to repeat the study protocol multiple times (four to six episodes per animal). The upshot of this approach was the likely preconditioning effect on the heart from the first episode affecting subsequent episodes. Thus, an extension of this study would be to compare the size, shape, and location of ischemic regions produced during the first episode with subsequent episodes.

7.2.1.3 Study Protocol

Kroll et al. [145], using canine studies, demonstrated that ATP levels were better maintained during demand ischemia, when compared to supply ischemia and attributed the results to protective effect of adenosine and adrenergic stimulation. This suggests that the pathway taken to reach a specific level of stress, whether demand or supply ischemia, could affect the onset of acute ischemia. An extension to our study would be to induce a given level of stress (e.g., elevated heart rate and reduced perfusion) using supply or demand ischemia study protocols on the same animal to determine if the pathway to stress affects the shape, size, and locations of acute myocardial ischemia.

7.2.1.4 Absence of ST Segment Depression on the Epicardium

A key finding from our study was the lack of epicardial ST segment depression to detect and localize nontransmural ischemia and suggests a complex and dynamic behavior of nontransmural bioelectric sources of ischemia. We used plunge needles to generate three-dimensional intramural surface maps. Moreover, since each plunge needle has 10 electrodes along its length, we can reconstruct up 11 (including the epicardium) cardiac potential distribution surface maps. An extension of this study could include a stepwise forward problem simulation from intramural needle surface 1 to intramural needle surface 2 and so on until we reach the epicardium. This approach would in theory provide a more systematic method to simulating epicardial potentials from intramural ischemic sources.

7.2.1.5 Primary ST Segment Depression on the Epicardium

Kligfield [207] suggested that metabolic severity of acute myocardial ischemia may be the primary factor driving exercise-induced ST segment depression. Based on our studies, we were able to produce primary ST segment depression (ST segment depression not adjacent to ST segment elevation) on the epicardial surface only in cases of demand ischemia at rapid heart rates. This result suggests that ST segment depression during demand ischemia is driven largely by increasing voltage gradients across the ischemic boundary. Thus, an extension of this study would be to conduct a forward problem simulation that evaluates a range of voltage gradients across the ischemic boundary and the effect on the epicardial potential distribution.

7.2.1.6 Masking Effect of Distributed Myocardial Ischemia

This research has focused on experimental evaluation of myocardial ischemia and its bioelectric sources. Based on our findings, we have suggested a refined source model of ischemia relative to its spatial organization and spatio-temporal evolution. In the future, this study could be augmented through computational modeling and simulation of ischemia using the proposed model. Specifically, an extension of this study could entail a forward problem simulation that compares a subendocardial ischemia source model to a distributed ischemia source model and determines whether the latter produces a masking effect on the resulting epicardial potential distribution.

7.2.2 Spatio-Temporal Evolution of Ischemia

The goal in the second study was to evaluate whether acute myocardial ischemia follows a similar pattern of spatial and temporal evolution as seen in myocardial infarction. The results from this study demonstrated that the spatio-temporal progression of acute myocardial ischemia is a more complex phenomenon characterized by multiple distinct regions that expand in all three directions and eventually merge together and become transmural. However, the relationship between the shape, size, location, and expansion pattern of these ischemic regions and their correlation with the myocardial fiber orientation and microvasculature has not yet been explored and could be an interesting future research topic. We briefly describe the correlation studies.

7.2.2.1 Correlation Study With Myocardial Fiber Orientation and Microvasculature

Based on our findings, we have suggested the possibility that the combination of microvasculature and the organization of cardiac fibers may also contribute to the more rapid expansion of ischemia along the circumferential and longitudinal directions as opposed to radially. Given that we can extract high-resolution, CT-based microvasculature images and DT-MRI-based organization of cardiac fibers, this idea could be further explored by doing a subject-specific qualitative and quantitative correlation study of cardiac fibers and microvasculature to the shape, size, location, and expansion of ischemic regions.

7.2.3 Sensitivity of Electrical Markers to Ischemia

The aim of the third study was to evaluate the sensitivity and specificity of epicardial electrical markers of acute myocardial ischemia. The key finding from this study was that the epicardial T-wave is a more sensitive index of acute ischemia than epicardial ST segment changes, especially in the early stages of acute ischemia development. Alternately, the ST segment remains a more specific marker to acute ischemia. These complementary strengths of the two markers suggest that a combination marker could potentially be a more reliable marker. In addition, there could be other temporal, integral, and potential difference markers that have not been evaluated and could be an interesting future research question. We describe a possible multivariate analysis approach to help answer these questions.

7.2.3.1 Multivariate Analysis of ST Segment and T-Wave Markers

An extension of the study would be conduct a multivariate analysis of different electrical markers (e.g., ST segment, T-wave, R-wave, S-wave, QRS complex, QT interval, QRS duration, STT interval, QRS integral, STT integral, and QRST integral) using statistical tools such as linear discriminant analysis, stepwise linear regression, etc., to identify markers sensitive or specific to acute ischemia. A further exploration of this idea could include creating a weighted scorecard of these markers, with the weights assigned based on the respective sensitivity and specificity scores.

7.2.4 Design of Experiments

We have been able to conduct robust studies based on the technology available to us. Specifically, the use of plunge needles enabled us to produce high-resolution three-dimensional intramural cardiac potential maps. In addition, with access to software tools from the SCI Institute, we were able to produce subject-specific spatial and functional

cardiac surface and volume potential maps. Even so, there are ways we can augment our experimental designs to improve our understanding of the bioelectric sources of ischemia. We describe some of these suggested improvements below.

7.2.4.1 Microspheres

The findings of this research depend on the assumption that local shifts in extracellular ST segment potentials can be detected with sufficient spatial resolution and that they reflect the underlying ischemia. Intramural extracellular ST segment potentials, an indirect marker of what is fundamentally a perfusion deficit, have been shown to be a sensitive marker for ischemia [129, 150] and correlate well with regional blood flow [147] and local gas tension measurements [186]. One way to augment this study would be to use fluorescent labeled microspheres, injected into coronary arteries to track regional blood flow deficits. This approach would complement our localized ST segment marker for ischemia. Microspheres traditionally have low spatial resolution (in the order of centimeters) but remain a trusted means of measuring perfusion.

7.2.4.2 Geometry Processing

The spatial resolution of our intramural recordings was 1.5 mm along the axial direction and 10 mm along the longitudinal direction, thus enabling a precise enough identification of intramural ischemia. The use of a three-dimensional Microscribe digitizer to digitally record the locations of preselected sock electrodes and plunge needles and subsequent registration to subject-specific mesh geometry has been basic to creating high-resolution three-dimensional and four-dimensional cardiac potential maps. The accuracy of the registration process was further improved by tracking the location of plunge needles from the anatomical MRI scans of the excised hearts and using it to register the digitally recorded electrode locations. Currently, there is variability from experiment to experiment, and it is possible to further improve the registration process and achieve higher precision and consistency across experiments. One possible approach to explore could be using depth cameras (e.g., Microsoft Kinect) that capture visual images (e.g., heart with sock and needle electrodes) along with per-pixel depth information and generate three-dimensional maps of the heart and electrode locations.

7.2.4.3 Experimental Setup

The experimental preparations we have employed to study ischemia include use of a cannula or the hydraulic occluder. The cannulation technique allows for controlled perfusion

of the heart by adjusting the rate of blood perfusate. However, the preparation can be tricky and can cause inadvertent tissue injury to the heart during the procedure. The use of a hydraulic occluder is a more convenient, less intensive, and relative injury-free procedure to achieve controlled perfusion. Although we have employed both techniques in the past, we migrated to using the hydraulic occluder for the majority of our experimental preparations. The calibration of fluid volume injected into the occluder allows for graded reductions in coronary perfusion. However, the regulation of perfusion using the occluder is less precise than using the cannulation technique as calibration of the fluid invariably includes air in the occluder that can never be completed removed. Thus, there are opportunities to improve upon the hydraulic occluder preparation. One likely approach is to employ a hydraulic pressure gauge to track cuff pressure and thus allow for occlusion at a definite cuff pressure in lieu of measuring the volume of the fluid injected into the occluder.

REFERENCES

[1] R. O'Rourke and P. O'Gara, *Hurst's the Heart - Diagnosis and Management of Patients with CID.* New York: McGraw-Hill, 2010.

[2] T. Thom, N. Haase, W. Rosamond, V. J. Howard, J. Rumsfeld, T. Manolio, Z. Zheng, K. Flegal, C. O'Donnell, S. Kittner, D. Lloyd-Jones, D. Goff, Y. Hong, R. Adams, G. Friday, K. Furie, P. Gorelick, B. Kissela, J. Marler, J. Meigs, V. Roger, S. Sidney, P. Sorlie, J. Steinberger, S. Wasserthiel-Smoller, M. Wilson, and P. Wolf, "Heart disease and stroke statistics - 2006 update: A report from the American Heart Association Statistics Committee and Stroke Statistics Subcommittee," *Circulation*, vol. 113, pp. 85–151, 2006.

[3] D. Hearse, "Myocardial ischaemia: Can we agree on a definition for the 21^{st} century?" *Cardiovascular Research*, vol. 28, pp. 1737–1744, 1994.

[4] E. Carmeliet, "Cardiac ionic currents and acute ischemia: From channels to arrhythmias," *Physiological Reviews*, vol. 79, pp. 917–1017, 1999.

[5] K. Reimer and R. Jennings, *The Heart and Cardiovascular System.* New York: Raven Press, 1992.

[6] R. Gianrossi, R. Detrano, D. Mulvihill, K. Lehmann, P. Dubach, A. Colombo, D. McArthur, and V. Froelicher, "Exercise-induced ST depression in the diagnosis of coronary artery disease. A meta-analysis," *Circulation*, vol. 80, pp. 87–98, 1989.

[7] D. Likhite, G. Adluru, N. Hu, C. McGann, and E. DiBella, "Quantification of myocardial perfusion with self-gated cardiovascular magnetic resonance." *Journal of Cardiovascular Magnetic Resonance*, vol. 17, no. 1, p. 14, 2015.

[8] K. Song, S. Kim, Y. Choe, W. Jung, S. Lee, S. Chang, Y. Choi, and J. Sung, "Integrated cardiac magnetic resonance imaging with coronary magnetic resonance angiography, stress-perfusion, and delayed-enhancement imaging for the detection of occult coronary artery disease in asymptomatic individuals." *International Journal of Cardiovascular Imaging*, p. 14, Apr 2015.

[9] K. Reimer, J. Lowe, M. Rasmussen, and R. Jennings, "The wavefront phenomenon of ischemic cell death. Myocardial infarct size vs duration of coronary occlusion in dogs," *Circulation*, vol. 56, pp. 786–794, 1977.

[10] R. Holland and H. Brooks, "Precordial and epicardial surface potentials during myocardial ischemia in the pig. A theoretical and experimental analysis of the TQ and ST segments," *Circulation Research*, vol. 37, pp. 471–480, 1975.

[11] D. Mirvis, "Physiologic bases for anterior ST segment depression in patients with acute inferior wall myocardial infarction," *American Heart Journal*, vol. 116, pp. 1308–1322, 1988.

[12] D. Li, A. Chot, and D. Kilpatrick, "Validation of a subendocardial ischaemia sheep model by intracoronary fluorescent microspheres," *Clinical and Experimental Pharmacology and Physiology*, vol. 23, pp. 111–118, 1996.

[13] M. Xin, E. Olson, and R. Bassel-Duby, "Mending broken hearts: Cardiac development as a basis for adult heart regeneration and repair," *Nature Reviews Molecular Cell Biology*, vol. 14, pp. 529–541, 2013.

[14] P. Macfarlane, A. van Oosterom, O. Pahlm, P. Kligfield, M. Janse, and J. C. (eds.), *Comprehensive Electrocardiology*. London: Springer-Verlag, 2011.

[15] C. Souders, S. Bowers, and T. Boudino, "Cardiac fibroblast. The renaissance cell," *Circulation Research*, vol. 105, pp. 1164–1176, 2009.

[16] M. Boyett, H. Honjo, and I. Kodama, "The sinoatrial node, a heterogeneous pacemaker structure," *Cardiovascular Research*, vol. 47, pp. 658–687, 2000.

[17] P. Iaizzo and A. Hill, *Handbook of Cardiac Anatomy, Physiology and Devices*, 2nd ed. New York: Springer Science and Business Media, 2009.

[18] P. Verdouw, M. van den Doel, S. de Zeeuw, and D. Duncker, "Animal models in the study of myocardial ischemia and ischaemic syndromes," *Cardiovascular Research*, vol. 39, pp. 121–135, 1998.

[19] J. Fedor, D. McIntosh, J. Rembert, and J. Greenfield, "Coronary and transmural myocardial blood flow responses in awake domestic pigs," *American Journal of Physiology*, vol. 235(4), pp. 435–444, 1978.

[20] D. Gregg, "Brief reviews: The natural history of coronary collateral development," *Circulation Research*, vol. 35, pp. 335–344, 1974.

[21] R. Hamlin, R. Burton, S. Leverett, and J. Burns, "Ventricular activation process in mini pigs," *Journal of Electrocardiology*, vol. 8, pp. 113–116, 1975.

[22] A. Guyton and J. Hall, *Guyton and Hall Textbook of Medical Physiology*, 13th ed. Philadelphia: Elsevier Saunders, 2006.

[23] H. H. Jr., "Molecular aspects of water transport," *Pediatrical Nephrology*, vol. 6, pp. 304–310, 1992.

[24] G. Benga, "Birth of water channel proteins - The aquaporins," *Cell Biology*, vol. 27, pp. 701–709, 2003.

[25] D. Sigg, D. Jaye, and Y. Xiao, *Cardiac Electrophysiology Methods and Models*. London: Springer, 2010.

[26] Y. Hirano, A. Moscucci, and C. January, "Direct measurement of L-type Ca^{++} window current in heart cells," *Circulation Research*, vol. 70, pp. 445–455, 1992.

[27] M. Sanguinetti and N. Jurkiewicz, "Two components of cardiac delayed rectifier K^+ current. Differential sensitivity to block by class III anti arrhythmic agents," *Journal of General Physiology*, vol. 96, pp. 195–215, 1990.

[28] M. Rocchetti, A. Besana, G. Gurrola, L. Possani, and A. Zaza, "Rate-dependency of delayed rectifier currents during the guinea-pig ventricular action potential," *Journal of Physiology*, vol. 534, pp. 721–732, 2001.

[29] S. Litovsky and C. Anzelevitch, "Transient outward current prominent in canine ventricular epicardium but not endocardium," *Circulation Research*, vol. 62, pp. 116–126, 1986.

[30] D. Liu and C. Anzelevitch, "Characteristics of the delayed rectifier current in canine ventricular epicardial, mid myocardial and endocardial myocytes," *Circulation Research*, vol. 76, pp. 351–365, 1995.

[31] A. Noma, T. Nakayama, Y. Kurachi, and H. Irisawa, "Resting K^+ conductances in pacemaker and non-pacemaker heart cells of the rabbit," *Japanese Journal of Physiology*, vol. 34, pp. 709–727, 1984.

[32] D. Noble, J. Denyer, H. Brown, and D. DiFrancesco, "Reciprocal role of inward currents I_b and I_f in controlling and stabilizing pacemaker frequency of rabbit SA node cells," *Proceedings Royal Society of London Biological Sciences*, vol. 250, pp. 199–207, 1992.

[33] D. DiFrancesco, "Pacemaker mechanisms in cardiac tissue," *Annual Review of Physiology*, vol. 55, pp. 451–467, 1993.

[34] R. Klabunde, *Cardiovascular Physiology Concepts*, 2nd ed. Philadelphia: Lippincott and Williams and Wilkins, 2011.

[35] D. Bers, "Cardiac excitation-contraction coupling," *Nature*, vol. 415, pp. 198–205, 2002.

[36] D. Scriven, P. Dan, and E. Moore, "Distribution of proteins implicated in EC coupling in rat ventricular myocytes," *Biophysics Journal*, vol. 79, pp. 2682–2691, 2000.

[37] C. Franzini-Armstrong, F. Protasi, and V. Ramesh, "Shape, size and distribution of calcium release units and coupons in skeletal and cardiac muscles." *Biophysics Journal*, vol. 77, pp. 1528–1539, 1999.

[38] R. Sitsapesan and A. Williams, "Regulation of gating of sheep cardiac SERCA channel by luminal calcium," *Journal of Membrane Biology*, vol. 137, pp. 215–226, 1994.

[39] K. Sipido, G. Callewaert, and E. Carmeliet, "Inhibition and rapid recovery of Ca^{++} current during Ca^{++} release from sarcoplasmic reticulum in guinea pig ventricular myocytes," *Circulation Research*, vol. 76(1), pp. 102–109, 1995.

[40] A. Harris, "Emerging issues of connexin channels: Biophysics fills the gap," *Quarterly Reviews of Biophysics*, vol. 34, pp. 325–472, 2001.

[41] M. Delmar, W. Coombs, P. Sorgen, H. Duffy, and S. M. Taffet, "Structural bases for the chemical regulation of connexin43 channels," *Cardiovascular Research*, vol. 62, pp. 268–275, 2004.

[42] S. Weidman, "Electrical constants of trabecular muscle from mammalian heart," *Journal of Physiology*, vol. 210, pp. 1041–1054, 1970.

[43] B. Taccardi, B. Punske, F. Sachse, X. Tricoche, P. Colli-Franzone, L. Pavarino, and C. Zabawa, "Intramural activation and repolarization sequences in the ventricles. Experimental and simulation studies," *Journal of Electrocardiology*, vol. 38, pp. 131–137, 2005.

[44] M. Valderrabano, "Influence of anisotropic conduction properties in propagation of action potential," *Progress Biophysics Molecular Biology*, vol. 94, pp. 144–168, 2007.

[45] L. Waldman, D. Nosan, F. Villarreal, and J. Covell, "Relation between transmural deformation and local myofiber direction in canine left ventricle," *Circulation Research*, vol. 63, pp. 550–562, 1988.

[46] S. Wickline, E. Verdonk, A. Wong, R. Shepard, and J. Miller, "Structural remodeling of human myocardial tissue after infarction. Quantification with ultrasonic backscatter," *Circulation*, vol. 85, pp. 259–268, 1992.

[47] A. Kleber, M. Janse, and V. Fast, *Handbook of Physiology: Cardiovascular System.* London: Oxford University Press, 2001.

[48] D. Durrer, R. VanDam, G. Freud, M. Janse, F. Mejler, and R. Arzabaecher, "Total excitation of the isolated human heart," *Circulation*, vol. 41, pp. 899–912, 1970.

[49] J. Cinca, M. Janse, H. Morena, J. Candell, V. Valle, and D. Durrer, "Mechanism and time course of the early electrical changes during acute coronary artery occlusion," *Chest*, vol. 77, pp. 188–204, 1980.

[50] R. Plonsey, "An extension of the solid angle formulation of an active cell," *Biophysics Journal*, vol. 5, pp. 663–666, 1965.

[51] R. Holland and M. Arnsdorf, "Solid angle theory and the ECG: Physiologic and quantitative interpretations," *Progress in Cardiovascular Disease*, vol. 19, pp. 431–457, 1977.

[52] R. Plonsey and R. Barr, *Bioelectricity: A Quantitative Approach*, 3rd ed. New York: Kluwer Academic Plenum, 2007.

[53] H. Burger, "The zero potential: A persistent error," *American Heart Journal*, vol. 49, pp. 581–586, July 1955.

[54] Z. Ihara, A. van Oosterom, and R. Hoekema, "Atrial repolarization observed during the PQ interval," *Journal of Electrocardiology*, vol. 39(3), pp. 290–297, 2006.

[55] N. Flowers, V. Shvartsman, H. Palakurthy, G. Som, and M. Sridharan, "Analysis of PR intervals in normal subjects and early studies in patients with abnormalities of conduction system using surface His bundle recordings," *Journal of American College of Cardiology*, vol. 2, pp. 939–946, 1983.

[56] R. Helm, "Electrocardiographic cancellation. Mathematical basis," *American Heart Journal*, vol. 60, pp. 251–265, 1960.

[57] M. Burgess, L. Green, K. Millar, R. Wyatt, and J. Abildskov, "The sequence of normal ventricular recovery," *American Heart Journal*, vol. 84(5), pp. 660–669, 1972.

[58] H. Kishida, J. Cole, and B. Surawicz, "Negative U wave: A highly specific but poorly understood sign of heart disease," *American Journal of Cardiology*, vol. 49, pp. 2030–2036, 1982.

[59] J. Lowe, R. Cummings, D. Adams, and E. Hull-Ryde, "Evidence that ischemic cell death begins in the subendocardium," *Circulation Research*, vol. 51, pp. 683–693, 1983.

[60] H. Sabbah and P. Stein, "Effect of acute regional ischemia on pressure in the subepicardium and subendocardium," *American Journal of Physiology*, vol. 242, pp. H240–H244, 1982.

[61] S. Rabbany, J. Kresh, and A. Noordergraaf, "Intramyocardial pressure: Interaction of myocardial fluid pressure and fiber stress," *American Journal of Physiology*, vol. 26, pp. H357–H364, 1989.

[62] T. Moir, "Subendocardial distribution of coronary blood flow and the effect of antianginal drugs," *Circulation Research*, vol. 30, pp. 621–627, 1972.

[63] V. Fuster, L. Badimon, and J. Badimon, "The pathogenesis of coronary artery disease and ACS," *New England Journal of Medicine*, vol. 326, pp. 242–250, 1992.

[64] R. Jennings, C. Ganote, and K. Reimer, "Ischemic tissue injury," *American Journal of Pathology*, vol. 81, pp. 179–198, 1975.

[65] E. Falk, "Pathogenesis of atherosclerosis," *Journal of American College of Cardiology*, vol. 47, pp. C7–C12, 2006.

[66] Y. Chatzizisis, A. Coskun, and M. Jonas, "Role of endothelial shear stress in the natural history of coronary atherosclerosis and vascular remodeling: Molecular, cellular and vascular behavior," *Journal of American College of Cardiology*, vol. 49, pp. 2379–2393, 2007.

[67] J. Schaar, J. Muller, and E. Falk, "Terminology for high-risk and vulnerable coronary artery plaques," *European Heart Journal*, vol. 25, pp. 1077–1082, 2004.

[68] S. Jadhav, W. Ferrell, and J. Petrie, "Microvascular function, metabolic syndrome and novel risk factor status in women with cardiac syndrome X," *American Journal of Cardiology*, vol. 97, pp. 1727–1731, 2006.

[69] K. Kobayashi and J. Neely, "Control of maximum rates of glycolysis in rat cardiac muscle," *Circulation Research*, vol. 44, pp. 166–175, 1979.

[70] C. Jones, J. Thomas, J. Parker, and R. Parker, "Acute changes in HEP, nucleotide derivatives and contractile force in ischemic and non-ischemic canine myocardium following coronary occlusion," *Cardiovascular Research*, vol. 94, pp. 163–167, 1976.

[71] K. Reimer, M. Hill, and R. Jennings, "Prolonged depletion of ATP and of the adenine nucleotide pool due to delayed resynthesis of adenine nucleotides following reversible myocardial ischemic injury in dogs," *Journal of Molecular Cell Cardiology*, vol. 13, pp. 229–239, 1981.

[72] G. V. der Vusse, T. Roemen, F. Prinzen, W. Coumans, and R. Reneman, "Uptake and tissue content of fatty acids in dog under normoxic and ischemic conditions," *Circulation Research*, vol. 50, pp. 538–546, 1982.

[73] A. Liedtke, "Alterations of carbohydrate and lipid metabolism in the acutely ischemic heart," *Progress in Cardiovascular Disease*, vol. 23, pp. 321–336, 1981.

[74] A. Katz and F. Messineo, "Lipid-membrane interactions and the pathogenesis of ischemic damage in the myocardium," *Circulatoin Research*, vol. 48, pp. 1–16, 1981.

[75] D. Rannels, R. Kao, and H. Morgan, "Effect of cardiac ischemia on protein degradation," *Circulation*, vol. 53, pp. 30–31, 1983.

[76] W. Gevers, "Generation of protons by metabolic processes in the heart cells," *Journal of Molecular Cell Cardiology*, vol. 9, pp. 867–873, 1977.

[77] J. Williamson, S. Schaeffer, C. Ford, and B. Safer, "Contribution of tissue acidosis to ischemic injury in the perfused rat heart," *Circulation*, vol. 53, pp. 3–14, 1976.

[78] B. Freeman and J. Crapo, "Biology of disease: Free radicals and tissue injury," *Lab Investigations*, vol. 47, pp. 412–426, 1982.

[79] R. Jennings, J. Schaper, M. Hill, C. Steenbergen, and K. Reimer, "Effect of reperfusion late in the phase of reversible ischemic injury. Changes in cell volume, electrolytes, metabolites and ultrastructure," *Circulation Research*, vol. 56, pp. 262–278, 1985.

[80] W. Basuk, K. Reimer, and R. Jennings, "Effect of repetitive brief episodes of ischemia on cell volume, electrolytes and ultrastructure," *Journal of the American College of Cardiology*, vol. 8, pp. 33A–41A, 1986.

[81] R. Jennings, "Myocardial ischemia revisited. The osmolar load, membrane damage, and reperfusion," *Journal of Molecular and Cellular Cardiology*, vol. 18, pp. 769–780, 1986.

[82] W. Cascio, T. Johnson, and L. Gettes, "Electrophysiologic changes in ischemic ventricular myocardium: Influence of ionic, metabolic and energetic changes," *Journal of Cardiovascular Electrophysiology*, vol. 6, pp. 1039–1062, 1995.

[83] A. Wilde and G. Aksnes, "Myocardial potassium ions and cell depolarization in ischemia and hypoxia," *Cardiovascular Research*, vol. 29, pp. 1–15, 1995.

[84] H. Morena, M.J.Janse, J. Fiolet, W. Krieger, H. Crijns, and D. Durrer, "Comparison of the effects of regional ischemia, hypoxia, hyperkalemia, and acidosis on intracellular and extracellular potentials and metabolism in the isolated porcine heart," *Circulation Research*, vol. 46, pp. 634–646, 1980.

[85] R. Gilmour and D. Zipes, "Different electrophysiological responses of canine endocardium and epicardium to combined hyperkalemia, hypoxia and acidosis," *Circulation Research*, vol. 46, pp. 814–825, 1980.

[86] W. Smith, W. Fleet, T. Johnson, C. Engle, and W. Cascio, "The Ib phase of ventricular arrhyhtmias in ischemic in situ porcine heart is related to changes in cell-to-cell coupling," *Circulation*, 1995.

[87] A. Kleber, C. Riegger, and M. Janse, "Electrical uncoupling and increase of extracellular resistance after induction of ischemia in isolated, arterially perfused rabbit papillary muscle," *Circulation Research*, vol. 61, pp. 271–279, 1987.

[88] S. Jain, R. Schuessler, and J. Saffitz, "Mechanisms of delayed electrical uncoupling induced by ischemic preconditioning," *Circulation Research*, vol. 92, pp. 1138–1144, 2003.

[89] A. Kleber, M. Janse, F. van Capelle, and D. Durrer, "Mechanism and time course of ST and TQ segment changes during acute regional myocardial ischemia in the pig heart determined by extracellular and intracellular recordings," *Circulation Research*, vol. 42, pp. 603–613, 1978.

[90] I. Kubota, M. Yamaki, T. Shibata, E. Ikeno, Y. Hosoya, and H. Tomoike, "Role of ATP-sensitive K^+ channel on ECG ST segment elevation during a bout of myocardial ischemia," *Circulation*, vol. 88, pp. 1845–1851, 1993.

[91] G. Yan and C. Antzelevitch, "Cellular basis for the normal T wave and the ECG manifestations of the Long-QT syndrome," *Circulation*, vol. 98, pp. 1928–1936, 1998.

[92] A. Arai, G. Pantely, W. Thoma, C. Anselone, and J. Bristow, "Energy metabolism and contractile function after 15 beats of moderate myocardial ischemia," *Circulation Research*, vol. 70, pp. 1137–1145, 1992.

[93] G. Gross, N. Farber, and H. Hardman, "Beneficial actions of superoxide dismutase and catalase in stunned myocardium of dogs," *American Journal of Physiology*, vol. 250, pp. H372–H377, 1986.

[94] S. Rahimtoola, "A perspective on the three large multi centered randomized clinical trials of coronary bypass surgery for chronic stable angina," *Circulation*, vol. 58, pp. 148–156, 1985.

[95] C. Murry, R. Jennings, and K. Reimer, "Preconditioning with ischemia: A delay of lethal cell injury in ischemic myocardium," *Circulation*, vol. 74, pp. 1124–1136, 1986.

[96] D. Yellon and J. Downey, "Preconditioning the myocardium: From cellular physiology to clinical cardiology," *Physiology Reviews*, vol. 83, pp. 1113–1151, 2003.

[97] L. Pescatello, *American College of Sports Medicine. Guidelines for Exercise Testing and Prescription*, 6th ed. Philadelphia: Lippincott, Williams and Wilkins, 2000.

[98] J. Viik, R. Lehtinen, and V. Turjanmaa, "Correct utilization of exercise electrocardiographic leads in differentiation of men with CAD from patients with low likelihood of CAD using peak exercise ST segment depression," *American Journal of Cardiology*, vol. 81, pp. 964–969, 1998.

[99] M. Geleijnse, P. Floretti, and J. Roelandt, "Methodology, feasibility, safety and diagnostic accuracy of dobutamine stress echocardiography," *Journal of American College of Cardiology*, vol. 30, pp. 595–606, 1997.

[100] K. Gould, K. Lipscomb, and G. Hamilton, "Physiologic basis for assessing critical coronary stenosis. Instantaneous flow response and regional distribution during coronary hyperemia as measures of coronary flow reserve," *American Journal of Cardiology*, vol. 33, pp. 87–94, 1974.

[101] M. Ragosta, A. Bishop, and L. Lipson, "Comparison between angiography and fractional flow reserve versus SPECT MPI for determining lesion significance in patients with multi vessel coronary disease," *American Journal of Cardiology*, vol. 99, pp. 896–902, 2007.

[102] J. Friedman, K. V. Train, and J. Maddahi, "Upward creep of the heart: A frequent source of false-positive reversible defects during SPECT," *Journal of Nuclear Medicine*, vol. 30, pp. 1718–1722, 1989.

[103] W. Janowitz, A. Agatston, and G. Kaplan, "Differences in prevalence and extent of coronary artery calcium detected by ultrafast CT in asymptomatic men and women," *American Journal of Cardiology*, vol. 72, pp. 247–254, 1993.

[104] G. Mowatt, J. Cook, and G. Hillis, "64-slice CT angiography in diagnosis and assessment of coronary artery disease: Systematic review and meta-analysis," *Heart*, vol. 372, pp. 1386–1393, 2008.

[105] D. Nash and S. Nash, "Ranolazine for chronic stable angina," *Lancet*, vol. 372, pp. 1335–1341, 2008.

[106] M. Agarwal, P. Mehta, and C. N. B. Merz, "Non-acute coronary syndrome anginal chest pain," *Medical Clinics of North America*, vol. 94, pp. 201–216, 2010.

[107] D. Lloyd-Jones, R. Adams, and M. Carnethon, "Heart disease and stroke statistics," *Circulation*, vol. 119, pp. 480–486, 2009.

[108] M. Blaha, S. Bansal, and R. Rouf, "A practical ABCDE approach to the metabolic syndrome," *Mayo Clinical Proceedings*, vol. 83, pp. 932–941, 2008.

[109] W. Evans and G. Sutton, "Painless cardiac infarction," *British Heart Journal*, pp. 259–272, July 1955.

[110] W. Samson and A. Scher, "Mechanism of ST segment alteration during acute myocardial injury," *Circulation Research*, vol. 8, pp. 780–787, 1960.

[111] W. Evans and H. Lloyd-Thomas, "The syndrome of the suspended heart," *British Heart Journal*, pp. 153–158, February 1956.

[112] L. Pordy, J. Kolker, M. Blumenthal, and A. Master, "Ergotamine tartrate and the 2-step exercise electrocardiogram in functional heart disturbance and in organic heart disease," *Annals New York City*, pp. 445–446, June 1949.

[113] M. Seigel and H. Feil, "Electrocardiographic studies during attacks of angina pectoris and of other paroxysmal pain," *Journal of Clinical Investigation*, pp. 795–806, July 1931.

[114] P. Salisbury, C. Cross, and P. Rieben, "Acute ischemia of inner layers of the ventricular wall," *American Heart Journal*, vol. 66, pp. 650–656, 1963.

[115] B. Brofman, D. Leighninger, and C. Beck, "Electrical instability of the heart: The concept of the current oxygen differential in CAD," *Circulation*, vol. 13, pp. 161–177, 1956.

[116] A. Katcher, G. Peirce, and J. Sayen, "Effects of experimental regional ischemia and levarterenol on RS-T segment and baseline of ventricular surface electrocardiograms obtained by direct-coupled amplification," *Circulation Research*, vol. 8, pp. 29–43, 1960.

[117] D. Streeter, H. Spotnitz, D. Patel, J. Ross, and E. Sonnenblick, "Fiber orientation in canine LV during diastole and systole," *Circulation Research*, vol. 24, pp. 339–347, 1969.

[118] D. Gregg and R. Patterson, "Functional importance of the coronary collaterals," *New England Journal of Medicine*, vol. 303-24, pp. 1404–1406, 1980.

[119] S. Brazzamano, J. Fedor, J. Rembert, and J. Greenfield, "Collateral conductance changes during a brief coronary occlusion in awake dogs," *Circulation*, vol. 72, pp. 225–232, 1985.

[120] A. Master, "Anoxic effects on the ECG produced by the 2-step test," *Annals New York City*, pp. 401–403, June 1950.

[121] I. Kroop, H. Jaffe, and A. Master, "The significance of RS-T elevation in acute coronary insufficiency," *Annals New York City*, p. 465, June 1949.

[122] S. Lau, S. Cohen, E. Stein, J. Haft, M. Kinney, M. Young, R. Helfant, and A. Damato, "Controlled heart rate by atrial pacing in angina pectoris: A determinant of ECG ST depression," *Circulation*, vol. 38, pp. 711–720, 1968.

[123] D. Mason, J. Spann, and R. Zelis, "New trends in treatment of angina pectoris," *California Medicine*, pp. 159–164, 1969.

[124] J. Talbot, R. Cosby, D. Levinson, G. Griffith, and M. Mayo, "Electrocardiograms and vectorelectrocardiograms," *California Medicine*, vol. 1, pp. 7–9, July 1956.

[125] D. Weitzman and E. Smith, "Ischaemic ECG in symptomless men," *British Heart Journal*, pp. 162–166, August 1959.

[126] J. D. Matis, "Reversible angina pectoris," *Chest*, vol. 34, pp. 450–454, 1958.

[127] L. Katz and H. Feinberg, "The relation of cardiac effort to myocardial oxygen consumption and coronary flow," *Circulation Research*, vol. 6, pp. 656–669, 1958.

[128] J. Sayen, W. Sheldon, G. Peirce, and P. Kuo, "Polarographic oxygen, the epicardial electrocardiogram and muscle contraction in experimental acute regional ischemia of the LV," *Circulation Research*, vol. 6, pp. 779–798, 1958.

[129] J. Sayen, G. Peirce, A. Katcher, and W. Sheldon, "Correlation of intramyocardial electrocardiograms with polarographic oxygen and contractility in the nonischemic and regionally ischemic left ventricle," *Circulation Research*, vol. 9, pp. 1268–1279, 1961.

[130] J. Boineau and M. Spach, "The relationship between the ECG and the electrical activity of the heart," *Journal of Electrocardiology*, vol. 1, pp. 117–124, 1968.

[131] E. Braunwald, J. Karliner, W. Ashburn, T. Kazamias, J. Ross, P. Maroko, B. Sobel, and N. Braunwald, "Research on the diagnosis and treatment of myocardial infarction," *California Medicine*, vol. 5, pp. 44–63, 1971.

[132] R. Balcon, J. Hoy, W. Malloy, and E. Sowton, "Hemodynamic comparisons of atrial pacing and exercise in patients with angina pectoris," *British Heart Journal*, vol. 31, pp. 168–171, 1969.

[133] J. Kjekshus, P. Maroko, and B. Sobel, "Distribution of myocardial injury and its relation to epicardial ST segment changes after coronary artery occlusion in the dog," *Cardiovascular Research*, vol. 6, pp. 490–499, 1972.

[134] T. Moir, "Study of luminal coronary circulation in the beating canine heart," *Circulation Research*, vol. 24, pp. 735–744, 1969.

[135] C. Mendez, W. Mueller, J. Meredith, and G. Moe, "Interaction of transmembrane potentials in canine Purkinje fibers and at Purkinje fiber-muscle junctions," *Circulation Research*, vol. 24, pp. 361–372, 1969.

[136] R. Kloner, C. Ganote, D. Whalen, and R. Jennings, "Effect of a transient period of ischemia on myocardial cells," *American Journal of Pathology*, vol. 74, pp. 399–423, 1974.

[137] P. Friedman, J. Stewart, J. Fenoglio, and A. Wit, "Survival of subendocardial Purkinje fibers after extensive MI in dogs," *Circulation Research*, vol. 33, pp. 597–611, 1973.

[138] R. Wilensky, J. Tranum-Jensen, R. Coronel, A. Wilde, J. Fiolet, and M. Janse, "The subendocardial border zone during acute ischemia of the rabbit heart: An electrophysiologic, metabolic and morphologic correlative study," *Circulation*, vol. 74, pp. 1137–1146, 1986.

[139] C. Steenbergen, C. Deleeuw, C. Barlow, B. Chance, and J. Williamson, "Heterogeneity of the hypoxic state in perfused rat heart," *Circulation Research*, vol. 41, pp. 606–615, 1977.

[140] M. Janse, J. Cinca, H. Morena, J. Fiolet, A. Kleber, G. de Vries, A. Becker, and D. Durrer, "The border zone in myocardial ischemia. An electrophysiological, metabolic and histochemical correlation in the pig heart," *Circulation Research*, vol. 44, pp. 576–588, 1979.

[141] R. Austin, G. Aldea, D. Coggins, A. Flynn, and J. Hoffman, "Profound spatial heterogeneity of coronary reserve - Discordance between patterns of resting and maximal myocardial blood flow," *Circulation Research*, vol. 67, pp. 319–331, 1990.

[142] C. Murry, V. Richard, K. Reimer, and R. Jennings, "Ischemic preconditioning slows energy metabolism and delays ultrastructural damage during a sustained ischemic episode," *Circulation Research*, vol. 66, pp. 913–931, 1990.

[143] Y. Birnbaum, S. Hale, and R. Kloner, "Progressive decrease in the ST segment elevation during ischemic preconditioning," *Journal of Molecular Cell Cardiology*, vol. 28, pp. 1493–1499, 1996.

[144] A. Arai, S. Grauer, C. Anselone, G. Pantely, and J. Bristow, "Metabolic adaptation to a gradual reduction in myocardial blood flow," *Circulation*, vol. 92, pp. 244–252, 1995.

[145] K. Kroll and G. Martin, "Comparison of myocardial ATP, blood flow, and cytosolic adenosine in demand ischemia and coronary occlusion," *American Journal of Physiology*, vol. 269, pp. 819–828, 1995.

[146] J. Karlsson, G. Templeton, and J. Willerson, "Relationship between epicardial ST changes and myocardial metabolism during acute coronary insufficiency," *Circulation Research*, vol. 32, pp. 725–730, 1973.

[147] J. Lekven, A. Ilebekk, E. Fonstelien, and F. Kil, "Relationship between ST segment elevation and local tissue flow during myocardial ischaemia in dogs," *Cardiovascular Research*, vol. 9, pp. 627–633, 1975.

[148] E. Braunwald and P. Maroko, "ST segment mapping. Realistic and unrealistic expectations," *Circulation*, vol. 54, pp. 529–532, 1976.

[149] J. Ross, "Electrocardiographic ST segment analysis in the characterization of myocardial ischemia and infarction," *Circulation*, vol. 53, pp. 173–181, 1976.

[150] I. Watanabe, T. Johnson, J. Buchanan, C. Engle, and L. Gettes, "Effect of graded coronary flow reduction on ionic, electrical, and mechanical indexes of ischemia in the pig," *Circulation*, vol. 76, pp. 1127–1134, 1987.

[151] H. Igarashi, M. Yamaki, I. Kubota, K. Ikeda, M. Matsui, K. Tsuiki, and S. Yasui, "Relation between localization of coronary artery disease and local abnormalities in ventricular activation during exercise tests," *Circulation*, vol. 81, pp. 461–469, 1990.

[152] D. Li, C. Li, A. Yong, and D. Kilpatrick, "Source of electrocardiographic ST changes in subendocardial ischemia," *Circulation Research*, vol. 82, pp. 957–970, 1998.

[153] Q. Li, "Transmyocardial ST potential distributions in ischemic heart disease," Ph.D. dissertation, University of Tasmania, Tasmania, Australia, 2005.

[154] R. MacLeod, B. Punske, B.Yilmaz, S. Shome, and B. Taccardi, "The role of heart rate in myocardial ischemia from restricted coronary perfusion," *Journal of Electrocardiology*, vol. 34, pp. 43–51, 2001.

[155] S. Shome, "Electrocardiographic mapping and characterization of myocardial ischemia," Ph.D. dissertation, University of Utah, Salt Lake City, USA, 2007.

[156] R. MacLeod, S. Shome, J. Stinstra, B. Punske, and B. Hopenfeld, "Mechanisms of ischemia-induced ST segment changes," *Journal of Electrocardiology*, vol. 38, pp. 8–13, 2005.

[157] W. Schaper, S. Bernotat-Danielowski, C. Nienaber, and J. Schaper, *The Heart and Cardiovascular System.* New York: Raven Press, 1992.

[158] J. Triana, X. Li, U. Jamaluddin, J. Thornby, and R. Bolli, "Post-ischemic myocardial stunning. Identification of major differences between open chest and conscious dog and evaluation of the oxygen radical hypothesis in the conscious dog," *Circulation Research*, vol. 69, pp. 731–747, 1991.

[159] T. Ihara, R. Shannon, and K. Komamura, "Effects of anaesthesia and recent surgery on diastolic function," *Cardiovascular Research*, vol. 28, pp. 325–336, 1994.

[160] R. Macleod, Q. Ni, and B. Punske, "Effects of heart position on the body-surface ECG," *Journal of Electrocardiology*, vol. 33, p. 229, 2000.

[161] D. Mirvis and R. Gordey, "Electrocardiographic effects of myocardial ischemia induced by atrial pacing in dogs with coronary stenosis. Repolarization changes with progressive left circumflex coronary artery narrowing," *Journal of American College of Cardiology*, vol. 4, pp. 1090–1098, 1983.

[162] G. Arisi, E. Macchi, C. Corradi, and R. Lux, "Epicardial excitation during ventricular pacing. Relative independence of breakthrough sites from excitation sequence in canine right ventricle," *Circulation Research*, vol. 71, pp. 840–849, 1992.

[163] J. Rogers, S. Melnick, and J. Huang, "Fiberglass needle electrodes for transmural cardiac mapping," *IEEE Transactions in Biomedical Engineering*, vol. 49, pp. 111–118, 2002.

[164] P. Ershler, K. Steadman, K. Moore, and R. Lux, "Systems for measuring and tracking electrophysiological distributions: Current tools for clinical and experimental cardiac mapping," *IEEE Transactions in Biomedical Engineering*, vol. 26, pp. 56–61, 1998.

[165] S. Institute, "Seg3D: Volume segmentation and processing tool," Scientific Computing and Imaging Institute (SCI), download from: http://www.scirun.org, 2015.

[166] R. Gonzalez and R. Woods, *Digitial Image Processing*, 3rd ed. New York: Prentice Hall, 2002.

[167] J. Weickert, *Anisotropic Diffusion in Image Processing*. Copenhagen: B. G. Teubner (Stuttgart), 1998.

[168] S. Institute, "BioMesh3D: Quality mesh generator for biomedical applications," Scientific Computing and Imaging Institute (SCI), download from: http://www.scirun.org, 2015.

[169] E. Haber and J. Modersitzki, "Numerical methods for image registration," *Inverse Problems*, vol. 20, pp. 1621–1638, 2004.

[170] J. Gower, "Generalized procrustes analysis," *Psychometrika*, vol. 40, pp. 33–51, 1975.

[171] W. Crum, T. Hartkens, and D. Hill, "Non-rigid image registration: Theory and practice," *British Journal of Radiology*, vol. 77, pp. S140–S153, 2004.

[172] A. Gorgels, "ST elevation and non-ST elevation acute coronary syndromes: Should the guidelines be changed?" *Journal of Electrocardiology*, vol. 46(4), pp. 318–323, 2013.

[173] K. Reimer and R. Jennings, "Myocardial ischemia, hypoxia and infarction," in *The Heart and Cardiovascular System*, H. Fozzard *et al.*, Eds. New York: Raven Press, 1986, pp. 1133–2101.

[174] R. Savage, G. Wagner, R. Ideker, S. Podolsky, and D. Hackel, "Correlation of postmortem anatomic findings with electrocardiographic changes in patients with myocardial infarction," *Circulation*, vol. 5, pp. 279–285, 1977.

[175] T. Hinohara, N. Hindman, R. White, R. Ideker, and G. Wagner, "Quantitative QRS criteria for diagnosing and sizing myocardial infarcts," *American Journal of Cardiology*, pp. 875–878, 1984.

[176] A. Kléber, "Extracellular potassium accumulation in acute myocardial ischemia," *Journal of Molecular and Cellular Cardiology*, vol. 16, pp. 389–394, 1984.

[177] A. Kléber, M. Janse, F. Wilms-Schopmann, A. Wilde, and R. Coronel, "Changes in conduction velocity during acute ischemia in ventricular myocardium of the isolated porcine heart," *Circulation*, vol. 73, pp. 189–198, 1986.

[178] R. Coronel, J. Fiolet, F. Wilms-Schopman, A. Schaapherder, T. Johnson, L. Gettes, and M. Janse, "Distribution of extracellular potassium and its relation to electrophysiologic changes during acute myocardial ischemia in the isolated perfused porcine heart," *Circulation*, vol. 77, pp. 1125–1138, 1988.

[179] R. Guyton, J. McClenathan, and G. Newman, "Significance of subendocardial ST segment elevation caused by coronary stenosis in the dog," *American Journal of Cardiology*, vol. 40, pp. 373–380, 1977.

[180] J. Edmunds, R. Gibbons, J. Breshahan, and I. Clements, "Significance of anterior ST depression in inferior wall acute myocardial infarction," *American Journal of Cardiology*, vol. 73, pp. 143–148, 1994.

[181] S. Shome, J. Stinstra, B. Hopenfeld, B. Punske, and R. MacLeod, "A study of the dynamics of cardiac ischemia using experimental and modeling approaches," in *Proceedings of the IEEE Engineering in Medicine and Biology Society 26th Annual International Conference*, IEEE EMBS. IEEE Press, 2004.

[182] S. Shome, S. Rossi, B. Punske, J. Stinstra, B. Hopenfeld, R. MacLeod, and B. Taccardi, "Anisotropic epicardial ST potential patterns reveal location and depth of ventricular necroses," in *Proceedings of the BMES 2004 Annual Fall Meeting*. BMES, 2004.

[183] S. Institute, "map3d: Interactive scientific visualization tool for bioengineering data," Scientific Computing and Imaging Institute (SCI), download from: http://www.scirun.org, 2015.

[184] P. Verdouw, B. Wolffebuttel, and J. Giessen, "Domestic pigs in the study of myocardial ischemia," *European Heart Journal*, vol. 4, pp. 61–67, 1983.

[185] P. Kovoor, C. Campbell, E. Wallace, K. Byth, B. Dewsnap, V. Eipper, J. Uther, and D. Ross, "Effects of simultaneous insertion of 66 plunge needle electrodes on myocardial activation, function, and structure," *PACE*, vol. 26, pp. 1979–1985, 2003.

[186] S. Khuri, J. Flaherty, J. O'Riordan, B. Pitt, R. Brawley, J. Donahoo, and V. Gott, "Changes in intramyocardial ST segment voltage and gas tensions with regional myocardial ischemia in the dog," *Circulation Research*, vol. 37, pp. 455–463, 1975.

[187] G. Buckberg, D. Fixler, J. Archie, and J. Hoffman, "Experimental subendocardial ischemia in dogs with normal coronary arteries," *Circulation Research*, vol. 30, pp. 67–81, 1972.

[188] E. Braunwald and P. Maroko, "The reduction of infarct size - An idea whose time (for testing) has come," *Circulation*, vol. 50, pp. 206–209, 1974.

[189] H. Smith, B. Singh, R. Norris, M. John, and P. Hurley, "Changes in myocardial blood flow and ST segment elevation following coronary artery occlusion in dogs," *Circulation Research*, vol. 36, pp. 697–705, 1975.

[190] J. Kjekshus, "Mechanism for flow distribution in normal and ischemic myocardium during increased ventricular preload in the dog," *Circulation Research*, vol. 33, pp. 489–499, 1973.

[191] J. Rouleau, L. Boerboom, A. Surjadhana, and J. Hoffman, "The role of autoregulation and tissue diastolic pressures in the transmural distribution of LV blood flow in anesthetized dogs," *Circulation Research*, vol. 45, pp. 804–815, 1979.

[192] R. Dunn and D. Griggs, "Transmural gradients in ventricular tissue metabolites produced by stopping coronary flow in the dog," *Circulation Research*, vol. 37, pp. 438–445, 1975.

[193] H. Fujiwara, M. Ashraf, S. Sato, and R. Millard, "Transmural cellular damage and blood flow distribution in early ischemia in pig hearts," *Circulation Research*, vol. 51, pp. 683–693, 1982.

[194] R. Ruffy, D. Lovelace, T. Mueller, S. Knoebel, and D. Zipes, "Relationship between changes in LV bipolar electrograms and regional myocardial blood flow during acute

coronary artery occlusion in the dog," *Circulation Research*, vol. 45, pp. 764–770, 1979.

[195] S. Kimura, A. Bassett, T. Furukawa, J. Cuevas, and R. Myerburg, "Electrophysiological properties and responses to simulated ischemia in cat ventricular myocytes of endocardial and epicardial origin," *Circulation Research*, vol. 66, pp. 469–477, 1990.

[196] B. Leshnower, H. Sakamoto, H. Hamamoto, A. Zeeshan, J. Gorman, and R. Gorman, "Progression of myocardial injury during coronary occlusion in the collateral-deficient heart: A non wavefront phenomenon," *American Journal of Physiology*, vol. 293, pp. 1799–1804, 2007.

[197] G. Wagner, *Marriott's Practical Electrocardiography*, 11th ed. Philadelphia: Lippincott Williams & Wilkins, 2008.

[198] K. Aras, B. Burton, D. Swenson, and R. MacLeod, "Sensitivity of epicardial electrical markers to acute ischemia detection," *Journal of Electrocardiology*, vol. 47(6), pp. 836–841, 2014.

[199] D. Mirvis, "Differential electrocardiographic effects of myocardial ischemia induced by atrial pacing in dogs with various locations of coronary stenosis," *Circulation*, vol. 68, pp. 1116–1126, 1983.

[200] L. Clerc, "Directional differences of impulse spread in trabecular muscle from mammalian heart," *Journal of Physiology*, vol. 255, pp. 335–346, 1976.

[201] A. Selwyn, E. Welman, and A. Jonathan, "ECG signs in experimental ischemia and infarction," *European Journal of Cardiology*, vol. 8, pp. 185–196, 1978.

[202] T. Huebner, M. Goernig, M. Schuepbach, E. Sanz, R. Pilgram, A. Seeck, and A. Voss, "Electrocardiographic and related methods of non-invasive detection and risk stratification in myocardial ischemia: State of the art and perspectives," *GMS German Medical Science*, vol. 8, pp. 1–19, 2010.

[203] B. Chaitman and J. Hanson, "Comparative sensitivity and specificity of exercise ECG lead systems," *American Journal of Cardiology*, vol. 47, pp. 1335–1349, 1981.

[204] S. Abboud, R. Cohen, A. Selwyn, P. Ganz, D. Sadeh, and P. Friedman, "Detection of transient myocardial ischemia by computer analysis of standard and signal averaged HF ECG in patients undergoing PTCA," *Circulation*, vol. 76, pp. 585–596, 1987.

[205] K. Yamada, M. Okajima, K. Hoki, M. Kohno, M. Kamijo, H. Tatematsu, S. Jen, A. Ito, Y. Nagata, H. Hayashi, H. Toyoshima, M. Wada, and O. Mizutani, "Studies on the mechanism of ST-T alterations of ECG," *Annual Report Nagoya University*, vol. 19, pp. 41–50, 1972.

[206] M. Miller, J. Thorvaldson, A. IIebekk, and J. Lekven, "Myocardial ischemia. Relationship between local flow, function, and ST segment elevation," *European Journal of Cardiology*, vol. 10, pp. 7–18, 1979.

[207] P. Kligfield, "Principles of simple heart rate adjustment of ST segment depression during exercise electrocardiography," *Cardiology Journal*, vol. 15, pp. 194–200, 2008.